

**MICROSPECTROSCOPIC STUDY OF COBALT SPECIATION AND
LOCALIZATION IN HYPERACCUMULATOR ALYSSUM MURALE**

by

Ryan V. Tappero

A dissertation submitted to the Faculty of the University of Delaware in
partial fulfillment of the requirements for the degree of Doctor of Philosophy in Plant
and Soil Sciences

Winter 2009

© 2009 Ryan V. Tappero
All Rights Reserved

UMI Number: HHI 1 € G

Copyright 2008 by
Væ] ^! [ÊÜ^ æ ÁÈ

All rights reserved

INFORMATION TO USERS

The quality of this reproduction is dependent upon the quality of the copy submitted. Broken or indistinct print, colored or poor quality illustrations and photographs, print bleed-through, substandard margins, and improper alignment can adversely affect reproduction.

In the unlikely event that the author did not send a complete manuscript and there are missing pages, these will be noted. Also, if unauthorized copyright material had to be removed, a note will indicate the deletion.

UMI[®]

UMI Microform HHI 1 € G
Copyright 2008 by ProQuest LLC
All rights reserved. This microform edition is protected against
unauthorized copying under Title 17, United States Code.

ProQuest LLC
789 East Eisenhower Parkway
P.O. Box 1346
Ann Arbor, MI 48106-1346

**MICROSPECTROSCOPIC STUDY OF COBALT SPECIATION AND
LOCALIZATION IN HYPERACCUMULATOR ALYSSUM MURALE**

by

Ryan V. Tappero

Approved: _____
Donald L. Sparks, Ph.D.
Chair of the Department of Plant and Soil Sciences

Approved: _____
Robin W. Morgan, Ph.D.
Dean of the College of Agriculture and Natural Resources

Approved: _____
Debra Hess Norris, M.S.
Vice Provost for Graduate and Professional Education

I certify that I have read this dissertation and that in my opinion it meets the academic and professional standard required by the University as a dissertation for the degree of Doctor of Philosophy.

Signed:

Donald L. Sparks, Ph.D.
Professor in charge of dissertation

I certify that I have read this dissertation and that in my opinion it meets the academic and professional standard required by the University as a dissertation for the degree of Doctor of Philosophy.

Signed:

Rufus L. Chaney, Ph.D.
Member of dissertation committee

I certify that I have read this dissertation and that in my opinion it meets the academic and professional standard required by the University as a dissertation for the degree of Doctor of Philosophy.

Signed:

Matthew A. Marcus, Ph.D.
Member of dissertation committee

I certify that I have read this dissertation and that in my opinion it meets the academic and professional standard required by the University as a dissertation for the degree of Doctor of Philosophy.

Signed:

Harsh Bais, Ph.D.
Member of dissertation committee

ACKNOWLEDGEMENTS

I thank my family and friends for their patience and encouragement throughout my academic studies at Cal Poly, SLO and the University of Delaware. I recognize my parents (Carole and Vance) along with my beloved sister (Noelle) and her family (Steven, Presley, and Reagan) for their continued interest and support. I take this opportunity to document the many helpful contributions from my friend, mentor and colleague, Dr. Markus Gräfe; I will miss our late-night adventures at the DOE national labs/ beamlines across the US (“What’s mine say?”). Likewise, I owe deep gratitude to my friend and fellow graduate student, Jen Seiter, particularly for her sanity during the times when I was most insane (No, you are the photon junkie).

I need to acknowledge our fine post-doctoral researchers, Drs. Edward Peltier (“Ted”), Tiffany Thomas (“T.N.T.”), Sanjai Parikh, and Matthew Ginder-Vogel (“Dr. Matt”) for contributing their ideas and time. I owe many thanks to my fellow students in the Sparks’ group (David, Jen, Brandon, Gautier, Masayuki, Saengdao, Mike, and Matt); I wish you all great success in your research efforts and careers.

I appreciate all who contributed their time and expertise to this research. I recognize Jennifer Ciconte (PhytoSystems) and Krystl Heidel-Tappero for their relentless efforts during the many hours spent at the Fischer Greenhouse, and I especially thank Krystl for assuming the co-pilot position on crucial beamtrips to Berkeley, Chicago, and New York. I thank the staff of the Plant and Soil Science Department (PLSC) for their friendliness and willingness to help (especially Kathy

Fleischut and Amy Broadhurst). I express sincere gratitude to “Uncle Jerry” Hendricks (PLSC Research Technician) for his friendship, reliability, and admiration of fine ale. It is hard to find original things to say about Jerry that have not been written time and again in other dissertation acknowledgements; I think this fact speaks of its own.

A significant portion of this research was performed outside the walls and halls of UD, and involved the assistance of numerous persons at research facilities across the US. I thank Drs. Ken Livi (John Hopkins University) and Kirk Czymmek (Delaware Biotechnology Institute; DBI) for their assistance with the electron probe micro-analysis (EPMA) components of this research. I owe special thanks to Sirine Fakra at the Advanced Light Source (ALS), Drs. Bruce Ravel, Matt Newville, Steve Sutton, and Mark Rivers at the Advanced Photon Source (APS), and Drs. Kumi Pandya, Mark Fuhrman, Paul Northrup, Tony Lanzirotti, and Lisa Miller at the National Synchrotron Light Source (NSLS) for their relentless ‘round-the-clock’ help and support while performing experiments at their fine laboratories. *Fiat lux!*

I owe so much to Dr. Donald L. Sparks (my mentor and Ph.D. advisor) for his leadership, support, guidance and encouragement throughout my stay at UD. I can not convey with words how much I truly admire and respect him; there is no question that he is the “rock” of the ESC research group (and Uncle Jerry is the “n’roll”). I sincerely appreciate the academic freedom he offers and the endless opportunities he selflessly provides for his students. He is a truly remarkable individual of

insurmountable integrity and honor; a gemstone within a semi-precious deposit, a crystalline, silicon-interlayered double hydroxide within a poorly-crystalline, alpha-hydroxide surface coating (lol). I wish the very best to Dr. and Joy Sparks; may the Pinot gods rain down on your heads.

Finally, I would like to acknowledge the members of my dissertation committee. I sincerely thank Dr. Harsh Bais (DBI) for his helpful advice, the use of his laboratory facilities, and his participation as a committee member. I take this opportunity to document the many helpful contributions from my buddy, Dr. Matthew A. Marcus (LBNL-ALS), who begrudgingly served as a committee member (“Foo-fer-aw”), but I still love him (D’oh!) because he is reluctant about most things at first (except hikes, squishies, and grubbing down with the “Ghost diner”). Matthew is one cool dude and I have a lot of fun working with him; I hope we can begrudgingly collaborate on additional projects and squishies in the years ahead (No Braggies!). Lastly, I need to express my respect and sincere gratitude to my comrade, mentor and committee member, Dr. Rufus L. Chaney (USDA-ARS), who has been like a surrogate father to me while I was away from ‘the Left Coast’; I am sure he recognizes all that I have gained from him and that no room exists in this document for the necessary detail. All I can say here is, “Dr. Chaney?” [Yes!] “I’m not worthy, I’m not worthy”. It is my hope that you and I will continue to “Disturb the dirt” together.

DEDICATION

Most of all I thank my wife, Krystl, for her perpetual interest, involvement, and personal sacrifice during the course of this research. Without her none of this would have been possible nor worth it. I dedicate this work to Krystl.

EPIGRAPH

“It’s a miracle that curiosity survives formal education”.

--Albert Einstein

TABLE OF CONTENTS

LIST OF TABLES	xii
LIST OF FIGURES	xiii
ABSTRACT	xvi
Chapter	
1 INTRODUCTION	1
1.1 Trace Elements in the Critical Zone	1
1.2 Synchrotron-based Spectromicroscopic Techniques	3
1.3 Trace Metals in Soil.....	4
1.4 Metalliferous Soils and Metallophytes	8
1.5 Phytoremediation: Metal Phytoextraction and Phytomining.....	10
1.6 Rhizosphere: Root-Microbe-Mineral-H ₂ O Interface	13
1.6.1 Rhizosphere Processes.....	13
1.6.2 Nutrient Acquisition and Phytoavailability	14
1.7 Trace Metals in Plants	19
1.7.1 Short-distance Transport.....	20
1.7.2 Membrane Transport	22
1.7.3 Metal Homeostasis in Hyperaccumulators	26
1.8 Research Questions and Objectives.....	30
1.9 References	34
2 HYPERACCUMULATOR <i>ALYSSUM MURALE</i> RELIES ON A DIFFERENT STORAGE MECHANISM FOR COBALT THAN FOR NICKEL	44
2.1 Summary.....	44
2.2 Introduction	45
2.3 Materials and Methods	49
2.3.1 Project Summary	49
2.3.2 Ebb and Flow Mesocosm Design	49
2.3.3 Plant Tissue Analysis.....	50

2.3.4	Electron Probe Micro-Analysis	50
2.3.5	Synchrotron X-ray Microfluorescence (SXRF) and Computed Microtomography (CMT)	51
2.4	Results	53
2.4.1	Plant Growth.....	53
2.4.2	Bulk Characterization of Metal Accumulation.....	54
2.4.3	Plant Tissue Microanalysis.....	56
2.5	Discussion.....	66
2.5.1	Metal Localization.....	67
2.5.2	Metal Interactions.....	70
2.5.3	Metal Tolerance and Sequestration	72
2.6	References	76
3	COBALT SPECIATION IN HYPERACCUMULATOR <i>ALYSSUM</i> <i>MURALE</i> USING BULK AND MICROFOCUSED X-RAY ABSORPTION SPECTROSCOPY	82
3.1	Summary.....	82
3.2	Introduction	82
3.3	Methods	86
3.3.1	Experimental Design	86
3.3.2	Plant Propagation and Cultivation.....	86
3.3.3	Plant Tissue Analysis.....	87
3.3.4	Extraction and Analysis of Naturally-bleeding Xylem Fluid	88
3.3.5	Electron Probe Micro-analysis	89
3.3.6	Bulk X-ray Absorption Spectroscopy.....	89
3.3.7	Synchrotron-based Spectromicroscopy	90
3.3.8	EXAFS Data Analysis	92
3.4	Results and Discussion	96
3.4.1	Plant Growth and Cobalt Accumulation.....	96
3.4.2	Organic Acids in Naturally-bleeding Xylem Fluid.....	97
3.4.3	Cobalt Localization and Elemental Associations using Synchrotron-based Spectromicroscopy and Electron Microprobe Analysis (EMPA)	101
3.4.4	Cobalt Speciation in the Bulk Samples	105
3.4.5	<i>In Situ</i> Cobalt Speciation in Hydrated <i>Alyssum</i> Leaves.....	115
3.5	References	126
4	SUMMARY AND RESEARCH NEEDS.....	131

APPENDICES

A CHAPTER 2 COPYRIGHT PERMISSIONS 138

LIST OF TABLES

Table 2.1	Shoot biomass and element concentrations for <i>Alyssum murale</i> plants 30 days after metal exposure.....	55
Table 2.2	Translocation factors (Shoot to root concentration ratio) for <i>Alyssum murale</i> plants 30 days after metal exposure	56
Table 3.1	Concentrations of major organic acids detected in naturally-bleeding xylem fluid collected from <i>Alyssum murale</i> plants.....	98
Table 3.2	Summary of Co speciation in hyperaccumulator <i>Alyssum murale</i>	107
Table 3.3	Linear combination fit results for the μ -XAFS spectra of hydrated leaves from Co-treated <i>A. murale</i> (shown in Figure 3.7)	119

LIST OF FIGURES

Figure 1.1	Dicot root cross-section displaying symplastic (A) and apoplastic (B) solute pathways	21
Figure 1.2	Conceptual model of membrane transport systems involved with solute absorption	24
Figure 1.3	Possible mechanisms of metal tolerance	29
Figure 2.1	μ -SXRF images of the Ni, Co, and Zn distributions in a hydrated <i>Alyssum murale</i> leaf from the Ni + Co + Zn treatment. Camera image shows the leaf region selected for SXRF imaging.....	57
Figure 2.2	μ -SXRF tricolor image (Ni, Co, and Ca) of a hydrated <i>Alyssum murale</i> leaf from the Ni + Co + Zn treatment plus a line profile (fluorescence intensity versus position) for a segment from the leaf center toward the leaf tip (indicated by arrow).....	58
Figure 2.3	μ -SXRF images of hydrated <i>Alyssum murale</i> leaves depicting colocalization of Co with (a) Mn and Ca at a leaf trichome (line profile across trichome) and with (b) sulfur near a leaf tip and margin. The Mn-rich zone (blue) surrounding the trichome base is displayed as an inset on the tricolor SXRF image (top panel).....	59
Figure 2.4	Fluorescence CMT cross-sectional images (5 μ m slices) of the Ni, Co, Zn, Mn, and Fe distributions in <i>Alyssum murale</i> fine root segments at 0.5 mm (bottom), 3 mm (middle), and 6 mm (top) from the root apex. Root was collected from the Ni + Co + Zn treatment.....	61
Figure 2.5	Backscattered electron (BSE) image of a leaf from Co-treated <i>Alyssum murale</i> with the corresponding SEM-EDS spectra from the leaf-tip and bulk-leaf regions (top panel); μ -SXRF image (Co and Ca) of a hydrated leaf from Co-treated <i>A. murale</i> with the corresponding Co K-edge k^3 -weighted $\chi(k)$ spectra (inset) and the Fourier transforms (FT) of μ -XAFS spectra from leaf-tip and bulk-leaf regions (bottom panel). An optical microscope image of a hydrated leaf from Co-treated <i>A. murale</i> is displayed as an inset (top panel).....	62

Figure 2.6	Differential absorption (DA-CMT) tomographic projections (5.1 μm slices) of hydrated <i>Alyssum murale</i> leaves depicting (a) Co distribution in the leaf-tip region, (b) Co distribution in the bulk-leaf region, (c) Co distribution in relation to the leaf cell structure (grey), and (d) Ni distribution in the leaf-tip and bulk-leaf regions. Leaves were collected from a Co-treated plant (a-c) and a Ni-treated plant (d). Sinograms recorded above and below the Co or Ni K-edge energy (+30 eV and -100 eV, respectively) were computationally reconstructed and the resulting projections were subtracted (above - below) to reveal the metal distribution in leaves. Distances are relative to the leaf tissue at the tip as determined from leaf structure images (i.e. below-edge projections).....	65
Figure 3.1	μ -SXRF image showing the distribution of Co (red), Mn (blue), and Ca (green) in a hydrated <i>Alyssum murale</i> leaf from the 50 μM treatment plus approximate regions on leaves where μ -EXAFS spectra were collected (indicated with circles).....	102
Figure 3.2	One-dimensional XRD pattern for a trichome on an <i>A. murale</i> leaf, numbers indicate respective d-spacing for characteristic calcite (CaCO_3) peaks. Inset, SEM image (center) and two-dimensional μ -XRD pattern (right) for the trichome	103
Figure 3.3	Representative one-dimensional XRD pattern for a Co-rich hotspot near the tip of a Co-treated <i>A. murale</i> leaf (upper line) and a synthetic, poorly-ordered hydrous Co silicate (lower line), numbers indicate respective d-spacing for several characteristic features of the Co-Phyllosilicate (syn. Co-Kerolite; $\text{Co}_3\text{Si}_4\text{O}_{10}(\text{OH})_2$). Inset, two-dimensional μ -XRD pattern (right) for the Co-rich hotspot.	103
Figure 3.4	EMPA backscattered electron (BSE) image of a leaf from a Co-treated <i>Alyssum murale</i> plant and associated X-ray fluorescence maps for Co, Si, Ca, Mg, S, Mn, and K (top panel) plus the corresponding energy-dispersive X-ray spectra (produced by spectral summation) for Co-enriched and bulk-leaf regions (next page)	105
Figure 3.5	Cobalt K-edge EXAFS spectra of bulk plant samples, raw k^2 -weighted $\chi(k)$ spectra (dotted line) and corresponding linear combinations fit (solid line)	108

Figure 3.6	Cobalt K-edge EXAFS spectra of Co reference compounds, k^3 -weighted $\chi(k)$ spectra and corresponding Fourier Transforms (modulus and imaginary part)	113
Figure 3.7	Cobalt K-edge μ -EXAFS spectra of hydrated leaves from Co-treated <i>A. murale</i> (dotted lines) and corresponding linear combinations fit (solid line)	118
Figure 3.8	Molecular-scale representations of the coordination environment in a Cobalt-rich Kerolite-like 2:1 trioctahedral phyllosilicate, a hydrous Co-carbonate hydroxide mineral precipitate, and a Co-fumarato coordination polymer	121

ABSTRACT

A vast amount of research on phytoremediation has been conducted over the past several decades since Chaney (1983) first proposed the idea of using accumulator plants to extract metals from anthropogenically-contaminated soils (phytoextraction) or metalliferous soils (phytomining), and noted the opportunity to recover metals of economic value by ashing the shoot biomass. Substantial research on metalliferous soils existed previously, and the use of metallophytes as geobotanical indicators for mineral prospecting had been well-established (Tkalic 1938; Brundin 1939; Cannon, 1960). The first three Ni hyperaccumulators discovered were of the genus *Alyssum* in the family *Brassicaceae* (*A. bertolonii* in 1948, *A. murale* Waldst. & Kit. in 1961, and *A. serpyllifolium* Desf. in 1969), although discoveries of other genera of accumulator plants rapidly added to the list of accumulators (Morrison, 1980). R.R. Brooks and co-workers conducted the majority of pioneering research to identify metal accumulators by large-scale surveys of metalliferous flora and analysis of metal concentrations in field specimens (plants and soils) as well as analysis of herbarium specimens (Brooks et al., 1974; Brooks 1977; Brooks et al., 1977a,b,c; Wither and Brooks, 1977; Brooks and Radford, 1978; Jaffré et al., 1979a,b; Morrison, 1980; Reeves et al., 1981, 1983). In time, research focus shifted from field-based

observations of metalliferous flora to laboratory-scale investigations of metal-specific “hyperaccumulators” with emphasis largely on metal phytoextraction from artificially-contaminated (single-metal) media. Encouraging results from laboratory investigations obtained under ideal conditions quickly fueled implementation of field-scale remediation. However, early efforts to apply phytoextraction in the field were marginally successful because a fundamental understanding of the mechanisms underlying metal accumulation and tolerance was lacking as was the necessary information regarding agronomic practices for cultivation of hyperaccumulator plants.

In the last decade, major advances in biotechnology and plant molecular biology offered new opportunities to gain fundamental insight to the mechanisms underlying metal homeostasis in accumulators, and provided the necessary tools for investigating *in vivo* the complex physiological and biochemical processes regulating metal tolerance and hyperaccumulation. Many early biogeochemical and phytochemical studies of hyperaccumulators that reported on plant-soil relationships, metal distributions in plants, and metal-ligand complex formation were conducted with *ex situ* analytical techniques. Recent advances in analytical techniques for *in situ* chemical measurements (e.g. synchrotron-based spectroscopic methods) have created new opportunities to relate knowledge of the biochemical pathways mediating plant metal homeostasis with molecular-scale information of the localization, associations, and speciation of the metals in plants. A more comprehensive understanding of the mechanisms involved in metal uptake by plants will lead to enhanced phytoextraction

through breeding programs or transgenic developments, and provide a greater potential to produce nutrient-fortified foods and to improve crop production on nutrient-poor soils.

In this investigation, a combination of novel *in situ* techniques (e.g. synchrotron-based spectroscopies), advanced *ex situ* analytical methods (e.g. electron microprobe analysis), and wet-chemical procedures (e.g. high performance liquid chromatography) were used to investigate the localization and speciation of cobalt in the Ni/ Co hyperaccumulator plant (*Alyssum murale*). Synchrotron-based microspectroscopic tools were applied to gain (sub)micrometer-scale information regarding the *in situ* chemical form (i.e. molecular speciation), spatial location, and elemental associations of the plant-accumulated metals (Co and Ni). The first research objective was to investigate aspects of Co accumulation and storage in *A. murale* and to determine the influence of simultaneous hyperaccumulation (i.e. Ni and Co) on metal localization. The second objective was to examine the molecular speciation of Co in various *A. murale* tissues (e.g. roots, stems, shoots, leaf tips) in an effort to improve our understanding of the biochemical mechanisms regulating Co transport and tolerance (i.e. metal homeostasis).

The research findings presented in Chapter 2 revealed a novel metal sequestration mechanism for accumulated Co (exocellular sequestration) that is potentially involved with Co tolerance in *A. murale*. Furthermore, the sequestration mechanism for Co is completely different from the intracellular mechanism used to

sequester Ni in *A. murale* (i.e. vacuolar compartmentalization) and other *Alyssum* hyperaccumulators; compartmentalization of metals in the epidermal cell vacuoles of leaves has been established as a key component of the (hyper)tolerance mechanism used by the majority of hyperaccumulator plants.

The research findings presented in Chapter 3 represent the first report on the occurrence of Co/Si-rich biogenic nanoparticles (e.g. Phytoliths with two-dimensional hydrous cobalt silicate domains) and other Cobaltian mineral precipitates (e.g. Widgiemoolthalite, Co-analogue) and polymers (e.g. Cobalt hydroxide fumarate coordination polymer, $[\text{Co}_3(\text{C}_4\text{H}_2\text{O}_4)_2]_x\text{H}_2\text{O}$) sequestered on the leaf surface of a metal hyperaccumulator plant.

Chapter 1

INTRODUCTION

1.1 Trace Elements in the Critical Zone

Large-scale environmental contamination is a menacing consequence of the Industrial Revolution. Widespread redistribution of metals in the “Critical Zone” can result in severe damage to air, soil, and water resources, thereby threatening the viability of natural ecosystems. The Critical Zone is the vital region of the near-surface environment which extends from the outer envelope of the vegetation down to the lower limits of the groundwater, and includes all fluid, mineral, gaseous, and biotic components supporting life on Earth. A heavy metal can be broadly defined as any element having metallic properties (ductility, conductivity, density, stability as cations, and ligand specificity) with an atomic number greater than 20 and a density greater than 5.0 g cm^{-3} (Adriano, 1986). Metal-enriched soils are prevalent in nature, originating from both anthropogenic and geogenic sources. Some significant anthropogenic inputs include spoil from metal mining operations, fallout from smelter/refinery emissions, waste disposal from electroplating and manufacturing, combustion of fossil fuels, and agricultural application of pesticides and biosolids (Adriano, 1986).

Metal contamination of surface and subsurface environments is a worldwide concern. Pollution assessment and remediation efforts represent a

significant financial burden for industries, governments, and taxpayers. In the U.S., trace metals account for 65 % of the contaminated Superfund sites where USEPA has signed Records of Decision (Lombi et al., 2001). Non-radioactive metals and metalloids of importance as environmental contaminants include arsenic (As), cadmium (Cd), chromium (Cr), cobalt (Co), copper (Cu), lead (Pb), mercury (Hg), nickel (Ni), and zinc (Zn). Several trace metals listed as priority environmental pollutants are “essential elements” for many living organisms, thus excessive quantities of essential elements are toxic to living systems.

The traditional approach for remediation of metal-contaminated soils is excavation and subsequent reburial at a hazardous waste management facility. *Ex situ* remediation strategies are expensive, costing ~\$1M/ acre (Raskin et al., 1997). Engineered remedial approaches (e.g. excavation, soil washing, electrokinetics) are energy intensive, inefficient, and rely on other disposal systems for containment. Alternative remediation strategies are necessary when vast areas of land have been contaminated, due in part to the high cost associated with the traditional remediation methods (e.g. dig and haul). Effective *in situ* remediation methods will need to be based on a sound understanding of the site-specific, spatial and temporal variations in contaminant speciation. Quantitative elemental speciation is requisite for long-term risk assessment and for the design and monitoring of remediation systems.

The significance of metal contamination in the environment (including the absorption of these elements by plants and animals) depends on the chemical form of

the metal (or its speciation). Speciation describes the chemical and physical (spatial distribution) state of an element in a biogeochemical setting. Molecular speciation encompasses the element identity, oxidation state, associations and complexes with dissolved species (e.g. metal-ligand bonds) or solids (e.g. surface precipitate), local coordination environment, and molecular geometry (Brown et al, 1999; Roberts et al., 2003). The speciation of elements determines their transport, reactivity, and toxicity in the natural environment; it controls contaminant mobility in soils, sediments and natural waters, interactions with other elements, and food-chain transfer mechanisms. In natural environments, elemental transformations (i.e. changes of chemical form/speciation) are governed by physiochemical-biological interfacial interactions, thus the role of interfacial processes in controlling the speciation of elements in soils and surrounding environments, especially the rhizosphere, which is the bottleneck of contamination of the terrestrial food chain, deserves increasing attention (Huang, P.M. 2008).

1.2 Synchrotron-based Spectromicroscopic Techniques

One of the most widely used synchrotron-based spectroscopic techniques in the geosciences is X-ray Absorption Spectroscopy (XAS). Its use has revolutionized our understanding of metal and other contaminant reactions and processes in natural systems such as soils and sediments. XAS can be used to ascertain important chemical information, such as oxidation state, information on

next-nearest neighbors, bond distances, and coordination numbers (i.e. speciation). It can be used to study most elements in crystalline or non-crystalline solid, liquid, or gaseous states over a concentration range of a few mg L^{-1} to the pure element.

Synchrotron-based spectromicroscopic tools (e.g. μ -XAS) can be used to investigate element speciation and distribution in natural, heterogeneous samples at the (sub)micron scale. Spectromicroscopic techniques of particular relevance to soil and environmental biogeochemistry include synchrotron X-ray microfluorescence (μ -SXRF), microfocused extended X-ray absorption fine structure spectroscopy (μ -EXAFS), X-ray microdiffraction (μ -XRD), computed microtomography (CMT), scanning transmission X-ray microscopy (STXM), and reflectance Fourier transform infrared microscopy (SR-FTIR). Several of these novel *in situ* analytical techniques can glean element-specific, molecular-scale chemical information from natural samples maintained at environmentally-relevant conditions (e.g. hydrated, ambient temperature and pressure, etc.), a major advantage over techniques that require a sample to be dried or subjected to ultrahigh vacuum or both. By utilizing these spectromicroscopic tools it is possible to determine, *in situ*, the speciation of elements in soils and plants (where speciation can vary over tens of microns), or investigate physiochemical-biological processes at complex environmental interfaces (e.g. root-microbe-mineral- H_2O interface).

1.3 Trace Elements in Soil

Soil functions as the primary sink for trace metals in the terrestrial environment ([Adriano, 1986](#)). Metals introduced into a soil system can experience one or more of the following fates: (1) dissolved in the soil solution, (2) bound (electrostatically) to exchange sites on soil solids or sorbed (covalently bonded) to soil constituents, (3) precipitated with other compounds in soils, (4) fixed or occluded within soil minerals, (5) bound with organic constituents, or (6) incorporated into the soil biomass. A few trace metals (Hg) and metalloids (As and Se) can be volatilized by biotic and abiotic reactions.

Soil exhibits a finite capacity for retaining trace elements. The primary factors influencing the capacity of a soil to retain trace metals include the soil pH and redox potential, soil organic matter content, cation exchange capacity, and soil mineralogy ([Adriano, 1986](#)). A substantial fraction of trace metals in soil are associated with soil solids (e.g. oxides/ hydroxides/ oxyhydroxides, clay minerals, and organic material); these solids exert controlling influence on the solubility, 'bioavailability', and reactivity of metals in soil ([Petruzzelli, 1989](#)). Only trace metals dissolved in the soil solution are readily available for absorption by plants and other organisms (i.e. 'bioavailable'). Metal-bearing soil solids control the free metal ion activity in soil solution through a dynamic 'equilibrium' established by the multitude of competing reactions occurring in soils (oxidation/reduction, ion exchange, sorption/desorption, precipitation/ dissolution, complexation/ coprecipitation). Therefore, the free metal ion activity in soil solution results from metal equilibria among the "clay"

minerals, organic matter (humic and fulvic acids, polysaccharides, and organic acids), soluble chelators, and hydrous oxides of Fe/ Mn/ Al; soil Eh/ pH conditions strongly affect these equilibria ([Lindsay, 1979](#)) as do the soil biota/ microbiota.

The capacity of soil to retain most trace metals increases with increasing pH, with the maximum occurring under neutral and slightly alkaline conditions ([Adriano, 1986](#)). Exceptions include As, Se, V, Mo, and Cr (VI), commonly being more mobile under basic or saline soil conditions. In general, trace metals are solubilized and become more mobile in acidic conditions, whereas the mobility of metalloids follows an opposite trend ([Lombi et al., 2001](#)).

The water content of soil influences biological and chemical oxidation-reduction reactions. In oxidized soils, redox potentials typically range from approximately + 400 mV to + 700 mV ([Sparks, 2003](#)). In sediments or flooded soils, redox potentials may range from around – 400 mV (strongly reduced) to + 700 mV (well oxidized). Sulfides of metal elements (e.g. As, Cu, Zn, Cd, Ni, Co, and Pb) may form under reducing conditions. The sulfides of these chalcophilic elements are relatively insoluble in reduced environments, thus their mobility and bioavailability are considerably less than under well-oxidized soil conditions. Exceptions include Fe and Mn which are more soluble under reduced conditions than oxidized conditions.

Several trace elements (Cu, Pb, Hg, Ni, Co, Mn, and others) exhibit rather high affinities for soil organic matter (SOM). Organic soil colloids have both ion exchange and chelator properties. Metals bind to the functional groups (e.g. carboxyl,

phenolic, and hydroxyl) on colloidal organic matter or humus-coated soil minerals (i.e. organo-inorgano complexes).

The soil capacity for retention of trace elements is best correlated with the surface area (amount and type of “clay”) and the soil metal oxide content (Adriano, 1986). The size definition for soil “clay” (i.e. soil separates less than 2 μm in equivalent diameter) inherently classifies most clay particles as colloids (< 1 μm diameter). Colloids are highly charged inorganic or organic materials with characteristically high surface area. Soil colloids represent the most chemically active portion of soil and provide the source of charge for nutrient retention (i.e. ion exchange). In general, the higher the cation exchange capacity (CEC) of a soil, the greater the potential of the soil to retain nutrient and metal cations; soil organic matter can be responsible for a high percentage of the measured CEC. Although anions are not retained on cation exchange sites, they can interact electrostatically (*outer-sphere complex*) with the positively-charged (anion exchange) sites on metal oxides, organic matter, or edge sites of phyllosilicate clay minerals. In addition to electrostatic interactions, metal(loid) anions and metal cations can form *inner-sphere complexes* with colloid surfaces.

Inner-sphere complexes are defined as covalent linkages between the adsorbed ion and the reactive surface, with no water of hydration between the adsorbed ion and the surface functional group (Sparks, 2003). Inner-sphere complex formation (chemisorption) proceeds via a ligand-exchange mechanism. Inner-sphere

complexes can be classified as monodentate, bidentate, tridentate, etc. depending on the number of bonds formed with the reactive surface. Bonding in multidentate complexes can be further classified as mononuclear or binuclear depending on the coordination of the adsorbate at the adsorptive surface; for the case of binuclear (bidentate) complex formation, the adsorbate enters into bridge coordination with functional groups of neighboring metal polyhedra that comprise the reactive surface. Several trace metals (including Co and Ni) and oxyanions (including phosphate, arsenate, and selenite) tend to chemisorb to metal oxide surfaces via a binuclear mechanism (McBride, 1994; Sparks, 2003). Sorption of metals and nutrient elements to soil colloids plays a vital role in determining their fate and transport in the “Critical Zone”.

1.4 Metalliferous Soils and Metallophytes

Metalliferous soils are prevalent in the environment, originating from both geogenic and anthropogenic activities. Natural inputs of trace metals result from windblown dust, volcanic eruptions, marine aerosols, and forest fires (Friedland, 1990). Metalliferous plant communities include flora naturally growing on serpentine soils (Ni-, Cr-, Mn-, Mg-, and Co-rich), seleniferous deposits (Se-rich soils), uraniferous deposits (U-rich soils), and calamine soils (Zn- and Cd-rich) (Brooks, 1983). Plants with the ability to colonize metal-enriched soils and metal-ore outcrops (*metallophytes*) have been noted for centuries (Thalius 1588; Caesalpino 1583), and

their early use as geobotanical indicators for mineral prospecting (Tkalic 1938; Brundin 1939; Cannon 1960) inspired detailed catalogues of the species that concentrate metals (*accumulators*; Brooks et al., 1977a). Many of these plants are now classified as *hyperaccumulators* if they exceed a benchmark concentration for a specific metal on a dry weight basis (e.g. 1,000 $\mu\text{g g}^{-1}$ for Ni, Co, Cu; 10,000 $\mu\text{g g}^{-1}$ for Zn; 100 $\mu\text{g g}^{-1}$ for Cd) (McGrath et al., 2002). An additional criterion used to classify metal hyperaccumulators is a shoot-to-root metal concentration ratio greater than unity (Baker 1981).

Hyperaccumulation of Ni was first reported for a specimen of *Alyssum bertolonii* Desv. with 1.1 % Ni (Minguzzi and Vergnano, 1948) that was collected during a survey of serpentine flora near Firenze, Italia. A short time later, Doksopulo (1961) reported shoot Ni concentrations exceeding 10 % (on an ash weight basis) for *A. murale* Waldst. & Kit., clearly indicating hyperaccumulator status for this taxon. A third accumulator taxon (*A. serpyllifolium* Desv. ssp. *lusitanicum* T.R. Dudley & P. Silva) (Menezes de Sequeira, 1969) discovered within this genus was a subspecies of a widespread southwestern European and North African species that was confined to serpentine soils around northeastern Portugal (Morrison 1980).

Beginning in the mid-seventies, the list of hyperaccumulators grew rapidly with the discoveries of numerous other genera native to serpentine soils on several continents including Australia (plus New Caledonia), Africa, and Europe. R.R. Brooks and co-workers conducted the majority of pioneering research to identify metal

accumulators through large-scale surveys of metalliferous flora and analysis of metal concentrations in field (soils and plants) and herbarium specimens (Brooks et al., 1974; Brooks 1977; Brooks et al., 1977a,b,c; Wither and Brooks, 1977; Brooks and Radford, 1978; Jaffré et al., 1979a,b; Morrison, 1980; Reeves et al., 1981, 1983).

Recognizing the first three Ni hyperaccumulators discovered were all from the genus *Alyssum*, surveys were conducted to systematically identify and study metalliferous flora belonging to the *Brassicaceae* (formerly *Cruciferae*) (Vergnano et al., 1977; Brooks and Radford, 1978; Vergnano Gambi and Gabbrielli, 1979; Reeves et al., 1981, 1983); *Alyssum* and *Thlaspi* are members of this family. A vast amount of research on hyperaccumulators has been conducted over the past several decades since Chaney (1983) first proposed the idea of using plants to extract metals from anthropogenically-contaminated or metalliferous soils (phytoextraction) and recognized the opportunity to recover metals of economic value by ashing the shoot biomass (phytomining).

1.5 Phytoremediation: Metal Phytoextraction and Phytomining

Phytoremediation is the use of green plants to remove contaminants from the environment or to render them harmless. It offers an aesthetically pleasing, solar-driven, reduced-cost method for *in situ* environmental decontamination.

Phytoremediation has been applied to a range of contaminants in a variety of contaminated media. Plants have been used to recover metals from contaminated soils

(*phytoextraction/ phytomining*), degrade organic contaminants *in planta* and in the rhizosphere (*phytodegradation*), remove contaminants from industrial and domestic wastewater streams (*rhizofiltration*), transform toxic contaminants into less toxic forms (*phytovolatilization*), and to stabilize contaminants *in situ* (*phytostabilization*) via rhizosphere sequestration and minimization of erosion and infiltration.

Phytoextraction is the use of pollutant-accumulating plants to remove metals or salts from contaminated soils, sediments, or sludge by concentrating them in harvestable parts. Hyperaccumulator plants concentrate trace metals in their harvestable biomass, thereby offering a sustainable treatment option for metal-contaminated sites (phytoextraction) and an opportunity to mine metal-enriched soils (phytomining). Cultivating hyperaccumulator plants on metal-rich soil and ashing the harvestable biomass to produce ore (bio-ore) and energy (biofuel) can be an economically viable alternative for metal recovery (Chaney et al., 2004).

Two basic strategies of phytoextraction have been employed: (1) *induced* (chelate-assisted) phytoextraction using high-biomass plants and (2) *continuous* phytoextraction using natural metal-accumulator plants (Salt et al., 1998). *Induced phytoextraction* relies on high biomass ‘crop’ plants in combination with exogenous applications of metal-mobilizing agents (chelators) to increase metal phytoavailability, alter root membrane integrity, and deliver a pulse of metals into shoots at an optimal time for high yield. The feasibility of chelate-assisted phytoextraction has been challenged in recent years (Chaney et. al., 2007) due in part to the high costs

associated with chelating agents and concerns of contaminant leaching to groundwater due to their (over)application.

Continuous phytoextraction relies on accumulator plants with the ability to concentrate metals in shoot tissue to abnormal levels and to accumulate them over a complete growth cycle. This degree of metal homeostasis is epitomized by the metal hyperaccumulator plants native to metalliferous soils. Specialized genetic and physiological processes allow these accumulator plants to absorb, translocate, compartmentalize, and tolerate high levels of metals *in planta*. Inherent disadvantages of using metal hyperaccumulators for continuous phytoextraction are their relatively low biomass, slow growth rates, and metal specificity (Salt et al., 1998). However, a mechanistic understanding of the physiological and biochemical processes underlying hyperaccumulation and (hyper)tolerance in metal hyperaccumulators will ultimately lead to enhanced phytoextraction through breeding programs and/or transgenic developments.

Several rate-limiting steps can be considered in the metal phytoextraction/ phytomining process: 1) metal acquisition from soil, 2) radial transport and xylem loading of metals into the root vasculature, and 3) metal sequestration in shoot tissues. The developing picture of metal homeostasis in hyperaccumulators suggests that accumulated metals can be sequestered in leaves as quickly as they can be loaded into the xylem parenchyma; likewise, metals can be loaded into the xylem as quickly as they can be transported across the plasma membrane of root epidermal cells. Thus, in

most cases, the kinetics for these active, carrier-mediated transport events is expected to be more rapid than the kinetics of metals release from soil and subsequent diffusion of the metal to the (rhizosphere) soil solution. Unfortunately, reliable methods to quantify the capacity of a 'bulk' soil to buffer changes in the 'bulk' concentration of a dissolved metal (i.e. soil metal buffer capacity) are currently lacking; however, several techniques developed in recent years (e.g. isotope exchange kinetics (IEK) and metal biosensor bacteria) show promise. Any influence plants may have on soil metal buffer capacity would most likely be observed as root-induced changes in metal speciation or bioavailability at the root-microbe-mineral-H₂O interface (rhizosphere).

1.6 Rhizosphere: Root-Microbe-Mineral-H₂O Interface

1.6.1 Rhizosphere Processes

The rhizosphere is a complex microenvironment consisting of the few millimeters of soil in the immediate vicinity of plant roots, which is directly influenced by root activity and associated soil microorganisms. The rhizosphere can be functionally defined as a highly dynamic, solar/ plant-driven microenvironment characterized by interactions between root processes and the dynamics of the associated microbial population ([Lombi et al., 2001](#)). The characteristics of the rhizosphere are modified by plants through root exudation, absorption of nutrients and contaminants, and root growth. Chemical changes in the rhizosphere are closely linked with plant nutritional status. The primary root-induced chemical modifications

influencing nutrient/ metal acquisition include: 1) pH fluctuations (e.g. response to N source or to a deficiency of P or Fe), 2) exudation of low molecular weight organic acids (LMWOA), 3) secretion of enzymes (e.g. phosphatases) and other biomolecules, 4) fluctuations in redox potential (E_h), and 5) perturbation of solid-solution equilibria (Gregory and Hinsinger, 1999) either by the creation of chemical gradients between bulk solution and roots (due to the removal of dissolved species from solution) or by a reduction of the free ion activity in solution via complex formation with organic or inorganic ligands released by roots (or associated microorganisms).

In general, these root-induced chemical perturbations act to increase the bioavailability of elements in the root zone above those levels in bulk soil. Naturally, one might hypothesize one or more of these processes were adapted by accumulator plants to achieve hyperaccumulation; however, it is clear these processes are not unique to hyperaccumulators whereas constitutive up-regulation of trans-membrane element transporters is a key trait for hyperaccumulation (Pence et al., 2000; Assunção et al., 2001; Bernard et al., 2004; Hanikenne et al. 2008; Chaney et al., 2007). Root-induced perturbations in the hyperaccumulator rhizosphere play an indirect role in nutrient/ metal acquisition by influencing the lability of metal pools in the soil adjacent to roots (i.e. 'rhizosphere effect on phytoavailability').

1.6.2 Nutrient Acquisition and Phytoavailability

Root-induced fluctuations in pH (via enhanced excretion of protons) or redox potential (via release of reducing compounds) can assist plants with acquisition

of sparingly-soluble nutrients (e.g. Fe and Mn). Additionally, some plants release enzymes to acquire nutrients from sparingly-soluble sources. For example, roots can secrete phosphatases capable of hydrolyzing a wide range of organic P-containing substances (Kochian, 2000). Perturbation of solid/ solution equilibria via root activity can be an important nutrient acquisition mechanism particularly for immobile nutrients (e.g. trace metals). Depletion zones for the relatively immobile elements in soil develop quickly around roots and root hairs, and plants must rely on diffusion of soluble species along chemical gradients to supply nutrients to roots. However, slow diffusion kinetics result for charged species in heterogeneous soils due to readsorption onto soil surfaces and to the tortuosity of flow paths.

Exudation of compounds by roots influences metal solubility and uptake through indirect effects on microbial activity, physical properties of the soil, and root-growth dynamics, and by direct effects through complexation, precipitation and oxidation-reduction reactions, and acidification (Uren and Reisenauer, 1988; Laurie and Manthey, 1994; McLaughlin et al., 1998). Root exudates include a wide variety of compounds that may either leak passively from epidermal cells in response to concentration gradients (diffusates, e.g. sugars, organic acids, amino acids, inorganic ions, oxygen), be actively excreted to facilitate internal metabolism (excretions, e.g. bicarbonate ions, protons, electrons, carbon dioxide), or be actively secreted to facilitate external processes (secretions, e.g. mucilage, allelopathic compounds, siderophores) (Uren and Reisenauer, 1988; Marschner, 1995).

A general role of root exudates in nutrient acquisition has been thoroughly evaluated (Uren and Reisenauer, 1988; Jones and Darrah, 1994; Jones et al., 1994; Marschner, 1995; Hinsinger 1998; Jones, 1998) and root-induced chemical modifications in the rhizosphere have been investigated extensively for P nutrition (Boland et al., 1994,1997; Neumann and Römheld, 1999; Zhang et al., 1997; Morel and Hinsinger, 1999), Fe deficiency (Chaney and Bell, 1987, Takagi et al., 1988; Marschner and Römheld, 1994; Jones et al., 1996; Bertrand and Hinsinger, 1998), and Al toxicity (Hue et al., 1986; Miyasaka et al., 1991; Delhaize et al., 1993; Kochian, 1995; Ryan et al., 1995; Pellet et al., 1996).

Evidence for root-induced mineral weathering has been provided for a variety of plant species and demonstrated with various primary and secondary minerals (Hinsinger and Jaillard, 1993; Hinsinger and Gilkes, 1997; Hinsinger et al., 2001; Gommers et al. 2005 and Thiry et al. 2005) as well as sequestered (sorbed or occluded) species (Parfitt, 1979; Hinsinger et al., 1992; Guzman et al., 1994; Hinsinger and Gilkes, 1995,1996,1997; Geelhoed et al., 1997; Bertrand et al., 1999). Gommers et al. (2005) and Thiry et al. (2005) recently investigated root-induced weathering of mica by *Salix viminalis* and observed transformation to vermiculite in the rhizosphere. Mineral stability influenced the degree of mineral weathering with greater transformation observed for trioctahedral micas than for dioctahedral mica (phlogopite > biotite > muscovite). Le Chatelier's principle partially explains the increased mineral weathering in the rhizosphere; plants are continually removing

reaction products that are linked to the 'equilibrium' between solid and solution (driving the reaction to the right).

Low molecular weight organic acids (LMWOAs) are common compounds in root exudates, and the most prevalent LMWOAs in the soil system are those participating in the tricarboxylic acid cycle (Krebs cycle), including *citrate*, *fumarate*, *malate*, *maleate*, *malonate*, *oxalate* and *succinate*. The amount and composition of exudates released into the rhizosphere are highly variable and dependent on plant species, variety, age, and physiochemical environment, including plant nutritional status and substrate mechanical impedance (Marschner et al., 1987; Jones 1998). Concentrations of major LMWOAs in bulk soil solution reported in the literature range from 0.1 to 100 $\mu\text{mol L}^{-1}$, although much higher concentrations are found in localized zones of intense biological activity (e.g. rhizosphere) (Jones 1998). For example, concentrations exceeding 4 mmol L^{-1} have been determined in soil solution of the proteoid root rhizosphere of white lupin (Dinkelaker et al., 1989; Braum and Helmke, 1995). LMWOAs are produced continuously in soils through microbial activity, decomposition processes and root exudation, but are considerably short-lived in solution due to complex formation, sorption to soil constituents, and microbial degradation. However, unlike neutral exudate components (e.g. glucose), the biodegradation of LMWOAs is highly dependent on sorption to soil surfaces (i.e. minimal biodegradation when sorbed to Fe and Al (hydr)oxides) and the formation of metal-LMWOA complexes, both cause a marked inhibition on biodegradation.

Organic acids in root exudates are able to mobilize P (and other sorbates) by ligand exchange, dissolution, and occupation of 'specific adsorption' sites (Neumann and Römheld, 1999). Many of these organic ligands (e.g. citrate and malate) can complex with metal ions to form a chelate. The chelated metal is relatively stable in solution and can migrate convectively with mass flow (toward plant roots) or follow a diffusion gradient. Even when these organic ligands do not directly complex with the metal contaminant, they can interact with functional groups on Fe, Mn, or Al surfaces (metal-oxide coatings) and release surface-bound metal sorbates into solution. Several organic acids (e.g. malate) can scavenge protons or supply electrons for reduction of metals (e.g. Mn) in the rhizosphere; the combination of reduction and complexation reactions may explain the huge Mn accumulation by plants known to exude high amounts of organic acids (e.g. white lupin). In addition to root exudates, the soil microbial biomass releases LMWOAs potentially involved in metal mobilization. One widespread case involves symbiotic fungi (*mycorrhizae*), which secrete organic acids (e.g. oxalate) to release P (and other sorbates) from Fe and Al complexes (Barber, 1995).

Overall, LMWOAs have been implicated in many soil processes, including mobilization and uptake of nutrients (e.g. P and micronutrients) and potentially toxic elements (e.g. trace metals) by plants and microorganisms (possibly as metal-ligand complexes); detoxification of metals (e.g. Al, Cd) by plants and microorganisms; microbe proliferation in the rhizosphere; and solute transport in the

soil profile (Marschner et al.,1987; Pohlman and McColl, 1988; Fox et al., 1990; Jones 1998). Direct *in vivo* mechanistic evidences to support the effects attributed to LMWOAs are limited, and in many situations are a matter of speculation (Jones, 1998). However, new approaches permitting micro-scale chemical measurements should provide a better understanding for the roles of LMWOAs in physiochemical-biological interfacial interactions.

Despite a lack of *in vivo* evidence supporting the many potential functions of LMWOAs in the rhizosphere, extensive geochemical evidence exists regarding their interactions with other ligands and metal ions on mineral surfaces, their interactions with metal species in solution (metal-ligand complex formation), and their involvement in reductive- and ligand-promoted dissolution of metal oxides and clay minerals.

1.7 Trace Elements in Plants

Plant roots draw water from the surrounding soil, resulting in a convective transfer of solutes toward roots (mass flow). Depending on how this flux of solutes relates with root uptake from the soil solution, solutes may accumulate or be depleted in the rhizosphere. Sparingly-soluble phases in soils (e.g. metal-bearing solids) maintain low concentrations of dissolved species thus their solutes become depleted in the rhizosphere and mass flow represents only a small portion of the actual flux absorbed by roots. This is typically the case for P and K among major nutrients and a

majority of trace elements (Lombi et al., 2001). With respect to hyperaccumulator plants, which have a high density of trans-membrane element transporters on roots, the metal (or metals) it accumulates would be rapidly depleted from the rhizosphere soil solution. The depletion of soluble species near the root surface results in diffusion toward the root along the created gradient. According to Le Chatelier's principle, the consequence of down gradient ion movement would be an additional release of metals from the metal-bearing solids needed to restore the chemical activity of the species in solution (perturbation of reaction equilibria between solid and solution). By rapid uptake of dissolved metals ions, hyperaccumulator plants cause significant perturbations to solid-solution 'equilibria', creating conditions that favor dissolution of the metal-bearing solid phases and over time alter the pool of phytoavailable (bioavailable) metals in the rhizosphere microenvironment.

1.7.1 Short-distance Transport

Solutes in the soil solution move toward plant roots by mass flow or diffusion. Solutes in contact with the root rhizodermis can travel toward the root endodermis by means of an apoplastic or symplastic pathway (Figure 1.1). The apoplast consists of the apparent free space within the cell wall continuum. Apoplastic movement within the free space (water-filled intercellular spaces) of the root cortex is thermodynamically passive.

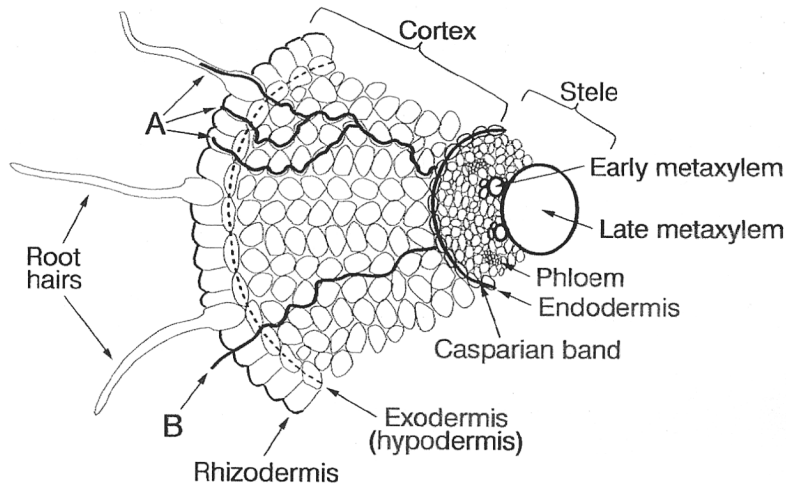


Figure 1.1. Dicot root cross-section displaying symplastic (A) and apoplastic (B) solute pathways (adapted from Marschner, 1995).

The main barrier to solute flux in the apoplast of roots occurs at the root endodermis (i.e. innermost layer of cells of the cortex). In the walls of the endodermis, the Casparian band (cells with hydrophobic incrustations of suberin) constitutes an effective barrier against passive solute movement. Therefore, the inner boundary of the apoplastic pathway occurs at the Casparian band (Barber, 1995). Solutes must enter the cytoplasm of root cells (i.e. cross the root cell plasma membrane) by means of membrane transport systems and pass from cell to cell via plasmodesmata (symplastic pathway). After crossing the Casparian band, solutes may re-enter the apoplast or travel symplastically to the vascular tissues where they are unloaded from xylem parenchyma into xylem vessels for long-distance transport to the stems and leaves. Solutes translocated to shoot xylem can be returned to the root via phloem transport.

The symplastic pathway may begin at the rhizodermis and root hairs, the exodermis, or the endodermis. Except in the case of young, developing roots lacking a fully developed Casparian band, membrane transport somewhere along the solute pathway to the xylem seems unavoidable. Recent advances in biotechnology and plant molecular biology have contributed significantly to elucidating the mechanisms involved in membrane transport.

1.7.2 Membrane Transport

Plants have evolved numerous proteins (*pumps, carriers, and channels*) to facilitate the transport of minerals, sugars, metabolites, and other compounds through the limiting membranes of cells and organelles. Transport is made possible by membrane-spanning proteins within the lipid bilayer. Similar to enzymes, transport systems exhibit some degree of substrate-specificity and may work to lower the activation energy required for transport. Membrane transport facilitates a wide range of essential processes, including turgor generation, nutrient absorption, waste product excretion, metabolite distribution and compartmentalization, and signal transduction (Raven et al., 1992).

Movement of a solute across a membrane is a function of the overall thermodynamic gradient established between the external and internal media. The energetic gradient for an uncharged solute is determined solely by the chemical potential difference (i.e. concentration gradient between internal and external media). However, the energetic gradient for a charged (ionic) solute is a function of the

chemical potential difference of the solute and the electrical potential difference of the aqueous media (*membrane potential*). A membrane potential results from an imbalance in the number of cations and anions across a membrane.

Membrane potentials arise across biological membranes in several ways. First, most cytosolic proteins bear a negative charge at a physiological pH of 7.5. This excess of negatively charged amino acid residues is countered largely by K^+ ions (Sanders and Bethke, 2000). Since the external concentration of K^+ is invariably less than the cytosolic concentration, the tendency of K^+ to leak from the cell generates an excess of negative charge inside. This combination of fixed, negative charges and mobile, positive charges is known as a Donnan potential. The other major factor exerting an influence on membrane potential is the transport of H^+ out of the cytosol. Pumping H^+ from the cytosol is achieved by metabolically-coupled pumps (usually ATPases).

Pumps catalyze transport of ions or complex organic molecules against their thermodynamic gradients (electrochemical potentials). Pumps are driven by ATP hydrolysis and generate the H^+ -electrochemical potential (or proton motive force (pmf)) across cell membranes by removing H^+ from the cytosol. The pmf generated by plasma membrane H^+ -pumping ATPase powers transport through a variety of carriers and influences ion channel activity through its impact on membrane potential. At steady state, continuing operation of electrogenic pumps requires compensating movement of countercharges through other transport systems (Figure 1.2).

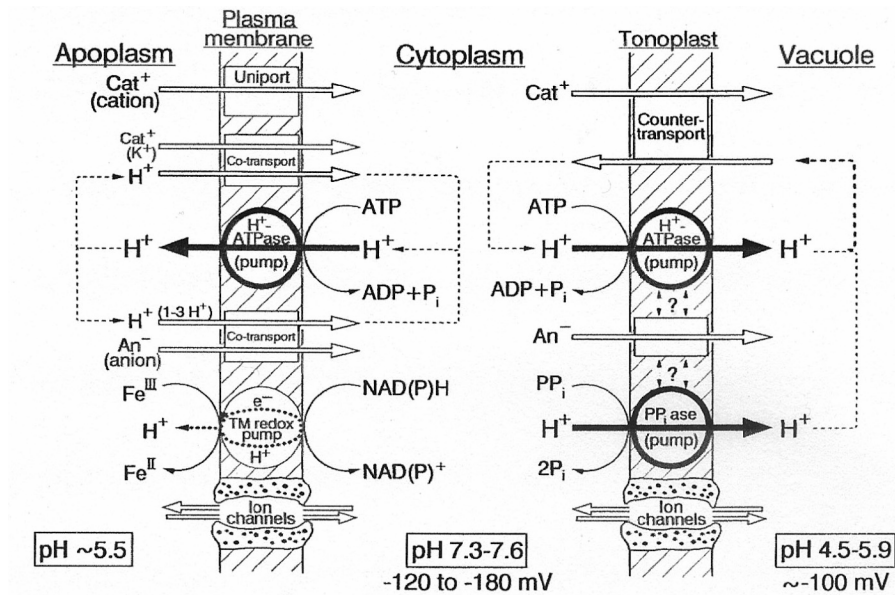


Figure 1.2. Conceptual model of membrane transport systems involved with solute absorption (adapted from Marschner, 1995).

Transport systems coupling the “downhill” flow of H^+ to the “uphill” flow of inorganic ions and solutes are called carriers. Carriers transport a vast array of ions and solutes (e.g. ions, sugars, and amino acids). The principle inorganic nutrients (including NH_4^+ , NO_3^- , $H_2PO_4^-$, K^+ , and SO_4^{2-}) are transported into cells by plasma membrane carriers (Sanders and Bethke, 2000). The transport of solutes by carriers is coupled with pmf-driven H^+ transport (pumps). As a result, the carrier substrate is translocated against its own electrochemical potential. The prominence of H^+ -coupled transport systems in plant cell plasma membranes illustrates that organisms living in relatively dilute media depend on energized solute transport (*active transport*). At the

plasma membrane, carriers are central to nutrient absorption from the soil and play fundamental roles in the mobilization and storage of metabolites.

Ion channels are ubiquitous in biological membranes. In contrast to pumps and carriers, the pmf plays no direct role in driving the passage of ions through channels. Ion flow through channels is passive. Thus, in contrast to pumps or ion-coupled carrier activity, the direction of flow of a particular ion through a channel is dictated simply by the electrochemical potential gradient for the ion. Most classes of ion channels in plant cells usually discriminate in favor of either cations or anions. Cation channels can be further subdivided into those selecting K^+ over other monovalent cations, those relatively non-selective among monovalent cations, and those selective for Ca^{2+} (Sanders and Bethke, 2000). Most plasma membrane anion channels allow permeation of a wide range of anions (including Cl^- , NO_3^- , $H_2PO_4^{2-}$, and organic acid anions). An even less selective channel has been observed in the plasma membrane of xylem parenchyma cells, and is almost as permeable to anions as it is to cations. In contrast to pumps and carriers, channels do not undergo conformational changes during transport and can catalyze ion fluxes of 10^6 to 10^8 molecules s^{-1} ; the turnover rates for pumps (on the order of 10^2 molecules s^{-1}) and carriers (on the order of 10^3 molecules s^{-1}) are correspondingly slower (Sanders and Bethke, 2000).

The transport of K^+ (mobile within cells, tissues, and whole plants) has been studied most extensively. Current evidence suggests two mechanisms operate to

mediate K^+ uptake. At low external concentrations, root cells often absorb K^+ against the electrochemical gradient for the cation. Under these circumstances, absorption must be mediated by a mechanism of active transport (either an ATP-driven ion pump or a secondarily active carrier). An alternative mechanism operating at higher external concentrations of K^+ is passive, and likely involves K^+ channels (Ravin et al., 1992). Similarly, root P absorption along with absorption of other important mineral anions (e.g. NO_3^{1-} and SO_4^{2-}) is mediated by H^+ -coupled cotransporters at low external concentrations, but can be mediated by channels at higher external concentrations.

1.7.3 Metal Homeostasis in Hyperaccumulators

Metals are transported across biological membranes as free ions (pumps or carriers), but could be absorbed by roots as low-molecular weight metal-ligand complexes (membrane channels). Metal transport from the root free space to the xylem vessels presumably involves two or more active, carrier-mediated transport events: (a) uptake at the plasma membrane of the root epidermal cells and (b) secretion into the vessels at the plasma membrane of the parenchyma cells bordering the xylem.

Enhanced metal uptake at the plasma membrane of root epidermal cells is possible due to the constitutive up-regulation of trans-membrane element transporters on hyperaccumulator roots (i.e. overexpression of the gene(s) which encode for a specific metal transporter). Lasat et al. (1996) reported Zn influx into the root cells of *Thalpi caerulescens* occurred at a much higher rate than for *T. arvensis* (non-accumulator). Furthermore, the gene encoding for Zn transporter (ZNT1) was found

to be highly expressed in the roots of *T. caerulea* even when plants were supplied with a high concentration of Zn, whereas ZNT1 was expressed in *T. arvense* roots only when Zn was deficient (Pence et al., 2000). Without an efficient route of entry into xylem vessels, metals would accumulate in the root symplasm, becoming sequestered in root epidermal cells/ cell vacuoles. Therefore, another carrier-mediated transport event is needed for xylem loading.

Transport of accumulated metals from the root symplasm into the xylem (i.e. xylem loading) apparently involves up-regulation of transporters in the plasma membrane of the parenchyma cells bordering the xylem vessels. For instance, HMA4 is among a large number of genes more highly expressed in *Arabidopsis halleri* (hyperaccumulator) than in *A. thaliana* (non-accumulator) and it encodes a plasma membrane protein of the 1_B family of transition metal pumps (Hanikenne et al. 2008). High HMA4 transcript levels are required for highly-efficient root-to-shoot Zn flux and for Zn hyperaccumulation in the shoots of *A. halleri*. Additionally, HMA4 alters the distribution of Zn within the roots of *A. halleri*; silencing of (A.h.)HMA4 impairs the release of Zn from the root symplasm into the apoplastic xylem vessels. Furthermore, relative transcript levels of IRT3 and ZIP4 (encode membrane transporters in the same family of proteins implicated in the cellular uptake of Zn) are correlated with HMA4 transcript levels, thus the high expression of these genes in roots of wild-type *A. halleri* appears to be a secondary consequence of increased HMA4 activity (Hanikenne et al. 2008). Therefore, transition metal transporters

localized in the plasma membrane of the parenchyma cells bordering the xylem vessels function to remove excess metals from the root symplasm, preventing the sequestration of metals in root cells and enhancing root-to-shoot transport. Expression of HMA4 is also observed in the cambium of leaves, which is consistent with a possible role of HMA4 in metal distribution within the leaf blade and the exclusion of metals from specific cell types (Hanikenne et al. 2008). Metal sensitivity resulting from the high HMA4-dependent metal flux into shoots of *A. thaliana* expressing (A.h.)HMA4 indicates that additional genes are needed to attain metal (hyper)tolerance.

Gene(s) encoding for transition metal transporters in the tonoplast (vacuolar membrane) of leaf epidermal cells or in the plasma membranes of specific cell types in plant shoots may be largely responsible for metal (hyper)tolerance in hyperaccumulators, potentially regulating the activity of the genes encoding for the metal transporters in the plasma membrane of the root epidermal cells (e.g. IRT3 or ZIP4) or in the plasma membrane of the parenchyma cells bordering the xylem vessels (e.g. HMA4). A more complete picture of metal hyperaccumulation and (hyper)tolerance mechanisms will evolve when the gene(s) that encode for metal transporters in the membranes of specific leaf cells (e.g. epidermal) and organelles (e.g. vacuoles) are discovered and characterized.

Metal tolerance in higher plants has been associated with reduced membrane transport, metal binding to cell walls, metal-tolerant enzymes, chelation of

metals by organic or inorganic ligands, and/or compartmentalization in the vacuole

(Figure 1.3).

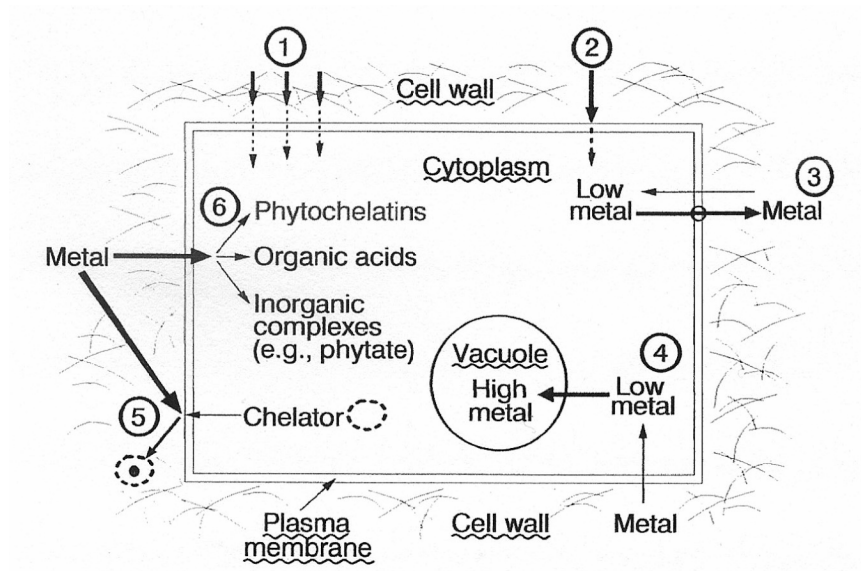


Figure 1.3. Possible mechanisms of metal tolerance (adapted from Marschner, 1995).

Note: (1) Binding to cell wall, (2) Restricted influx through plasma membrane, (3) Active efflux, (4) Compartmentalization in vacuole, (5) Chelation at the cell wall-plasma membrane interface, (6) Chelation in the cytoplasm.

Accumulator plants attain (hyper)tolerance to metals through “chemical binding” (*detoxification*) and “intracellular sequestration” (*compartmentalization*) (Brooks et al., 1977; Baker 1981; Küpper & Kroneck 2005); an exocellular sequestration mechanism for Co has been observed with Ni hyperaccumulator species of *Alyssum* (Tappero et al., 2007). Free metal ions are the most cytotoxic form of trace metals (Schat et al., 2000). Hyperaccumulators rely on common intercellular ligands (e.g. Krebs’ acids) for detoxification of free metal ions. Vascular and cellular fluids contain a complex mixture of inorganic ions (e.g. SO_4^{2-}) as well as organic (e.g. citric;

malic) and amino acids (e.g. histidine) that can bind metal cations, thus a large proportion of metals absorbed by hyperaccumulator roots do not exist as free metal ions *in planta*.

Tolerance pathways are typically metal specific (Schat et al., 2000; Walker & Bernal, 2004), relying on unique physiological processes to mediate metal transport across particular cell membranes (e.g. vacuolar tonoplast). Leaf cells play a crucial role in metal (hyper)tolerance for the vast majority of hyperaccumulators; metals are compartmentalized in the epidermal cell vacuoles where they do not disrupt important metabolic functions (Küpper et al., 2001; Küpper & Kroneck 2005). Metals are generally absent from guard and subsidiary cells within the stomatal complex, but metal accumulation has been observed within mesophyll cells bordering the leaf epidermis and at the base of leaf trichomes.

1.8 Research Questions and Objectives:

Information regarding metal speciation, localization (e.g. tissue, cells, and organelles) and elemental associations in accumulator plants is crucial to unraveling the mechanisms of hyperaccumulation and (hyper)tolerance. Recent advances in micro-analytical techniques for *in situ* chemical measurements (e.g. synchrotron-based spectromicroscopic methods) have created new opportunities to relate existing knowledge of the biochemical processes regulating plant metal homeostasis with submicroscopic spatial and chemical information concerning the form of metals *in planta* (molecular speciation). A more comprehensive understanding of the

mechanisms involved in metal uptake by accumulator plants will lead to enhanced phytoextraction through breeding programs or transgenic developments as well as provide a greater potential to produce nutrient-fortified foods and improve crop production on marginal (nutrient-poor) soils.

The general research objective was to use a multi-technique, multi-scale experimental approach to extend our understanding of the mechanisms of *metal acquisition, accumulation, and (hyper)tolerance* in the commercial hyperaccumulator *Alyssum murale* (Waldst. & Kit.) by linking *in situ* spectromicroscopic information and macroscopic observations with existing knowledge about the physiological processes controlling plant metal homeostasis.

The research project components can be summarized as follow:

1. Elucidate the effect of co-contaminant metals (Co and Zn) on Ni phytoextraction and localization in the Ni/ Co hyperaccumulator *Alyssum murale*;

Hyperaccumulator plants used to extract Ni from Ni-rich soil (e.g. industrial brownfields or serpentine soils) must be tolerant of co-contaminants. Two categories of soil suitable for Ni phytomining include serpentine soils (naturally enriched with Ni) and industrially-contaminated soils. Serpentine soils develop from ultramafic parent material and contain significant quantities of Ni, Co, Cr, Mn, Fe, and Zn. The Ni : Co ratios in serpentine soils typically range from five to ten. Anthropogenic metal inputs generally involve discharge of a mixed-element waste

stream. For instance, emissions from Ni smelters are typically enriched with other trace metals from the ore (e.g. Co, Cu, Pb, and Zn). Hyperaccumulator plants used to extract Ni from metal-enriched soils must be tolerant of co-contaminants. Therefore, the effects of metal co-contaminants on the physiology and biochemistry of hyperaccumulators, and ultimately on the efficiency of metal phytoextraction, is of concern for metal recovery efforts.

The objectives of this study were to evaluate the effect of co-contaminant metals (Co and Zn) on Ni accumulation by *Alyssum murale*, observe potential metal interactions in plants, and investigate the impact of simultaneous hyperaccumulation on metal localization. *Alyssum* plants in perlite culture were contained in ebb and flow cultivation devices and exposed (4 weeks) to Ni-enriched nutrient solutions containing basal or elevated concentrations (50 μM) of Co or Zn (Ni, Ni + Co, Ni + Zn, Ni + Co + Zn). Metal localization and elemental associations in plants were investigated with synchrotron X-ray fluorescence (SXRF) and tomography (CMT).

2. Determine *in planta* Co speciation in *A. murale* and identify metal detoxification and sequestration mechanisms;

Previous work with Ni hyperaccumulators has demonstrated the importance of organic and amino acids in plant metal homeostasis. For example, Ni absorbed by *Alyssum* roots is complexed by intercellular ligands (e.g. free histidine) (Krämer et al., 1996). Metal-ligand complex formation plays a role in radial transport

and xylem loading (Kerkeb and Krämer, 2003). Metals loaded into the xylem are complexed by ligands in the vascular system (e.g. organic acids produced by Krebs cycle), which function in metal detoxification and long distance transport to shoots. Nickel translocated to shoots of *Alyssum* is unloaded from the xylem, redistributed to epidermal tissue, transported across the tonoplast membrane, and sequestered as a metal-ligand complex in cell vacuoles. Vacuolar sequestration (in epidermal cells) provides a permanent sink for metal storage in plants isolated from photosynthetically active tissues (Krämer et al., 2000), and has been recognized as a primary feature of the Ni tolerance mechanism. Several *Alyssum* species have the ability to accumulate cobalt, but little is known about the ligands involved in Co detoxification, transport, and sequestration (i.e. Co tolerance and accumulation mechanisms).

The objectives of this study were to identify the Co species sequestered at leaf tips/ margins of *A. murale* and to determine the *in planta* speciation of Co using a multi-technique, multi-scale experimental design including metal accumulation studies, xylem fluid extraction and analysis (liquid chromatography), and molecular-scale spectroscopic investigations of accumulated cobalt (X-ray and electron microscopies).

1.9 References

- Adriano, D.C. 1986. Trace elements in the terrestrial environment. pp. 1-18. Springer-Verlag Inc., New York, NY.
- Antonovics, J., A.D. Bradshaw, and R.G. Turner. 1971. Heavy metal tolerance in plants. *Adv. Ecol. Res.* 7:1-85.
- Assunção, A.G.L., P.D. Martins, S. Folter, R. Vooijs, H. Schat, and M.G.M. Aarts. 2001. Elevated expression of metal transporter genes in three accessions of the metal hyperaccumulator *Thlaspi caerulescens*. *Plant Cell Environ.* 224:217-226.
- Baker, A.J.M. 1981. Accumulators and excluders - strategies in the response of plants to heavy metals. *Journal of Plant Nutrition* 3:643-654.
- Barber, S.A. 1995. Soil Nutrient Bioavailability: A mechanistic approach. John Wiley & Sons, New York, NY.
- Bernard, C., N. Roosens, P. Czernic, M. Lebrun, and N. Verbruggen. 2004. A novel CPx-ATPase from the cadmium hyperaccumulator *Thlaspi caerulescens*. *FEBS Lett.* 569:140-148.
- Bertrand, I. and P. Hinsinger. 1998. Dissolution of an iron oxyhydroxide in the rhizosphere of various crop species. *J. Plant. Nutr.* 23:1559-1577.
- Bertrand, I., P. Hinsinger, B. Jaillard, and J.C. Arvieu. 1999. Dynamics of phosphorus in the rhizosphere of maize and rape grown on synthetic, phosphated calcite and goethite. *Plant and Soil* 211:111-119.
- Boland, N.S., R. Naidu, S. Mahimairaja, and S. Baskaran. 1994. Influence of low molecular weight organic acids on the solubilization of phosphates. *Biol. Fert. Soils.* 18:311-319.
- Boland, N.S., J. Elliot, and P.E.H. Gregg. 1997. Enhanced dissolution of phosphate rocks in the rhizosphere. *Biol. Fert. Soils.* 24:169-174.
- Braum, S.M. and P.A. Helmke. 1995. White lupin utilizes soil phosphorus that is unavailable to soybean. *Plant Soil* 176:95-100.
- Brooks, R.R. 1977. Copper and cobalt uptake by *Haumaniastrum* species. *Plant Soil* 48:541-544.

- Brooks, R.R. 1983. Biological methods of prospecting for minerals. John Wiley & Sons, Inc., New York, NY.
- Brooks, R.R. and C.C. Radford. 1978. Nickel accumulation by European species of the genus *Alyssum*. Proc. R. Soc. Lond. B. 200:217-224.
- Brooks, R.R. and E.D. Wither. 1977. Nickel accumulation by *Rinorea bengalensis* (Wall). J. Geochem. Explor. 7:295-300.
- Brooks, R.R., J.A. McCleave, and E.K. Schofield. 1977b. Cobalt and nickel uptake by the *Nyssaceae*. Taxon 26:197-204.
- Brooks, R.R., J.A. McCleave, and F. Malaisse. 1977c. Copper and cobalt in African species of *Crotalaria* L. Proc. R. Soc. Lond. B. 197:231-236.
- Brooks, R.R., J. Lee, R.D. Reeves, and T. Jaffré. 1977a. Detection of nickeliferous rocks by analysis of herbarium specimens of indicator plants. Journal of Geochemical Exploration 7:49-57.
- Brooks, R.R., J. Lee, and T. Jaffré. 1974. Some New Zealand and New Caledonian plant accumulators of nickel. J. Ecol. 62:493-499.
- Brown, G.E. Jr., A.L. Foster, and J.D. Ostergren. 1999. Mineral surfaces and bioavailability of heavy metals: A molecular-scale perspective. Proceedings of the National Academy of Sciences 96:3388-3395.
- Brundin N.H. 1939. Method of locating metals and minerals in the ground. U.S. Patent 2158980.
- Caesalpino A. 1583. De plantis libri XVI: 369. Marescotti, Firenze. (Quoted in Proctor and Woodell, 1975).
- Cannon, H.L. 1960. Botanical prospecting for ore deposits. Science 132:591-598.
- Chaney RL. 1983. Plant uptake of inorganic waste constituents. In: Parr JF, Marsh PB, Kla JM, eds. *Land treatment of hazardous wastes*. Park Ridge, USA: Noyes Data Corp., 50-76.
- Chaney R.L., J.S. Angle, and Y.M. Li. 2004. Method for phytomining of nickel, cobalt, and other metals from soil. US patent 5,944,872.

Chaney, R.L. and P.F. Bell. 1987. Complexity of iron nutrition: Lessons for plant-soil interaction research. *J. Plant Nutr.* 10:963-994.

Chaney, R.L., J.S. Angle, C.L. Broadhurst, C.A. Peters, R.V. Tappero, and D.L. Sparks. 2007. Improved understanding of hyperaccumulation yields commercial phytoextraction and phytomining technologies. *J. Environmental Quality* 36:1429-1443.

Delhaize, E., P.R. Ryan, and P.J. Randall. 1993. Aluminum tolerance in wheat (*Triticum aestivum* L.) II. Aluminum-stimulated excretion of malic acid from root apices. *Plant Physiol.* 103:695-702.

Dinkelaker, B., V. Römheld, and H. Marschner. 1989. Citric acid excretion and precipitation of calcium citrate in the rhizosphere of white lupin (*Lupinus albus* L.). *Plant Cell Environ.* 12:285-292.

Doksopulo, E.P. 1961. Nickel in rocks, soils, waters, and plants adjacent to the talc deposits of the Chorchanskaya Group. Thesis, Izdatel vo Tbiliskovo Univ.

Fox, T.R., N.B. Comerford, and W.W. McFee. 1990. Phosphorus and aluminum release from a spodic horizon mediated by organic acids. *Soil Sci. Soc. Am. J.* 54:1763-1767.

Friedland, A.J. 1990. The movement of metals through soils and ecosystems. pp. 8-17. *In: A. J. Shaw (ed.) Heavy metal tolerance in plants: Evolutionary aspects.* CRC Press, Boca Raton, FL.

Geelhoed, J.S., G.R. Findenegg, and W.H. Van Riemsdijk. 1997. Availability to plants of phosphate adsorbed on goethite: experiment and simulation. *Eur. J. Soil Sci.* 48:473-481.

Gommers, A., Y. Thiry, and B. Delvaux. 2005. Rhizospheric mobilization and plant uptake of radiocesium from weathered micas: I. Influence of potassium depletion. *J. Environ. Qual.* 34:2167-2173.

Gregory, P.J. and P. Hinsinger. 1999. New approaches to studying chemical and physical changes in the rhizosphere: an overview. *Plant and Soil* 211:1-9.

Guzman, G., E. Alcantara, V. Barron, and J. Torrent. 1994. Phytoavailability of phosphate adsorbed on ferrihydrite, hematite, and goethite. *Plant and Soil* 159:219-225.

- Hanikenne, M., I.N. Talke, M.J. Haydon, C. Lanz, A. Nolte, P. Motte, J. Kroymann, D. Weigel, and U. Krämer. 2008. Evolution of metal hyperaccumulation required cis-regulatory changes and triplication of HMA4. *Nature* 453:391-396.
- Hinsinger, P. 1998. How do plant roots acquire mineral nutrients? Chemical processes involved in the rhizosphere. *Adv. Agron.* 64:225-265.
- Hinsinger, P. and B. Jaillard. 1993. Root induced release of interlayer potassium and vermiculitization of phlogopite as related to potassium in the rhizosphere of ryegrass. *J. Soil Sci.* 44:525-534.
- Hinsinger, P. and R.J. Gilkes. 1995. Root-induced dissolution of a reactive phosphate rock in the rhizosphere of two lupin species grown in alkaline soil. *Aust. J Soil Res.* 33:477-489.
- Hinsinger, P. and R.J. Gilkes. 1996. Mobilization of phosphate from phosphate rock and alumina-sorbed phosphate by the roots of ryegrass and clover as related to rhizosphere pH. *Eur. J. Soil Sci.* 47:533-544.
- Hinsinger, P. and R.J. Gilkes. 1997. Dissolution of phosphate rock in the rhizosphere of five plant species grown in an acid, P-fixing mineral substrate. *Geoderma* 75:231-249.
- Hinsinger, P., O.N.F. Barro, M.F. Benedetti, Y. Noack, and G. Callot. 2001. Plant-induced weathering of a basaltic rock: experimental evidence. *Geochimica et Cosmochimica Acta* 65:137-152.
- Hinsinger, P., B. Jaillard, and J.E. Dufey. 1992. Rapid weathering of a trioctahedral mica by the roots of ryegrass. *Soil Sci. Soc. Amer. J.* 56:977-982.
- Huang, P.M. 2008. Impacts of Physiochemical-Biological Interactions on Metal and Metalloid Transformations in Soils: An Overview. pp. 3-52. *In: Violante, A., P.M. Huang, and G.M. Gadd (ed.) Biophysio-Chemical Processes of Heavy Metals and Metalloids in Soil Environments.* John Wiley & Sons, Inc. New York, NY.
- Hue, N.V., G.R. Craddock, and F. Adams. 1986. Effect of organic acids on aluminum toxicity in subsoils. *Soil Sci. Soc. Am. J.* 50:28-34.
- Jaffré, T., R.R. Brooks, and J.M. Trow. 1979a. Hyperaccumulation of nickel by *Geissois* species. *Plant Soil* 51:157-162.

- Jaffré, T., W.J. Kersten, R.R. Brooks, and R.D. Reeves. 1979b. Nickel uptake by the *Flacourtiaceae* of New Caledonia. *Proc. R. Soc. Lond. B* 205:385-394.
- Jones, D.L. 1998. Organic acids in the rhizosphere-a critical review. *Plant Soil* 205:25-44.
- Jones, D.L. and P.R. Darrah. 1994. Role of root derived organic acids in the mobilization of nutrients from the rhizosphere. *Plant Soil* 166:247-257.
- Jones, D.L., P.R. Darrah, and L.V. Kochian. 1996. Critical evaluation of organic acid mediated iron dissolution in the rhizosphere and its potential role in root iron uptake. *Plant Soil* 180:57-66.
- Juillot, F., G. Morin, P. Ildefonse, T.P. Trainor, M. Benedetti, G. Calas, and G.E. Brown. 2003. Occurrence of Zn/Al hydrotalcite in smelter-impacted soils from northern France: Evidence from EXAFS spectroscopy and chemical extractions. *Am. Mineral.* 88:509-526.
- Kerkeb, L. and U. Krämer. 2003. The role of free histidine in xylem loading of nickel in *Alyssum lesbiacum* and *Brassica juncea*. *Plant Physiology* 131: 716-724.
- Kochian, L.V. 1995. Cellular mechanisms of aluminum toxicity and resistance in plants. *Annu. Rev. Plant Physiol. Plant Mol. Biol.* 46:237-60.
- Kochian, L.V. 2000. Molecular physiology of mineral nutrient acquisition, transport, and utilization. pp. 1204-1249. *In: Buchanan, B.B., W. Gruissemann, and R. L. Jones (ed.) Biochemistry and molecular biology of plants. American Society of Plant Physiologists, Rockvill, MD.*
- Krämer, U., J.D. Cotter-Howells, J.M. Charnock, A.J.M Baker, and J.A.C. Smith. 1996. Free histidine as a metal chelator in plants that accumulate nickel. *Nature* 379:635-638.
- Krämer, U., I.J. Pickering, R.C. Prince, I. Raskin, and D.E. Salt. 2000. Subcellular localization and speciation of nickel in hyperaccumulator and non-accumulator *Thlaspi* species. *Plant Physiology* 122:1343-1354.
- Küpper, H. and P.M.H. Kroneck. 2005. Heavy metal uptake by plants and cyanobacteria. pp. 97-142. *In: Sigel, A., H. Sigel, and R. Sigel (ed.) Metal ions in Biological Systems, vol. 44. Marcel Dekker, New York, NY.*

- Küpper, H., E. Lombi, F.J. Zhao, G. Wieshammer, and S.P. McGrath. 2001. Cellular compartmentation of nickel in the hyperaccumulator *Alyssum lesbiacum*, *Alyssum bertolonii*, and *Thlaspi goesingense*. *J. Exp. Bot.* 52:2291-2300.
- Lasat, M.M., A.J.M. Baker, and L.V. Kochian. 1996. Physiological characterization of root Zn²⁺ absorption and translocation to shoots in Zn hyperaccumulator and nonaccumulator species of *Thlaspi*. *Plant Physiology* 112:1715-1722.
- Laurie, S.H. and J.A. Manthey. 1994. The chemistry and role of metal ion chelation in plant uptake processes. pp. 165-172. *In: J.A. Manthey, D.E. Crowley, and D.G. Luster (ed.) Biochemistry of metal micronutrients in the rhizosphere.* Lewis Publishers, Boca Raton, FL.
- Lindsay, W. L. 1979. Chemical equilibria in soils. John Wiley and Sons, New York, NY.
- Lombi, E., W.W. Wenzel, G.R. Gobran, and D.C. Adriano. 2001. Dependency of phytoavailability of metals on indigenous and induced rhizosphere processes. pp. 3-24. *In: Gobran, G.R., W.W. Wenzel, and E. Lombi (ed.) Trace elements in the rhizosphere.* CRC Press, Boca Raton, FL.
- Manceau, A., B. Lanson, M.L. Schlegel, J.C. Harge, M. Musso, L. Eybert-Berard, J.L. Hazemann, D. Chateigner, and G.M. Lambelle. 2000b. Quantitative Zn speciation in smelter-contaminated soils by EXAFS spectroscopy. *Am. J. Sci.* 300:289-343.
- Marschner, H. 1995. Ion Uptake Mechanisms of Individual Cells and Roots: Short Distance Transport. pp. 6-78. *In: H. Marschner Mineral Nutrition of Higher Plants (2nd Ed.).* Academic Press, London.
- Marschner, H. and V. Römheld. 1994. Strategies of plants for acquisition of iron. *Plant Soil* 165:261-274.
- Marschner, H., V. Römheld, and I. Cakmak. 1987. Root-induced changes of nutrient availability in the rhizosphere. *J. Plant Nutr.* 10:1175-1184.
- McBride, M. B. 1994. Environmental chemistry of soils. pp. 121-168. Oxford University Press, Inc., New York, NY.
- McGrath, S.P., F.J. Zhao, and E. Lombi. 2002. Phytoremediation of metals, metalloids, and radionuclides. *Advances in Agronomy* 75:1-56.

- McLaughlin, M.J., E. Smolders, and R. Merckx. 1998. Soil-root interface: physicochemical processes. pp. 233-277. *In*: P.M. Huang, D.C. Adriano, T.J. Logan, and R.T. Checkai (ed.) Soil chemistry and ecosystem health. SSSA Spec. Publ. 52. SSSA, Madison, WI.
- Menezes de Sequeira, E. 1969. Toxicity and movement of heavy metals in serpentinitic rocks (Northeastern Portugal). *Agron. Lusit.* 30:115-154.
- Minguzzi, C. and O. Vergnano. 1948. Il contenuto di nichel nell ceneri di *Alyssum bertolonii* Desv. *Mem. Soc. Tosc. Sci. Nat. A* 55:49-77.
- Miyasaka, S.C., J.C. Buta, R.K. Howell, and C.D. Foy. 1991. Mechanisms of Al tolerance in snapbeans. Root exudation of citric acid. *Plant Physiol.* 96:737-743.
- Morel, C. and P. Hinsinger. 1999. Root-induced modifications of the exchange of phosphate ion between soil solution and soil solid phase. *Plant Soil* 211:103-110.
- Morrison, Richard S. 1980. Aspects of the accumulation of cobalt, copper, and nickel by plants. Thesis (PhD in Chemistry). Massey University Library, Palmerton North, New Zealand.
- Nachtegaal, M., M.A. Marcus, J.E. Sonke, J. Vangronsveld, K.J.T. Livi, D. van Der Lelie, and D.L. Sparks. 2005. Effects of *in situ* remediation on the speciation and bioavailability of zinc in a smelter contaminated soil. *Geochim. et Cosmochim. Acta* 69:4649-4664.
- Neumann, G. and V. Römheld. 1999. Root excretion of carboxylic acids and protons in phosphorus-deficient plants. *Plant and Soil* 211:121-130.
- Parfitt, R.L. 1979. The availability of P from phosphate-goethite bridging complexes: desorption and uptake by ryegrass. *Plant Soil* 53:55-65.
- Pellet, D.M., L.A. Papernik, and L.V. Kochian. 1996. Multiple aluminum-resistance mechanisms in wheat: roles of root apical phosphate and malate exudation. *Plant Physiol.* 112:591-597.
- Pence, N.S., P.B. Larsen, S.D. Ebbs, D.L. Letham, M.M. Lasat, D.F. Garvin, D. Eide, and L.V. Kochian. 2000. The molecular physiology of heavy metal transporter in the Zn/Cd hyperaccumulator *Thlaspi caerulescens*. *Proceedings of National Academy of Sciences, USA* 97:4956-4960.

- Petruzzelli, G. 1989. Recycling wastes in agriculture: Heavy metal bioavailability. *Agri. Ecosys. Environ.* 27:493-503.
- Pohlman, A.A. and J.G. McColl. 1988. Soluble organics from forest litter and their role in metal dissolution. *Soil Sci. Soc. Am. J.* 52:265-271.
- Proctor, J. and S.R.J. Woodell. 1975. The ecology of serpentine soils. *Adv. Ecol. Res.* 9:255-366.
- Raskin, I., R.D. Smith, and D.E. Salt. 1997. Phytoremediation of metals: Using plants to remove pollutants from the environment. *Curr. Opin. Biotechnol.* 8:221-226.
- Ravin, P.H., R.F. Evert, and S.E. Eichhorn. 1992. The movement of water and solutes in plants. pp. 616-635. *In: Ravin, P.H., R.F. Evert, and S.E. Eichhorn (ed.) Biology of Plants.* Worth Publishers, New York, NY.
- Reeves, R.D., R.R. Brooks, and R.M. MacFarlane. 1981. Nickel uptake by Californian *Streptanthus* and *Caulanthus* with particular reference to the hyperaccumulator *S. polygaloides* Gray (*Brassicaceae*). *Am. J. Bot.* 68:708-712.
- Reeves, R.D., R.R. Brooks, and T.R. Dudley. 1983. Uptake of nickel by species of *Alyssum*, *Bornmuellera* and other genera of Old World Tribus Alysseae. *Taxon.* 32:184-192.
- Roberts, D.R., R.G. Ford, and D.L. Sparks. 2003. Kinetics and mechanisms of Zn complexation on metal oxides using EXAFS spectroscopy. *Journal of Colloid and Interface Science* 263:364-376.
- Ryan, P.R., E. Delhaize, and P.J. Randall. 1995. Characterization of Al-stimulated efflux of malate from the apices of Al-tolerant wheat roots. *Planta* 196:103-110.
- Salt, D.E., R.D. Smith, and I. Raskin. 1998. Phytoremediation. *Annual Review of Plant Physiology and Plant Molecular Biology* 49:643-668.
- Sanders, D. and P. Bethke. 2000. Membrane transport. pp. 110-158. *In: Buchanan, B. B., W. Gruissemann, and R.L. Jones (ed.) Biochemistry and molecular biology of plants.* American Society of Plant Physiologists, Rockville, MD.
- Schat H., M. Llugany, and R. Bernhard. 2000. Metal-specific patterns of tolerance, uptake, and transport of heavy metals in hyperaccumulating and nonhyperaccumulating metallophytes. pp. 171-188. *In: Terry N. and G. Bañuelos*

(ed.) Phytoremediation of Contaminated Soil and Water. Lewis Publishers, Boca Raton, FL.

Sparks, D.L. 2003. Environmental Soil Chemistry (2nd Ed.). Academic Press, London. pp. 207-244.

Stumm, W., G. Furrer, E. Wieland, and B. Zinder. 1985. The effects of complex-forming ligands on the dissolution of oxides and aluminosilicates. pp. 55-74. *In*: Drever, J.I. (ed.) The Chemistry of Weathering. Reidel Publishing Co., Dordrecht.

Takagi, S., S. Kamei, and M. Yu. 1988. Efficiency of iron extraction from soil by mugenic acid family phytosiderophores. *J. Plant. Nutr.* 11:643-651.

Tappero, R., E. Peltier, M. Gräfe, K. Heidel, M. Ginder-Vogel, K.J.T. Livi, M.L. Rivers, M.A. Marcus, R.L. Chaney, and D.L. Sparks. 2007. Hyperaccumulator *Alyssum murale* relies on a different metal storage mechanism for cobalt than for nickel. *New Phytologist* 175:641-654.

Thalium 1588. (Quoted in Antonovics et al., 1971).

Thiry, Y., A. Gommers, A. Iserentant, and B. Delvaux. 2005. Rhizospheric mobilization and plant uptake of radiocesium from weathered micas: II. Influence of mineral alterability. *J. Environ. Qual.* 34:2171-2180.

Tkalich, S.M. 1938. Experience in the investigation of plants as indicators in geological exploration and prospecting. *Vest. Dal'nevost. Fil. Akad. Nauk.* 32:3-25. SSSR.

Uren, N.C. and H.M. Reisenauer. 1988. The role of root exudates in nutrient acquisition. *Adv. Plant Nut.* 3:79-114.

Vergnano Gambi, O. and R. Gabbrielli. 1979. Ecophysiological and geochemical aspects of nickel, chromium, and cobalt accumulation in the vegetation of some Italian ophiolitic outcrops. *Ofioliti* 4:199-208.

Vergnano Gambi, O., L. Pancaro, and C. Formica. 1977. Investigations on nickel accumulating plant: *Alyssum bertolonii* Desv.: I. Nickel, calcium, and magnesium content and distribution during growth. *Webbia* 32:175-188.

Voegelin, A. and R. Kretzschmar. 2005. Formation and dissolution of single and mixed Zn and Ni precipitates in soil: evidence from column experiments and extended X-ray absorption fine structure spectroscopy. *Environ. Sci. Technol.* 39:5311-5318.

Walker, D.J. and M.P. Bernal. 2004. The effects of copper and lead on growth and zinc accumulation of *Thlaspi caerulescens* J. and C. Presl: Implications for phytoremediation of contaminated soils. *Water Air Soil Pollut.* 151:361-372.

Wither, E.D. and R.R. Brooks. 1977. Hyperaccumulation of nickel by some plants of Southeast Asia. *J. Geochem. Explor.* 8:579-583.

Zhang, F.S., J. Ma, and Y.P. Cao. 1997. Phosphorus deficiency enhances root exudation of low-molecular weight organic acids and utilization of sparingly soluble inorganic phosphates by radish (*Raphanus sativus* L) and rape (*Brassica napus* L.) plants. *Plant Soil* 196:261-264.

Chapter 2

HYPERACCUMULATOR *ALYSSUM MURALE* RELIES ON A DIFFERENT STORAGE MECHANISM FOR COBALT THAN FOR NICKEL

2.1 Summary

Nickel (Ni) hyperaccumulator *Alyssum murale* has been developed as a commercial crop for phytoremediation/phytomining Ni from metal-enriched soils. Metal co-tolerance, accumulation, and localization were investigated for *A. murale* exposed to metal co-contaminants. *A. murale* was irrigated with Ni-enriched nutrient solutions containing basal or elevated concentrations of cobalt (Co) or zinc (Zn). Metal localization and elemental associations were investigated *in situ* with synchrotron X-ray microfluorescence (SXRF) and computed-microtomography (CMT). *A. murale* hyperaccumulated Ni and Co ($>1000 \mu\text{g g}^{-1}$ DW) from mixed-metal systems. Zinc was not hyperaccumulated. Elevated Co or Zn concentrations did not alter Ni accumulation or localization. SXRF images showed uniform Ni distribution in leaves and preferential localization of Co near leaf tips/margins. CMT images revealed 1) leaf epidermal tissue was enriched with Ni but devoid of Co, 2) Co was localized in the apoplasm of leaf ground tissue, and 3) Co was sequestered on leaf surfaces near the tips/margins. Cobalt-rich mineral precipitates form on leaves of Co-treated *A. murale*. Specialized biochemical processes linked with Ni (hyper)tolerance

in *A. murale* do not confer (hyper)tolerance to Co. *A. murale* relies on a different metal storage mechanism for Co (exocellular sequestration) than for Ni (vacuolar sequestration).

2.2 Introduction

Large-scale metal contamination can result in irreversible environmental damage, and remediation efforts represent a substantial financial burden for industry, government, and taxpayers. Anthropogenic metal inputs include spoil from metal mining operations, fallout from refinery emissions, waste disposal, electroplating, combustion of fossil fuels, and agricultural application of pesticides and biosolids (Adriano 1986). Traditional remediation efforts (e.g. excavation, burial, and contaminant isolation) are not feasible for large-scale impacts, thus alternative remediation strategies are necessary when vast areas of land have been contaminated. Hyperaccumulator plants concentrate trace metals in their harvestable biomass (Brooks et al., 1977), thereby offering a sustainable treatment option for metal-contaminated sites (phytoextraction) and an opportunity to mine metal-rich soils (phytomining) (Chaney 1983). Cultivating nickel (Ni) hyperaccumulator plants on metal-enriched soils and ashing the harvestable biomass to produce Ni ore (bio-ore) is an economically viable alternative for metal recovery (Chaney et al., 2004).

Soils suitable for Ni phytomining include serpentine soils and industrially-contaminated soils. Serpentine soils develop from ultramafic parent material, thus

contain appreciable quantities of Ni, cobalt (Co), chromium (Cr), manganese (Mn), iron (Fe), and zinc (Zn). The Ni : Co ratios in serpentine soils typically range from five to ten. Anthropogenic metal inputs generally involve discharge of a mixed-element waste stream. For instance, emissions from Ni smelters are typically enriched with other trace metals from the ore (e.g. copper (Cu), Co, lead (Pb), and Zn). Heavy metals are incorporated into (metallo)enzymes and thereby toxic to living organisms in excessive amounts. Cobalt contamination is an environmental concern, and the radionuclide ^{60}Co is classified as a priority pollutant (Hamilton 1994).

Hyperaccumulator plants used to extract Ni from metal-enriched soils must be tolerant of co-contaminants. Therefore, the effects of metal co-contaminants on the physiology and biochemistry of hyperaccumulators and ultimately on the efficiency of metal phytoextraction is of concern for metal recovery efforts.

Several first-row transition metals (e.g. Co and Ni) have important roles in biological systems as activators of enzymes or as key components of enzyme systems. Cobalt is essential for *Rhizobium* (associate symbiotically with legume roots for N_2 fixation), free-living nitrogen-fixing bacteria (e.g. *Azotobacter* spp.), and cyanobacteria. However, there is no evidence Co has a direct role in the metabolism of higher plants (Marschner 1995). Nickel is the element most recently classified as an “essential” plant nutrient (Welch 1995) and is a key component of the Ni-containing enzyme urease (Dixon et al., 1975). Transmembrane transport systems with specificity for Ni or Co have not been identified in higher plants.

Nickel hyperaccumulator *Alyssum murale*, an herbaceous perennial (*Brassicaceae* family) native to Mediterranean serpentine soils, has been developed as a commercial crop for phytoremediation/phytomining (Chaney et al., 1983, 2004; Li et al., 2003a). Hyperaccumulator species of *Alyssum* (hereafter referred to as ‘*Alyssum*’) accumulate Co from Co-enriched soils; cobalt accumulation is most efficient in mildly-acidic soils, while Ni is most effectively accumulated from neutral soils (Li et al., 2003b; Kukier et al., 2004). *Alyssum* sequesters Ni via epidermal compartmentalization, a metal sequestration strategy exploiting leaf epidermal tissue as the sink for metal storage. Epidermal cell vacuoles are responsible for Ni sequestration in *Alyssum* (Krämer et al., 1997a, 2000; Broadhurst et al., 2004a,b); vacuolar sequestration has been recognized as a key component of cellular-level metal tolerance (i.e. (hyper)tolerance) for several hyperaccumulator species (Heath et al., 1997; Mesjasz-Przybylowicz et al., 1997; Küpper et al., 1999, 2000, 2001; Frey et al., 2000; Bidwell et al., 2004; Küpper & Kroneck 2005). However, Co sequestration in *Alyssum* epidermal cell vacuoles has not been reported previously.

Information regarding metal localization (e.g. tissue, cells, and organelles) and elemental associations in accumulator plants is crucial to understanding the mechanisms of hyperaccumulation and tolerance. Synchrotron-based techniques such as X-ray microfluorescence (SXRF) and computed-microtomography (CMT) can be used to image (*in situ*) elements in hyperaccumulator plants. SXRF imaging of an intact, transpiring thallium (Tl) accumulator (*Iberis intermedia*) showed Tl distributed

throughout the vascular network, and X-ray absorption spectroscopy (XAS) identified aqueous Tl(I) as the primary species in plant tissue (Scheckel et al., 2004). X-ray CMT imaging techniques such as differential absorption (DA-CMT) and fluorescence microtomography (F-CMT) resolve the three-dimensional distribution of elements within a sample, and hydrated biological specimens can often be analyzed with minimal or no sample preparation and alteration. DA-CMT and F-CMT were used to visualize Fe localization in seeds of mutant and wild-type *Arabidopsis*, revealing Fe storage in seeds was mediated by the vacuolar Fe transporter (VIT1) (Kim et al., 2006). F-CMT and DA-CMT showed Ni enrichment in leaf epidermal tissue of *A. murale* grown in Ni-contaminated soils (McNear et al., 2005).

Soils naturally-enriched or industrially-contaminated with Ni typically have co-contaminants present; however, the influence of common metal co-contaminants on Ni hyperaccumulation remains poorly understood. In the present work, the effect of Co and Zn on Ni accumulation and localization in *A. murale* was examined. Metal localization and elemental associations in plants were investigated with X-ray and electron microscopies and X-ray microtomography. Particular emphasis was placed on the phenomenon of “simultaneous hyperaccumulation” (Ni & Co) and its relationship to metal co-tolerance.

2.3 Materials and Methods

2.3.1 Project Summary

Alyssum murale (Waldst. & Kit.) accession 'Kotodesh' (common name madwort or yellowtuft) was tested for growth and metal uptake in response to elevated Co and Zn concentrations in pseudo-hydroponic culture. Cobalt was selected as a competing divalent metal based on its geogenic association with Ni (co-occurrence in serpentine soils, metal ores, and smelter/refinery emissions) and because previous research indicated *Alyssum* hyperaccumulates Co. Zinc was selected as a divalent metal because it is a common contaminant in surface soils and is not hyperaccumulated by *Alyssum*.

2.3.2 Ebb and Flow Mesocosm Design

Each ebb and flow mesocosm consisted of two nest and stack totes (L.K. Goodwin Co. model 35180 & 35185), a water pump (Rio[®] 400 by Taam Inc.) fitted with 1.27 cm diameter tubing, and fill/drain and overflow plumbing accessories (American Hydroponics). A pump was placed in the reservoir and pump tubing was connected to the plant tray via the fill/drain plumbing accessory. Overflow plumbing consisted of a riser used to maintain the solution level (5 cm) in the plant tray when the pump was running. Ebb and flow systems were flooded for 15 minutes every eight hours, and solution remaining in the tray drained to the reservoir by gravity following each flooding cycle. Mesocosms contained 5 to 10 L of nutrient solution and six individual plants in 10 cm pots.

2.3.3 Plant Tissue Analyses

Plants were harvested after 30 days metal exposure and analyzed for total

metal and nutrient content. Immediately following harvest, shoots were rinsed in deionized water to remove adhering particles. Roots were meticulously separated from the perlite media and rinsed with 0.001 M CaCl₂ followed by deionized water. Plant material was oven-dried at 65° C to a constant weight (~48 h). Dry plant tissue was ground with a plastic herb grinder (420 Grinder Company) and homogenized. Plant tissue samples were acid digested using a modified EPA 3051 method. For each sample, 0.50 g (\pm 0.05) of tissue was microwave digested in 10 mL of concentrated HNO₃. Digests were filtered (0.22 μ m) and brought to 30 mL total volume with deionized water. Samples were analyzed by ICP-AES using yttrium (Y) as an internal standard. Sample duplicates were within 5 % agreement, and the Ni, Co, and Zn levels measured for NIST spinach standard (2385) were within the range specified by NIST. Statistical analyses were performed in Minitab 12. ANOVA with mean separation by Tukey's HSD ($P < 0.05$) was used to test statistical significance of the treatment effects on yield and elemental composition of plant tissue.

2.3.4 Electron Probe Micro-Analysis

A. murale leaves from a Co-treated plant were imaged with a scanning electron microscope (SEM) and energy dispersive X-ray Spectroscopy (EDS) spectra were collected from leaf-tip and bulk-leaf regions. Backscattered electron images (BSE) and EDS spectra were recorded using a JEOL 8600 Superprobe equipped with an EDAX light-element EDS detector and GENESIS software. The beam energy was set at 20 keV and the beam current at 30 nA (~2 μ m spot). Leaves were mounted onto

a conductive carbon stub and desiccated (CaCl_2) for 48 h prior to analysis. Samples were sputter-coated with carbon to minimize charging effects.

2.3.5 Synchrotron X-ray Microfluorescence (SXRF) and Computed Microtomography (CMT)

Metal localization and elemental associations in *A. murale* plants were investigated with SXRF and CMT. SXRF images were acquired from beamline 10.3.2 of the Advanced Light Source (ALS) at Lawrence Berkeley National Laboratory (Berkeley, CA) (Marcus et al., 2004). Briefly, this beamline uses Kirkpatrick-Baez (K-B) mirrors to produce a focused spot (5 to 16 μm) of hard X-rays with tunable energy achieved via a Si(111) monochromator. Incident energy was typically fixed at 10 keV to excite all target elements simultaneously. Plant tissue (hydrated) was excised from live plants and mounted directly to the sample stage with no further preparation. Samples were rastered in the path of the beam by an XY stage oriented in a plane 45° to the beam, and X-ray fluorescence was detected by a 7-element Canberra Ultra LE-Ge detector positioned 90° to the incident beam. Elemental maps were collected from a 1 to 3 mm^2 area using a step size of 5 μm (fine map) or 20 μm (coarse map) and a dwell time of 100 ms. In order to isolate the Co signal from contributions due to Ni and Fe fluorescence, SXRF images were collected at 50 eV above and below the Co K-edge energy (7.709 keV) and then subtracted to generate a difference map. Sulfur and Co were imaged simultaneously with the incident energy fixed at 1.5 keV above the sulfur K-edge (2472 eV) and the monochromator tuned to pass the third

harmonic and fundamental (used to excite the Co K-edge), preventing the Co signal from swamping out the S signal. Additionally, a small He-purged chamber was attached onto the end of the detector and positioned in tight proximity to the sample to minimize the air path and reduce absorption of the low energy X-rays.

Microtomography data (DA-CMT & F-CMT) were collected at GeoSoilEnviroCARS (GSECARS) beamline 13-BM-D and 13-ID-C of the Advanced Photon Source at Argonne National Laboratory (Argonne, IL) ([Rivers et al., 2006](#); [Sutton et al., 2002](#)). Specimens imaged by F-CMT were immersed in liquid nitrogen, freeze-dried under vacuum (-180° C), and mounted to a wooden shaft with epoxy resin as described by [McNear et al. \(2005\)](#). Leaf specimens imaged by DA-CMT were maintained in a high-humidity environment during data collection (~1 hr). A leaf was removed from a live plant and immediately placed into a Kapton tube. Dampened cotton was positioned in the tube both above and below the leaf, and the tube was sealed with modeling clay then fixed to a wooden shaft at one end for insertion into the rotation axis of the XYθ stepping stage.

DA-CMT data collection involved exposing the sample to a wide-fan X-ray beam, measuring the transmitted X-rays (converted to visible light via a single-crystal scintillator then projected onto a fast charged-coupled device area detector with a 10x microscope objective), rotating the sample by a small angle for repeat exposure, and continuing the measurements until the sample had been rotated from 0° to 180°. DA-CMT data were collected using 0.25° steps and a 3 s dwell time. Hardware

configurations selected for DA-CMT imaging provided optical resolution of 5.12 μm with a 3.27 x 2.59 mm (H x V) field of view. Data were acquired with the incident X-ray beam energy set ~ 100 eV below the Co K-edge (7709 eV) or Ni K-edge (8333 eV) energy and then repeated with the beam energy set ~ 30 eV above the absorption edge. Sinograms were reconstructed using the Gridrec-based software (Dowd et al., 1999). Above- and below-edge data arrays were subtracted and the difference matrices were used to generate the tomographic projections depicting the metal distribution in hydrated leaf tissue.

F-CMT imaging of roots involved a similar procedure although the samples were rotated and translated in a microfocused beam (incident energy fixed at 10 keV) and the fluorescence intensities for multiple elements were recorded simultaneously using a 16-element Ge array detector. F-CMT data were collected using 1.5 to 3° steps, a 1 s dwell time, and 5 μm translation steps.

2.4 Results

2.4.1 Plant Growth

All treatments resulted in healthy-looking plants at harvest, and metal treatments did not significantly ($P < 0.05$) affect shoot biomass (Table 2.1). Cobalt-treated plants (Ni + Co & Ni + Co + Zn) had mild chlorosis on new growth, signifying the initial Fe concentration in nutrient solution was inadequate. Plants from the Ni + Co + Zn treatment were less chlorotic than plants exposed to Ni + Co, indicating the

elevated concentration of Zn reduced the antagonism between Co and Fe. Cobalt-induced Fe deficiency was alleviated during the second week of metal exposure by increasing the Fe concentration in all nutrient solutions to 20 μM . Plants recovered quickly and new growth appeared non-chlorotic. Although differences in shoot biomass between treatments were insignificant, the slight depression in yield for these Co-treated plants can be attributed to reduced growth during this brief period of mild Fe deficiency chlorosis.

2.4.2 Bulk Characterization of Metal Accumulation

Elevated aqueous concentrations (50 μM) of Co or Zn in nutrient solution did not significantly ($P < 0.05$) affect shoot Ni concentration in *A. murale* (Table 2.1). Plants absorbed Co and Ni to a similar extent from equimolar solution; root transport systems had comparable ability to shuttle these metals into the vasculature. Zinc was not hyperaccumulated by *A. murale*.

A metal bioconcentration factor (BCF), ratio of metal concentration in shoot tissue to metal concentration in growth media, evaluates the potential for a plant to concentrate a metal. *A. murale* initially supplied with 50 μM Ni ($\sim 3 \text{ mg L}^{-1}$ solution) had a shoot Ni concentration averaging 1550 $\mu\text{g g}^{-1}$ DW (BCF ~ 500). In contrast, maximal Zn BCF was 46 (Ni + Zn). Cobalt BCFs were 532 (Ni + Co) and 702 (Ni + Co + Zn). Clearly, *A. murale* concentrated Ni and Co against a substantial chemical potential gradient.

Table 2.1. Shoot biomass and element concentrations for *Alyssum murale* plants 30 days after metal exposure.

Ni-Co-Zn treatment	Shoot biomass	Element concentration in shoot tissue of <i>Alyssum murale</i>					
		Ni	Co	Zn	Mn	Fe	S
μM	g DW	$\mu\text{g g}^{-1}\text{ DW}$					
50 - 0 - 0	7.42 a (1.74)	1610 a (189)	— —	60.4 a (6.45)	244 a (11.2)	33.3 a (2.61)	5800 a (815)
50 - 0 - 50	7.60 a (0.92)	1540 a (302)	— —	149 b (42.6)	263 a (31.9)	38.4 a (9.64)	6550 a (978)
50 - 50 - 0	6.30 a (0.65)	1650 a (85.1)	1570 a (178)	69.3 a (4.76)	322 b (12.9)	33.5 a (1.40)	8320 b (787)
50 - 50 - 50	6.40 a (0.95)	1410 a (139)	2070 b (252)	129 b (20.1)	339 b (29.5)	30.8 a (1.49)	8980 b (730)

Values are mean (\pm SD); $n = 5$. Different letters within a column indicate significant difference ($P < 0.05$) with Tukey HSD comparison.

A translocation factor (TF), ratio of element concentration in shoot tissue to element concentration in root tissue, estimates the translocation efficiency of a plant, and the TF for a hyperaccumulated metal is typically greater than one. *A. murale* was efficient at translocating Ni (TF ~2) and Co (TF ~3), but Zn (TF ~0.1) was not translocated to any unusual extent (Table 2.2). Nickel TF was not significantly altered by elevated concentrations of Co or Zn, indicating minimal effects from the metal co-contaminants. Sulfur and Mn translocation were significantly ($P < 0.05$) affected by the metal treatments, and maximal S TF (~0.9) and Mn TF (~1.6) were observed for plants from the Ni + Co + Zn treatment.

Correlations between the concentration of one metal in shoot tissue and the concentration of other metals or nutrients can help identify elemental interactions in plants. Cobalt-treated *A. murale* (Ni + Co & Ni + Co + Zn) had significantly ($P < 0.001$) higher shoot concentrations of S and Mn than untreated plants, indicating uptake of these elements was related to Co accumulation. *A. murale* had significantly

($P = 0.018$) higher shoot Co concentrations when the Zn concentration was elevated in nutrient solution (Table 2.1). Maximal shoot Co concentration ($2065 \mu\text{g g}^{-1}$) and shoot Co accumulation ($13.2 \text{ mg plant}^{-1}$) were observed for plants from the Ni + Co + Zn treatment.

Table 2.2. Translocation factors (Shoot to root concentration ratio) for *Alyssum murale* plants 30 days after metal exposure.

Ni-Co-Zn treatment (μM)	Ni	Co	Translocation factors			
			Zn	Mn	Fe	S
50 - 0 - 0	1.8 a (0.16)	— —	0.09 a (0.01)	0.44 a (0.05)	0.09 a (0.01)	0.53 a (0.07)
50 - 0 - 50	2.0 a (0.14)	— —	0.07 a (0.01)	0.78 b (0.08)	0.12 a (0.06)	0.58 a (0.06)
50 - 50 - 0	1.9 a (0.30)	2.7 a (0.31)	0.12 b (0.02)	0.85 b (0.12)	0.11 a (0.02)	0.80 b (0.07)
50 - 50 - 50	2.0 a (0.27)	3.2 a (0.34)	0.07 a (0.01)	1.57 c (0.24)	0.09 a (0.02)	0.86 b (0.08)

Values are mean (\pm SD); $n = 5$. Different letters within a column indicate significant difference ($P < 0.05$) with Tukey HSD comparison.

2.4.3 Plant Tissue Microanalysis

Metal localization and elemental associations in *A. murale* were investigated with SXRF, CMT, SEM-EDS, and XAS. Two-dimensional (2D) SXRF images of *A. murale* leaves revealed a distinctive localization pattern for Co relative to Ni and Zn. Nickel distribution in leaves was essentially uniform, although the fluorescence intensity was slightly elevated in the midrib region (Figure 2.1). A uniform Ni distribution was anticipated for 2D leaf images because *Alyssum* sequesters Ni within the epidermal layers. Nickel localization was not altered in *A. murale* plants exposed to mixed-metal systems (Ni + Co, Ni + Zn, Ni + Co + Zn). Nickel distributions were comparable for both young and old leaves.

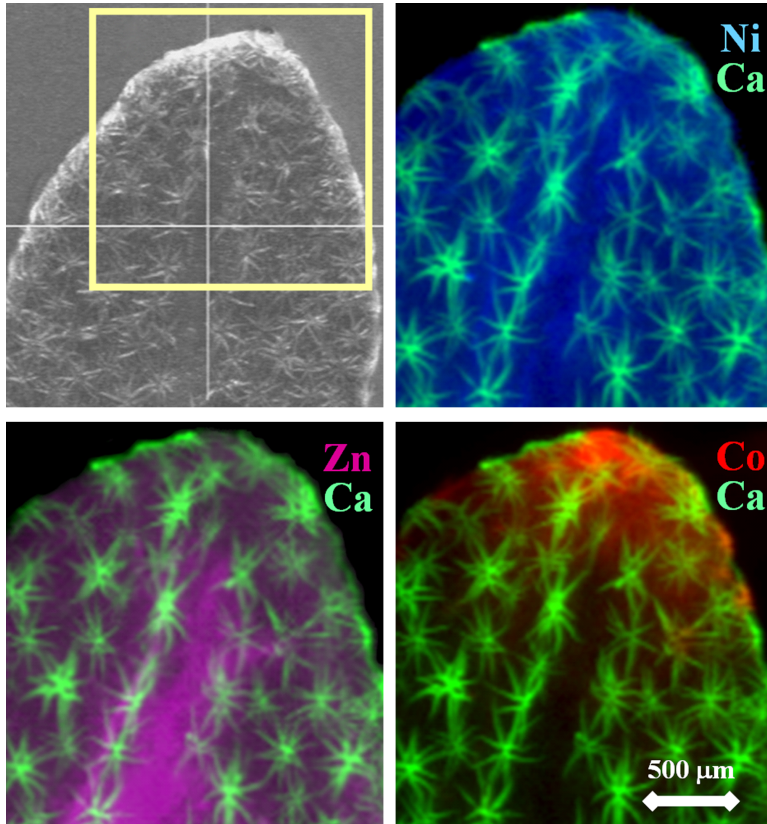


Figure. 2.1. μ -SXRF images of the Ni, Co, and Zn distributions in a hydrated *Alyssum murale* leaf from the Ni + Co + Zn treatment. Camera image shows the leaf region selected for SXRF imaging

Zinc distribution in *A. murale* leaves appeared similar to nickel; however, elevated fluorescence intensity in the midrib region was more evident in SXRF images of Zn than Ni because the Zn fluorescence signal was not dominated by the epidermal cell layers (i.e. more uniform metal distribution through leaf). Zinc was not hyperaccumulated by *A. murale* and would not be preferentially compartmentalized in epidermal tissue. Zinc distributions were comparable for both young and old leaves.

In contrast to Ni and Zn distributions, Co was preferentially localized at the tips and margins of *A. murale* leaves (Figure 2.1). Similar Co localization patterns have been reported for various non-accumulator plants investigated using autoradiography (^{60}Co radiotracer) (Gustafson 1956; Langston 1956; Handreck & Riceman 1969). Cobalt localization in *A. murale* was consistent for young and old leaves, but Co enrichment near leaf tips was more common on older leaves than younger leaves.

Spatial associations in leaves were visualized by combining fluorescence data from individual elements into a multi-color image and plotting a line profile. An SXRF image of Co, Ni, and Ca localization in an *A. murale* leaf revealed a color gradient (blue plus red light = magenta) near the leaf tip as a result of the uniform Ni distribution and the irregular Co distribution in the leaf (Figure 2.2).

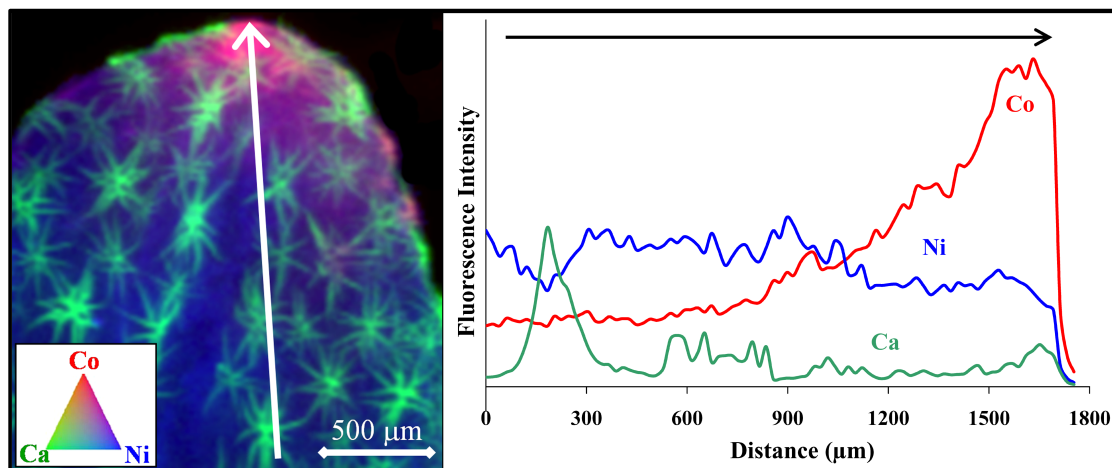


Figure. 2.2. μ -SXRF tricolor image (Ni, Co, and Ca) of a hydrated *Alyssum murale* leaf from the Ni + Co + Zn treatment plus a line profile (fluorescence intensity versus position) for a segment from the leaf center toward the leaf tip (indicated by arrow)

A line profile generated for a segment from the leaf center toward the leaf tip showed the substantial increase in the Co signal coincided with a subtle decrease in the Ni signal; cobalt and Ni were not preferentially co-localized in leaves.

Spatial associations of Co with Mn and S coincided with statistically significant correlations in bulk shoot concentrations. Cobalt-treated plants (Ni + Co & Ni + Co + Zn) had the highest shoot concentrations of Mn and S (Table 2.1) and the highest S translocation factors (Table 2.2). SXRf images of Co and Mn in *A. murale* leaves revealed co-localization of these elements at leaf trichomes (Figure 2.3).

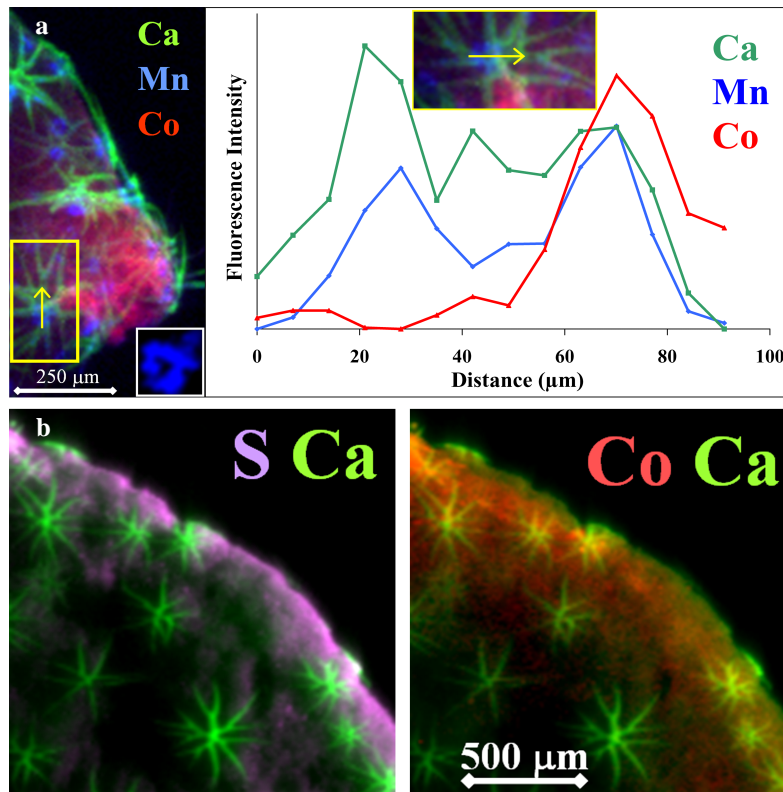


Figure 2.3. μ -SXRf images of hydrated *Alyssum murale* leaves depicting co-localization of Co with (a) Mn and Ca at a leaf trichome (line profile across trichome) and (b) with sulfur near a leaf tip and margin. The Mn-rich zone (blue) surrounding the trichome base is displayed as an inset on the tricolor SXRf image (top panel).

A Mn-rich zone surrounds the base of *A. murale* trichomes (Figure 2.3 inset) and could sequester Ni or Co. SXRF images of S and Co in *A. murale* leaves indicated co-localization of these elements near leaf tips/margins (Figure 2.3). Sulfur and Co were spatially correlated, but preliminary XANES data did not indicate a direct chemical association.

Metal localization in *A. murale* roots was investigated with microtomography. F-CMT images of *A. murale* fine root segments (0.5 mm, 3 mm, and 6 mm from the root apex) revealed distinctive metal partitioning patterns as a function of distance from the root tip (i.e. tissue age and function) (Figure 2.4). Nickel, Co, and Fe were localized in the root vasculature (procambium) at 0.5 mm from the apex; the root tip appeared most active in the absorption of these metals. In the root segment at 6 mm from the apex, these metals were predominantly confined to the epidermis, signifying sorption to surface functional groups, mucilage, bacterial biofilms, or metal oxide plaques on the root surface. Additionally, metal enrichment was discernible in the vasculature but was absent from the pith. Similar localization patterns were reported by Fellows et al. (2003) who investigated europium (Eu) uptake in living roots of *Avena sativa* and observed maximal fluorescence intensities in the apical tissue at the root tip and within the zone of root maturation (up to 500 μm basipetally), while elevated fluorescence from highly-differentiated root tissue was observed at the epidermis. Metal localization patterns in the *A. murale* root segment at 3 mm from the apex were intermediate to those observed at 0.5 mm and 6 mm;

elevated Ni and Co levels were observed in the vascular cylinder and at the root epidermis. Zinc and Mn localization patterns in *A. murale* roots were distinctive from Ni, Co, and Fe and from one another (Figure 2.4). Zinc was predominantly localized in isolated domains within the root at 0.5 mm, 3 mm, and 6 mm from the apex, while Mn was sporadically localized at the epidermis.

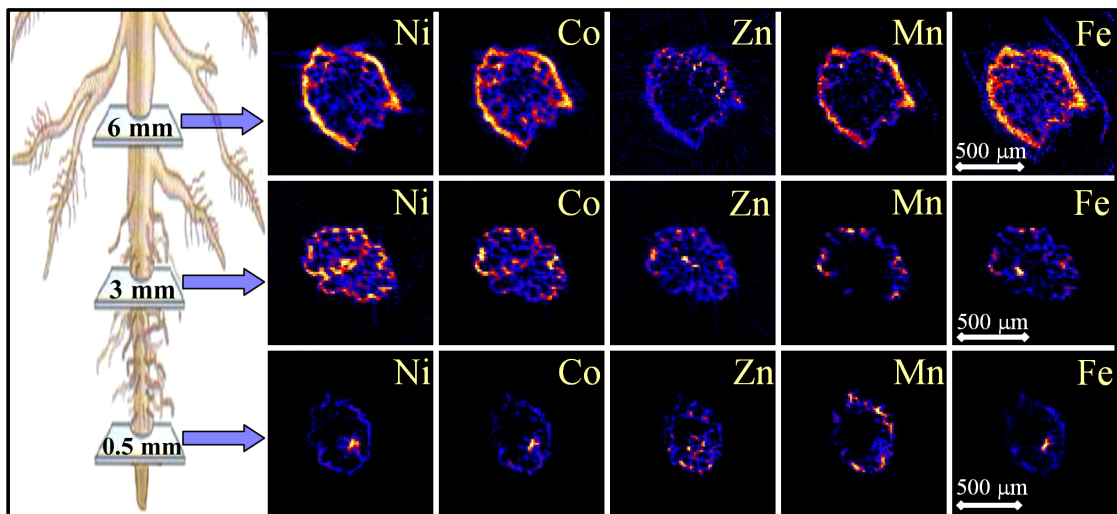


Figure 2.4. Fluorescence CMT cross-sectional images (5 µm slices) of the Ni, Co, Zn, Mn, and Fe distributions in *Alyssum murale* fine root segments at 0.5 mm (bottom), 3 mm (middle), and 6 mm (top) from the root apex. Root was collected from the Ni + Co + Zn treatment.

A separate experiment conducted with *A. murale* plants exposed to a Co-enriched nutrient solution verified the Co localization phenomenon observed in the metal interaction study was not a result of simultaneous hyperaccumulation, thus Co localization had not been altered in plants exposed to elevated Ni and Zn concentrations. Cobalt accumulated by *A. murale* was ultimately deposited on leaf

surfaces near the tips/margins. Cobalt on the surface of leaves was visible by optical microscopy (Figure 2.5 inset).

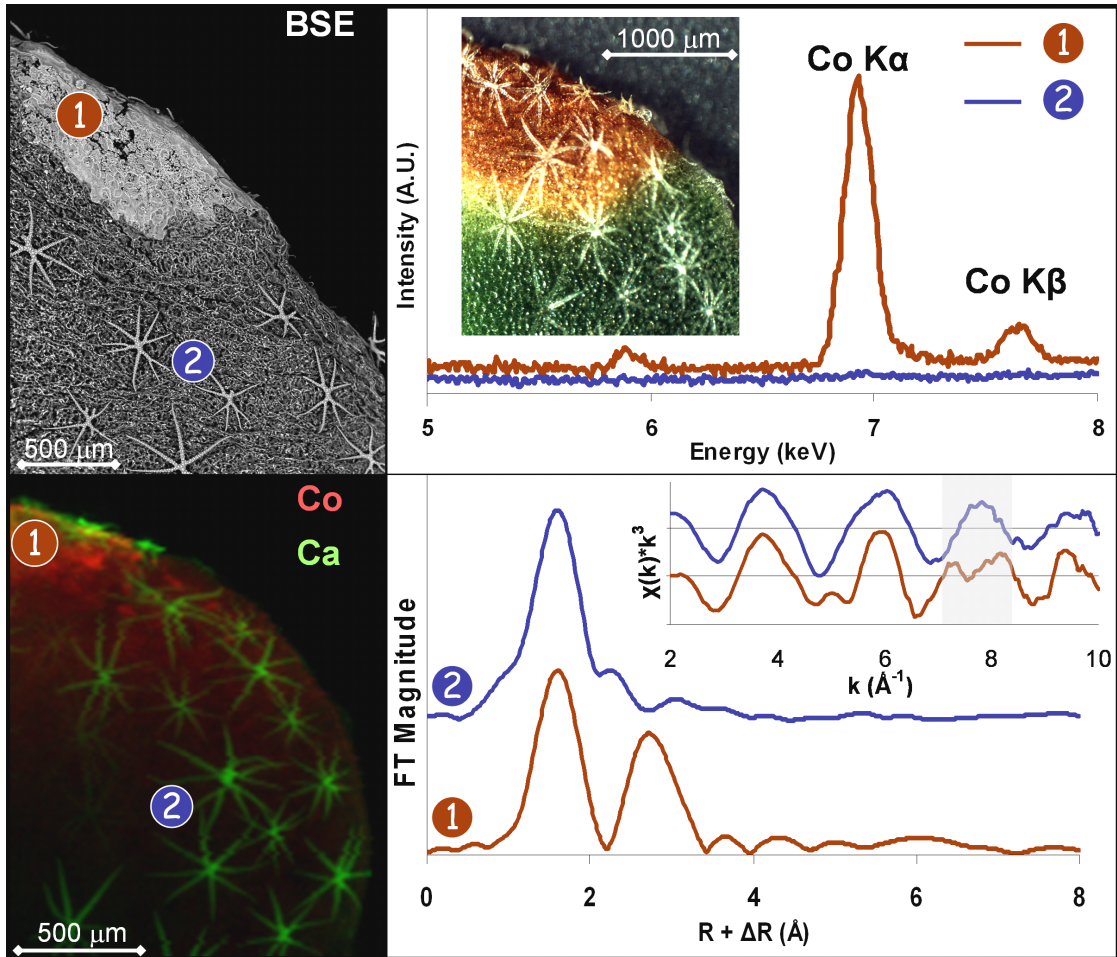


Figure 2.5. Backscattered electron (BSE) image of a leaf from Co-treated *Alyssum murale* with the corresponding SEM-EDS spectra from the leaf-tip and bulk-leaf regions (top panel); μ -SXRF image (Co and Ca) of a hydrated leaf from Co-treated *A. murale* with the corresponding Co K-edge k^3 -weighted $\chi(k)$ spectra (inset) and the Fourier transforms (FT) of μ -XAFS spectra from leaf-tip and bulk-leaf regions (bottom panel). An optical microscope image of a hydrated leaf from Co-treated *A. murale* is displayed as an inset (top panel).

Backscattered electron (BSE) images showed a coating on the leaf surface near tips/margins, and X-ray microanalysis (SEM-EDS) indicated the coating was a Co-rich phase (Figure 2.5). The electron microprobe beam penetrated only a few microns into the sample, thus the recorded signals were emitted from the leaf surface or cuticle layer; a comparison of EDS spectra from the Co-rich and bulk-leaf regions further supports the finding of a Co-rich phase deposited on the exterior of leaves. Leaf images from the optical microscope and SEM corroborate the Co distribution observed with SXRF (Figure 2.5). Micro-XAS spectra collected from hydrated *A. murale* leaves revealed the oxidation state of Co in plants was Co(II); artificial Co oxidation was not observed in this study but Co(III) can result from sample alteration in the X-ray beam and by ligand stabilization with multidentate amine ligands (e.g. EDTA). Spectra collected at the Co-rich region near the tip showed striking differences from spectra collected at the bulk-leaf region. The Co k^3 -weighted $\chi(k)$ spectrum from the Co-rich region had a beat pattern near 5 \AA^{-1} and a split oscillation between 7 and 8.5 \AA^{-1} whereas the $\chi(k)$ spectrum from the bulk-leaf region did not have these characteristic structural features (Figure 2.5 inset); spectra with several frequencies (e.g. Co-rich spot 1) are indicative of a long-range ordered binding environment such as that in a mineral structure, while spectra dominated by a single frequency (e.g. Bulk-leaf spot 2) are indicative of a short-range ordered environment. An evaluation of the Co-binding environment (*ab initio* model) for Co-rich spot 1 provided distances and numbers of Co-Co pairs that are characteristic of an edge-sharing layered framework.

A strong second-shell feature (heavy backscattering atom) and a third metal shell at about twice this distance (indicative of a brucite-like hydroxide sheet) was present in the Fourier transform (FT) from the Co-rich region but was absent in the FT from the bulk-leaf region (Figure 2.5). Cobalt accumulated by *A. murale* formed cobalt-rich mineral precipitate(s) on the leaf surface. Detailed characterization of the Co phase(s) formed on leaves and the ligands involved with Co transport and detoxification are reported in the next chapter of the dissertation.

DA-CMT images (i.e. virtual cross-sections) of a hydrated leaf from Co-treated *A. murale* revealed a lack of metal enrichment in epidermal tissue (Figure 2.6). Cobalt near leaf tips (< 30 μm) was localized predominantly on the leaf exterior. In addition to Co enrichment on the leaf surface, DA-CMT slices at 20 to 30 μm below the leaf tip showed Co localized in isolated regions inside the leaf associated with the vascular system. Cobalt was consistently observed on the exterior of leaves, but deposition on leaf surfaces was less prevalent at greater distances from the leaf tip. Images from several hundreds to thousands of microns below the leaf tip showed a predominance of Co distributed around the leaf ground tissue (intercellular); the distribution between cells was interpreted as Co in the leaf apoplasm (Figure 2.6). Cobalt enrichment was more prevalent in the region composed of spongy mesophyll than palisade mesophyll; spongy mesophyll contains fewer chloroplasts and many intercellular spaces linked to the outside via stomata.

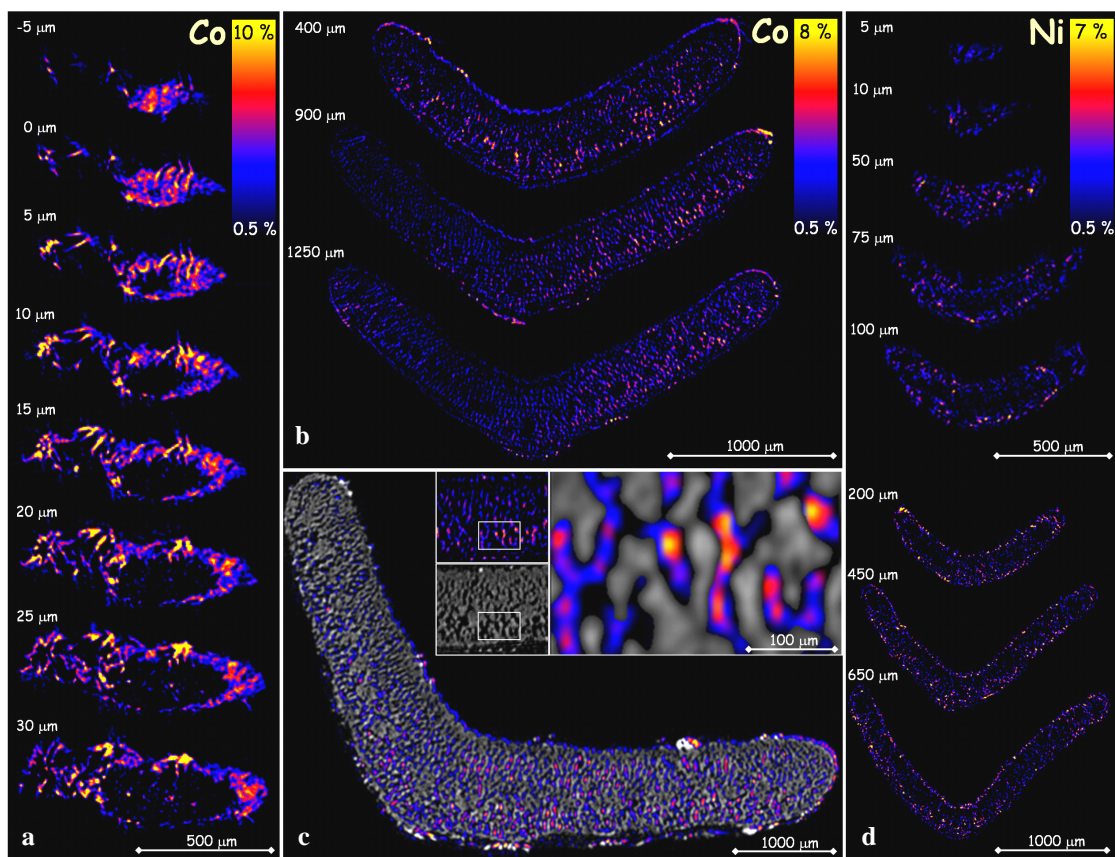


Figure 2.6. Differential absorption (DA-CMT) tomographic projections (5.1 μm slices) of hydrated *Alyssum murale* leaves depicting (a) Co distribution in the leaf-tip region, (b) Co distribution in the bulk-leaf region, (c) Co distribution in relation to the leaf cell structure (grey), and (d) Ni distribution in the leaf-tip and bulk-leaf regions. Leaves were collected from a Co-treated plant (a-c) and a Ni-treated plant (d). Sinograms recorded above and below the Co or Ni K-edge energy (+30 eV and -100 eV, respectively) were computationally reconstructed and the resulting projections were subtracted (above - below) to reveal the metal distribution in leaves. Distances are relative to the leaf tissue at the tip as determined from leaf structure images (i.e. below-edge projections).

Regions with elevated Co or Ni were frequently observed in proximity to leaf trichomes; however, Co enrichment was associated with the trichome structures on the leaf surface (i.e. some Co on the leaf surface was trapped in the space between the

trichome branches and the leaf tissue) while Ni was associated with the basal portion of trichomes. DA-CMT images of a hydrated leaf from Ni-treated *A. murale* showed metal enrichment in the epidermis (Figure 2.6); this result is consistent with other studies of Ni compartmentalization in *Alyssum* which have shown Ni sequestration in epidermal cell vacuoles (Krämer et al., 1997a, 2000; Broadhurst et al., 2004a,b). In addition to epidermal localization, Ni was observed within leaf ground tissue. In contrast to Co, a fraction of Ni in ground tissue occupied the same spaces as mesophyll cells, and this Ni distribution was interpreted as partial metal enrichment of mesophyll tissue.

2.5 Discussion

At a fundamental level, mechanisms of metal tolerance and hyperaccumulation in *Alyssum* remain poorly understood. *A. murale* hyperaccumulates Ni and Co, but Zn is not accumulated to abnormal levels. Elevated Co or Zn concentrations (50 μM) do not alter Ni accumulation or localization, thus *A. murale* can be used to recover Ni from most metal-enriched soils containing these metal co-contaminants. *A. murale* is more tolerant to Ni than Co; nickel (hyper)tolerance is attained via epidermal compartmentalization (i.e. vacuolar sequestration). *A. murale* does not sequester Co in epidermal cells; cobalt in the xylem or leaf apoplasm is excreted from leaves and subsequently sequestered on leaf surfaces as sparingly-soluble precipitate(s). Therefore, the specialized biochemical

processes linked to Ni (hyper)tolerance in *A. murale* do not confer (hyper)tolerance to Co.

2.5.1 Metal Localization

Cobalt is preferentially localized at leaf tips/margins while Ni is ultimately sequestered in epidermal cells. Vacuolar sequestration is a key strategy for metal tolerance because leaf epidermal cells provide an effective sink for the accumulated metal. Metal concentrations exceeding 0.35 M were measured in epidermal cell vacuoles of a Zn hyperaccumulator (Küpper et al., 1999). McNear et al. (2005) imaged Ni (DA-CMT) in an *A. murale* leaf and reported, in addition to epidermal enrichment, elevated Ni accumulation on/in the leaf tip; furthermore, it was suggested leaf tips function as an additional reservoir for Ni when concentrations exceed the finite capacity of cell vacuoles. However, McNear et al. (2005) did not consider their leaf tip was curled such that the epidermal layers near the tip were oriented parallel to the incident X-ray beam regardless of the rotation angle, thus the beam exclusively ‘sampled’ metal-enriched epidermal tissue in this region leading to the erroneous impression of elevated Ni on/in the leaf tip (i.e. bright voxels (3D pixels) in these upper slices resulted from Ni in the epidermis). Upper slices from the DA-CMT movie (supplementary information, McNear et al., 2005) reveal a lack of Ni enrichment near the point of the leaf (i.e. actual leaf tip); nonetheless, these slices afford a rare glimpse of Ni localization across leaf epidermal tissue.

Clear differences between Ni and Co localization suggest *A. murale* uses a different metal sequestration mechanism for Co than for Ni. While Ni is redistributed to leaf epidermal cells and subsequently transported across the tonoplast for long-term sequestration in vacuoles (Krämer et al., 1996, 1997a, 2000; Broadhurst et al., 2004a,b), Co does not have an efficient route of entry into epidermal cells.

Considering the serpentine (ultramafic) origin of *Alyssum*, a cellular-level tolerance mechanism for Co may not have been naturally selected because the Ni : Co ratio in these soils is relatively large. Additionally, Co is typically retained more strongly by the soil components (e.g. Mn oxides) than Ni and thereby less phytoavailable (Sparks 2003). Therefore, mechanisms other than vacuolar sequestration must be operating to cope with the elevated Co concentrations in plant tissue.

A. murale leaves apparently lack the transport system needed to sequester Co in epidermal cells, thus accumulated Co resides in the xylem and the leaf apoplasm. Mass flow and diffusion gradients in the apoplasm will cause Co to redistribute in leaves. Water loss via transpiration will move Co toward leaf surfaces and margins where transpiration is maximal. Cobalt principally follows the transpiration stream and results in Co enrichment at leaf tips/margins (Kabata-Pendias & Kabata 1984). When transpiration is low (e.g. night), root pressure will cause exudation of xylem fluid from the ventilation pores (hydathodes) located at the points of the leaf margin to where veins extend (i.e. guttation). Guttation fluids of plants from ultramafic soils have been reported to contain elevated metal (e.g. Mn)

concentrations (Mizuno et al., 2002). For example, *Minuartia verna* grown in metal-contaminated soil accumulated Cu and Zn in leaves and excreted these metals onto leaf surfaces via hydathodes (Neumann et al., 1997).

Cobalt accumulated by *A. murale* is ultimately deposited on leaf surfaces. Cobalt enrichment on leaf surfaces is evident from X-ray microtomography (DA-CMT), X-ray microanalysis (SEM-EDS), optical microscopy, and visual inspection of Co-treated *A. murale* leaves. Similar observations were made by Vergnano & Hunter (1952) who noted red-colored leaf tips on plants exposed to Co-enriched nutrient solution. Cobalt deposition at *A. murale* leaf tips is most prevalent on older leaves. For many plant species, older leaves have the highest concentrations of elements such as Co because evapotranspiration continues as long as the leaf is attached to the plant (Malik et al., 2000). Deposition of sparingly-soluble Co species near the tips/margins of *A. murale* leaves is corroborated by *in situ* microspectroscopic analyses (DA-CMT & μ -XAS) revealing weight percent Co(II) is sequestered on leaf surfaces and forms cobalt-rich mineral precipitate(s). Metal tolerant *Arabidopsis halleri* (formerly *Cardaminopsis halleri*) grown in a Zn- and Cu-contaminated soil had mixed-metal precipitate(s) on leaf surfaces (Neumann & zur Nieden 2001).

Elevated regions of Ni and Co occur consistently in proximity to the trichomes on *A. murale* leaves, and the Mn-rich zone surrounding the base of trichomes may be partially responsible for this metal enrichment. Simultaneous hyperaccumulation of Mn and Ni occurred in the basal compartment of the non-

glandular trichomes on *Alyssum* leaves (Broadhurst et al., 2004b). Metal enrichment of glandular leaf trichomes has been observed in non-accumulators such as Cu with *Cannabis sativa* (Arru et al., 2004) and Zn/Cd with *Nicotiana tabacum* (Choi et al., 2001; Sarret et al., 2006). Currently, no consensus exists for the role of Mn in Ni (or Co) sequestration in *Alyssum* or whether the basal compartment of trichomes on hyperaccumulator leaves functions as a significant repository for accumulated metals (Krämer et al., 1997b; Psaras et al., 2000; Küpper et al., 2000, 2001; McNear et al., 2005).

2.5.2 Metal Interactions

Shoot Ni concentrations are not appreciably affected for *A. murale* plants cultivated in mixed-metal systems containing less than 50 μM Co or Zn. Plants from the Ni + Co + Zn treatment have the highest shoot Co concentrations, suggesting Zn has a synergistic effect on Co uptake; the effects of Co on plants was reviewed by Palit et al. (1994) who noted Zn often interacts synergistically with Co. Cobalt-treated *A. murale* (Ni + Co & Ni + Co + Zn) had significantly higher shoot S and Mn concentrations than untreated plants. Enhanced S uptake by plants and elevated S in Co-rich leaf regions may be related to a charge balance requirement. Other researchers have found highly significant correlations between S and Ni in individual cells of *Alyssum* using SEM-EDX and attributed the co-localization to SO_4^{2-} functioning as a counter ion (Küpper et al., 2001; Broadhurst et al., 2004a). Enhanced Mn uptake by *A. murale* plants from the Ni + Co & Ni + Co + Zn treatments may be related to the

stability of transition metal complexes; the Irving-Williams series (Irving & Williams 1948) predicts displacement of Mn from anionic functional groups (e.g. root cell wall surfaces) in the presence of Ni, Co, or Zn.

Competition between metals is not evident under the conditions imposed in this study. Cobalt frequently interacts antagonistically with Ni, Fe, and Mn in plants (Kabata-Pendias & Kabata 1984; Palit et al., 1994), and antagonistic interactions between Ni and Co are observed for *Alyssum* species under specific experimental conditions. For instance, Gabbrielli et al. (1991) evaluated Co and Zn tolerance and uptake in the Ni hyperaccumulator *Alyssum bertolonii* and suggested plants were tolerant to Co and Zn but noted these metals compete with Ni accumulation; this antagonistic interaction occurred with *Alyssum* seedlings during a toxicity assay (i.e. very high metal concentrations). *Alyssum* plants hyperaccumulated Co (1320 mg kg⁻¹ DW) from a Co-amended soil but accumulated significantly less Co (< 20 mg kg⁻¹ DW) from a refinery-contaminated soil with a high Ni to Co ratio (70 : 1) (Malik et al., 2000). Cobalt and Ni accumulation by *Alyssum* species in single and mixed-metal media (several hundred mg kg⁻¹ metal) was investigated by Homer et al. (1991) who attributed lower Ni levels in plants to suppressed Ni uptake by Co ions.

Nickel and Co are expected to interact antagonistically due to competition for semi-selective transport proteins in roots, while Zn is not expected to interfere appreciably with Ni absorption (except by cation competition) because it is not hyperaccumulated by *Alyssum*. High Ni and Co concentrations will increase

competition for root metal transporters and for intercellular ligands participating in metal absorption, long-distance transport, or metal detoxification. Exposure of the hyperaccumulator *Alyssum lesbiacum* to Ni resulted in a dose-dependent increase in xylem fluid Ni concentration and free histidine (Krämer et al., 1996); thermodynamic calculations (Geochem PC) predicted nearly all free histidine (> 97 %) was complexed with Ni. Kerkeb & Krämer (2003) later suggested a role for free histidine in radial transport and xylem loading of Ni in *Alyssum*. Nickel/Co antagonism in *Alyssum* may be related to competition for intercellular ligands. Ligands with a greater affinity for Ni than for Co can facilitate selective accumulation (Still & Williams 1980); however, selective accumulation or antagonistic interactions may not be evident unless the free metal ion (Ni + Co) concentration exceeds the concentration of metal-binding ligands.

2.5.3 Metal Tolerance and Sequestration

Metal tolerance and accumulation mechanisms in *A. murale* do not appear directly correlated. *A. murale* concentrates Ni in shoot tissue to abnormal levels (hyperaccumulation mechanism) and has a Ni-specific tolerance mechanism (vacuolar sequestration) to prevent damage to photosynthetically active tissue. Similarly, *A. murale* concentrates Co in shoot tissue but lacks an equivalent cellular-level sequestration mechanism to confer Co tolerance. In fact, Morrison (1980) noted *Alyssum* is less tolerant to Co than Ni. An underlying relationship between metal accumulation and tolerance remains unclear. For instance, variability in Zn tolerance between populations of *Thlaspi caerulescens* from a Zn-mine contaminated and an

uncontaminated site was not associated with a variation in the ability to accumulate Zn, suggesting tolerance and hyperaccumulation were independent traits (Ingrouille & Smirnoff 1986). Similarly, high metal transport ability was coupled with low metal tolerance in the non-accumulator *Thlaspi arvense* (Krämer et al., 1997a). While correlations between hyperaccumulation and tolerance have been observed in populations of taxonomically-related hyperaccumulator and non-accumulator species (Homer et al., 1991; Krämer et al., 1996, 1997a; Chaney et al., 1997; Salt & Krämer, 2000), intraspecies comparisons have revealed independent genetic variation in these two traits for *Thlaspi caerulescens* (Macnair et al., 1999, 2000; Schat et al., 2000; Pollard et al., 2002; Frérot et al., 2005) and *Arabidopsis halleri* (Macnair et al., 1999; Bert et al., 2003).

Tolerance strategies are typically metal specific (Schat et al., 2000; Walker & Bernal 2004), relying on unique biochemical processes to mediate metal transport across cell membranes (e.g. vacuolar tonoplast) as well as intercellular ligands for chelation of metals (Schat et al., 2000). Previous research has identified the importance of organic and amino acids in metal transport and detoxification in hyperaccumulators (e.g. *Alyssum* and *Thlaspi*). Since free metal ions are the most cytotoxic form of trace elements (e.g. Co and Ni), accumulator plants need specialized tolerance mechanisms to prevent disruption of normal metabolic functions.

Accumulator plants attain (hyper)tolerance through chemical binding (detoxification)

and intracellular sequestration (Brooks et al., 1977; Baker 1981; Küpper & Kroneck 2005).

A. murale plants alleviate Co toxicity via an exocellular sequestration mechanism. Depending on the definition of tolerance, one can argue *A. murale* achieves Co tolerance through a chemical-binding mechanism, presumably involving O and N donor ligands, coupled to an exclusion mechanism involving excretion (possibly via hydathodes) and deposition of the metal on leaf surfaces. Deposition on leaf surfaces exposes the metal species to diverse environmental conditions (e.g. microbial activity, dehydration, light, etc.) and can lead to formation of sparingly-soluble phases via molecular-level restructuring. Cobalt excreted from *A. murale* forms cobalt-rich mineral precipitate(s) on leaf surfaces. Several component mechanisms of metal tolerance can be recognized: 1) metal detoxification via complexation with ligands, 2) metal sequestration in cellular compartments, 3) metal sequestration via exocellular deposition, and 4) metal detoxification by formation of sparingly-soluble phases.

Ultimately, understanding the physiological and biochemical processes underlying metal acquisition, accumulation, and tolerance will permit optimization of metal phytoextraction and aid developments in the production of nutrient-fortified foods. A mechanistic understanding of the highly selective metal transport system linked to Ni tolerance in *A. murale* (vacuolar transporter of leaf epidermal cells) should prove useful for identifying metal transporter(s) in roots or xylem, thus offering

insight to the lack of metal selectivity at the plant-mineral-H₂O interface.

Accumulator plants with the capacity for “simultaneous hyperaccumulation” can evolve with a cellular-level tolerance mechanism for one metal (Ni) but may not develop a similar mechanism to confer (hyper)tolerance for a co-accumulated metal (Co), especially when environmental conditions limit the need for adaptation (e.g. low bioavailability in the natural environment). These data agree with previous hypotheses and support observations suggesting metal tolerance and accumulation mechanisms can be independent. Accumulator plants lacking cellular-level tolerance for an accumulated metal must resort to alternate sequestration strategies to maintain metal homeostasis; *A. murale* relies on an extracellular sequestration mechanism for Co. *A. murale* can be used to remediate Co-enriched soils or industrial wastewater in select circumstances, and Ni phytomining can occur successfully with elevated Co or Zn in (soil) solution.

References

- Adriano DC. 1986. *Trace Elements in the Terrestrial Environment*. New York, USA: Springer-Verlag Inc., 1-18.
- Arru L, Rognoni S, Baroncini M, Bonatti PM, Perata P. 2004. Copper localization in *Cannabis sativa* L. grown in a copper-rich solution. *Euphytica* 140:33-38.
- Baker AJM. 1981. Accumulators and excluders- strategies in the response of plants to heavy metals. *J. Plant. Nutr.* 3:643-654.
- Bert V, Meerts P, Saumitou-Laprade P, Salis P, Gruber W, and Verbruggen N. 2003. Genetic basis of Cd tolerance and hyperaccumulation in *Arabidopsis halleri*. *Plant Soil* 249:9-18.
- Bidwell SD, Crawford SA, Woodrow IE, Sommer-Knudsen J, Marshall AT. 2004. Sub-cellular localization of Ni in the hyperaccumulator *Hybanthus floribundus* (Lindley) F. Muell. *Plant Cell Environ.* 27:705-716.
- Broadhurst CL, Chaney RL, Angle JA, Erbe EF, Mangel TK. 2004a. Nickel localization and response to increasing Ni soil levels in leaves of the Ni hyperaccumulator *Alyssum murale*. *Plant Soil* 265: 225-242.
- Broadhurst CL, Chaney RL, Angle JS, Mangel TK, Erbe EF, Murphy CA. 2004b. Simultaneous hyperaccumulation of nickel, manganese, and calcium in *Alyssum* leaf trichomes. *Environ. Sci. Technol.* 38:5797-5802.
- Brooks RR, Lee J, Reeves RD, Jaffré T. 1977. Detection of nickeliferous rocks by analysis of herbarium specimens of indicator plants. *J. Geochem.Explor.* 7:49-57.
- Chaney RL. 1983. Plant uptake of inorganic waste constituents. In: Parr JF, Marsh PB, Kla JM, eds. *Land treatment of hazardous wastes*. Park Ridge, USA: Noyes Data Corp., 50-76.
- Chaney RL. 1988. Plants can utilize iron from Fe-N, N'-di-(2-hydroxy-benzoyl)-ethylenediamine-N, N'-diacetic acid, a ferric chelate with 10^6 greater formation constant than Fe-EDDHA. *J. Plant Nutr.* 11:1033-1050.
- Chaney RL, Malik M, Li YM, Brown SL, Brewer EP, Angle JS, Baker AJM. 1997. Phytoremediation of soil metals. *Curr. Opin. Biotechnol.* 8:279-284.

- Chaney RL, Angle JS, Li YM. 2004. Method for phytomining of nickel, cobalt, and other metals from soil. US patent 5,944,872.
- Choi YE, Harada E, Wada M, Tsuboi H, Morita Y, Kusano T, Sano H. 2001. Detoxification of cadmium in tobacco plants: formation and active excretion of crystals containing cadmium and calcium through trichomes. *Planta* 213:45-50.
- Dixon NE, Gazola C, Blakeley RL, Zerner B. 1975. Jack bean urease (EC 3.5.1.5), a metalloenzyme. A simple biological role for nickel? *J. Am. Chem. Soc.* 97:4131-4133.
- Dowd BA, Campbell GH, Marr RB, Nagarkar VV, Tipnis SV, Axe L, Siddons DP. 1999. Developments in synchrotron X-ray computed microtomography at the National Synchrotron Light Source. Proceedings of SPIE, Developments in X-ray Tomography II, 3772:224-236.
- Fellows RJ, Wang Z, Ainsworth CC. 2003. Europium uptake and partitioning in Oat (*Avena sativa*) roots as studied by laser-induced fluorescence spectroscopy and confocal microscopy profiling technique. *Environ. Sci. Technol.* 37:5247-5253.
- Frérot H, Lefèbvre C, Petit C, Collin C, Dos Santos A, Escarré J. 2005. Zinc tolerance and hyperaccumulation in F 1 and F 2 offspring from intra and interecotype crosses of *Thlaspi caerulescens*. *New Phytol.* 165:111-119.
- Frey B, Keller C, Zierold K, Schulin R. 2000. Distribution of Zn in functionally different leaf epidermal cells of the hyperaccumulator *Thlaspi caerulescens*. *Plant Cell Environ.* 23:675-687.
- Gabbrielli R, Mattioni C, Vergnano O. 1991. Accumulation mechanisms and heavy metal tolerance of a nickel hyperaccumulator. *J. Plant Nutr.* 14:1067-1080.
- Gustafson FG. 1956. Absorption of ⁶⁰Co by leaves of young plants and its translocation through the plant. *Am. J. Bot.* 43:157-160.
- Hamilton EI. 1994. The geobiochemistry of cobalt. *Sci. Total Environ.* 150:7-39.
- Handreck KA & Riceman DS. 1969. Cobalt distribution in several plant species grown in culture solutions. *Australian Journal of Agricultural Research* 20:213-226.
- Heath SM, Southworth D, Allura JAD. 1997. Localization of nickel in epidermal subsidiary cells of leaves of *Thlaspi montanum* var. *siskiyouense* (Brassicaceae) using energy-dispersive X-ray microanalysis. *Int. J. Plant. Sci.* 158:184-188.

- Homer FA, Morrison RS, Brooks RR, Clemens J, Reeves RD. 1991. Comparative studies of nickel, cobalt, and copper uptake by some nickel hyperaccumulators of the genus *Alyssum*. *Plant Soil* 138:195-205.
- Ingrouille MJ & Smirnoff N. 1986. *Thlaspi caerulescens* J. & C. Presl. (*T. alpestre* L.) in Britain. *New Phytol.* 102:219-233.
- Irving H & Williams RJP. 1948. Order of stability of metal complexes. *Nature* 6:746-747.
- Kabata-Pendias A & Kabata H. 1984. *Trace elements in soils and plants*. Boca Raton, USA: CRC Press Inc., 238-246.
- Kerkeb L & Krämer U. 2003. The Role of Free Histidine in Xylem Loading of Nickel in *Alyssum lesbiacum* and *Brassica juncea*. *Plant Physiol.* 131:716-724.
- Kim SA, Punshon T, Lanzirotti A, Li L, Alonso JM, Ecker JR, Kaplan J, Guerinot ML. 2006. Localization of iron in *Arabidopsis* seed requires the vacuolar membrane transporter VIT1. *Science* 314:1295-1298.
- Krämer U, Cotterhowells JD, Charnock JM, Baker AJM, Smith JC. 1996. Free histidine as a metal chelator in plants that accumulate nickel. *Nature* 379:635-638.
- Krämer U, Grime GW, Smith JAC, Hawes CR, Baker AJM. 1997b. Micro-PIXE as a technique to study nickel localization in leaves of the hyperaccumulator plant *Alyssum lesbiacum*. *Nucl. Instr. Meth. in Phys. Res. B* 130:346-350.
- Krämer U, Smith RD, Wenzel WW, Raskin I, Salt DE. 1997a. The role of metal transport and tolerance in nickel hyperaccumulation by *Thlaspi goesingense* Halacsy. *Plant Physiol.* 115:1641-1650.
- Krämer U, Pickering IJ, Prince RC, Raskin I, Salt DE. 2000. Subcellular localization and speciation of nickel in hyperaccumulator and non-accumulator *Thlaspi* species. *Plant Physiol.* 122:1343-1354.
- Kukier U, Peters CA, Chaney RL, Angle JS, Roseberg RJ. 2004. The effect of pH on metal accumulation in two *Alyssum* species. *J. Environ. Qual.* 33:2090-2102.
- Küpper H, Zhao FJ, McGrath SP. 1999. Cellular compartmentation of zinc in leaves of the hyperaccumulator *Thlaspi caerulescens*. *Plant Physiol.* 119:305-311.

- Küpper H, Lombi E, Zhao FJ, McGrath SP. 2000. Cellular compartmentation of cadmium and zinc in relation to other elements in the hyperaccumulator *Arabidopsis halleri*. *Planta* 212:75-84.
- Küpper H, Lombi E, Zhao FJ, Wieshammer G, McGrath SP. 2001. Cellular compartmentation of nickel in the hyperaccumulator *Alyssum lesbiacum*, *Alyssum bertolonii*, and *Thlaspi goesingense*. *J. Exp. Bot.* 52:2291-2300.
- Küpper H & Kroneck PMH. 2005. Heavy metal uptake by plants and cyanobacteria. In: Sigel A, Sigel H, Sigel R eds. *Metal ions in Biological Systems*, vol. 44. New York, USA: Marcel Dekker, 97-142.
- Langston R. 1956. Distribution patterns of radioisotopes in plants. *Proc. Am. Soc. Hort. Sci.* 68:370-376.
- Li YM, Chaney RL, Brewer E, Roseberg R, Angle JS, Baker AJM, Reeves R, Nelkin J. 2003a. Development of a technology for commercial phytoextraction of nickel: economic and technological considerations. *Plant Soil* 249:107-115.
- Li YM, Chaney RL, Brewer EP, Angle JS, Nelkin J. 2003b. Phytoextraction of nickel and cobalt by hyperaccumulator *Alyssum* species grown on nickel-contaminated soils. *Environ. Sci. Technol.* 37:1463-1468.
- Macnair MR, Bert V, Huitson SB, Saumitou-Laprade P, Petit D. 1999. Zinc tolerance and hyperaccumulation are genetically independent characters. *Proc. Roy. Soc. B.* 266:2175-2179.
- Macnair MR, Tilstone GH, Smith SE. 2000. The genetics of metal tolerance and accumulation in higher plants. In: Terry N, Bañuelos G, eds. *Phytoremediation of Contaminated Soil and Water*. Boca Raton, USA: Lewis Publishers, 235-250.
- Malik M, Chaney RL, Brewer EP, Li Y, Angle JS. 2000. Phytoextraction of soil cobalt using hyperaccumulator plants. *Int. J. Phytoremed.* 2:319-329.
- Marcus MA, MacDowell AA, Celestre R, Manceau A, Miller T, Padmore HA, Sublett RE. 2004. Beamline 10.3.2 at ALS: a hard X-ray microprobe for environmental and materials sciences. *J. Synchrotron Rad.* 11: 239-247.
- Marschner H. 1995. *Mineral nutrition of higher plants* (2nd ed.). New York, USA: Academic Press.

- McNear Jr. DH, Peltier E, Everhart J, Chaney RL, Newville M, Rivers M, Sutton S, Sparks DL. 2005. Application of quantitative fluorescence and absorption-edge computed microtomography to image metal compartmentalization in *Alyssum murale*. *Environ. Sci. and Technol.* 39: 2210-2218.
- Mesjasz-Przybylowicz J, Przybylowicz WJ, Prozesky VW, Pineda CA. 1997. Quantitative micro-PIXE comparison of elemental distribution in Ni-hyperaccumulating and non-accumulating genotypes of *Senecio coronatus*. *Nucl. Instr. Meth. Phys. Res. B* 130:368-373.
- Mizuno N, Takahashi A, Wagatsuma T, Mizuno T, Obata H. 2002. Chemical composition of guttation fluid and leaves of *Petasites japonicus* var. *giganteus* and *Polygonum cuspidatum* growing on ultramafic soil. *Soil Sci. Plant Nutr.* 48:451-453.
- Morrison Richard S. 1980. *Aspects of the accumulation of cobalt, copper, and nickel by plants*. PhD thesis, Massey University, Palmerston North, New Zealand.
- Norkus E, Vaskelis A, Griguceviciene A, Rozovskis G, Reklaitis J, and Norkus P. 2001. Oxidation of cobalt(II) with air oxygen in aqueous ethylenediamine solutions. *Transition Metal Chemistry* 26:465-472.
- Neumann D, zur Nieden U, Schwieger W, Leopold I, Lichtenberger O. 1997. Heavy metal tolerance of *Minuartia verna*. *J. Plant Physio.* 151:101-108.
- Neumann D, zur Nieden U. 2001. Silicon and heavy metal tolerance of higher plants. *Phytochem.* 56:685-692.
- Palit S, Sharma A, Talukder G. 1994. Effects of cobalt on plants. *Bot. Rev.* 60:149-181.
- Pollard AJ, Powell KD, Harper FA, Smith JAC. 2002. The genetic basis of metal hyperaccumulation in plants. *Crit. Rev. Plant Sci.* 21:539-566.
- Psaras GK, Constantinidis T, Cotsopoulos B, Manetas Y. 2000. Relative abundance of nickel in the leaf epidermis of eight hyperaccumulators: evidence that the metal is excluded from both guard cells and trichomes. *Ann. Bot.* 86:73-78.
- Rivers M & Wang Y. 2006. Recent developments in microtomography at GeoSoil-EnviroCARS. In: Bonse U, ed. *Developments in X-ray tomography V*. Proc. SPIE, 6318(OJ-):1-15.

- Salt DE & Krämer U. 2000. Mechanism of metal hyperaccumulation in plants. In: Raskin L, Ensley BD, eds. *Phytoremediation of Toxic Metals*. New York, USA: John Wiley, 231-236.
- Sarret G, Harada E, Choi YE, Isaure MP, Geoffroy N, Birschwilks M, Clemens S, Fakra S, Marcus MA, Manceau A. 2006. Trichomes of tobacco excrete zinc as Zn-substituted calcium carbonate and other Zn-containing compounds. *Plant Physiol.* 141:1021-1034.
- Schat H, Llugany M, Bernhard R. 2000. Metal-specific patterns of tolerance, uptake, and transport of heavy metals in hyperaccumulating and nonhyperaccumulating metallophytes. In: Terry N, Bañuelos G, eds. *Phytoremediation of Contaminated Soil and Water*. Boca Raton, USA: Lewis Publishers, 171-188.
- Scheckel KG, Lombi E, Rock SA, McLaughlin MJ. 2004. *In vivo* synchrotron study of Thallium speciation and compartmentalization in *Iberis intermedia*. *Environ. Sci. Technol.* 38:5095-5100.
- Sparks DL. 2003. *Environmental Soil Chemistry (2nd ed.)*. New York, USA: Academic Press, 133-186.
- Still ER & Williams RJP. 1980. Potential methods for selective accumulation of Nickel(II) ions by plants. *J. Inorg. Biochem.* 13:35-40.
- Sutton S, Bertsch PM, Newville M, Rivers M, Lanzirotti A, Eng P. 2002. Microfluorescence and microtomography analyses of heterogeneous earth and environmental materials. In: Fenter PM, Rivers M, Sturchio N, Sutton S, eds. *Applications of Synchrotron Radiation in Low-temperature Geochemistry and Environmental Science Vol. 49*. Washington DC, USA: Mineralogical Society of America, 429-483.
- Vergnano O. & Hunter JG. 1952. Nickel and cobalt toxicities in Oat plants. *Annals of Botany* 17:317-329.
- Walker DJ & Bernal MP. 2004. The effects of copper and lead on growth and zinc accumulation of *Thlaspi caerulescens* J. and C. Presl: Implications for phytoremediation of contaminated soils. *Water Air Soil Pollut.* 151:361-372.
- Welch RM. 1995. Micronutrient nutrition of plants. *Crit. Rev. Plant Sci.* 14:49-82.

Chapter 3

COBALT SPECIATION IN THE NICKEL/ COBALT HYPERACCUMULATOR

ALYSSUM MURALE: AN *IN SITU* MICROSPECTROSCOPIC INVESTIGATION

3.1 Summary

In this study, the chemical form of Co in roots, stems, leaves, and leaf tips of *Alyssum murale* were investigated *in situ* using bulk and microfocused X-ray absorption fine structure spectroscopy (XAFS). Metal localization and elemental associations in plant tissues were investigated with synchrotron-based X-ray fluorescence imaging (SXRF) and scanning electron microscopy (SEM-EDX). Xylem fluid chemistry was determined with high performance liquid chromatography. The ligands involved in Co transport and detoxification in the Ni/ Co hyperaccumulator *A. murale* were identified as well as the chemical forms of Co preferentially sequestered on leaf tips.

3.2 Introduction

Unique metallophyte plant species (hyperaccumulators) have evolved an ability to concentrate trace metals in their harvestable biomass, and thereby offer a sustainable method for treatment of metal contaminated sites (phytoremediation) and an opportunity to mine metal rich soils (phytomining) (Chaney 1983). Metal

hyperaccumulator plants can absorb, translocate, and compartmentalize about 100 times more metals in aerial tissue than normal crop plants. Several plants in the *Brassicaceae* family (including *Alyssum*) have demonstrated the ability to hyperaccumulate Ni (up to 10,000 mg/kg) in previous laboratory and field studies. Cultivating hyperaccumulator plants on Ni-rich soils and ashing the harvestable biomass to produce Ni ore (bio-ore) is an economically sound alternative for metal recovery (Chaney 1983; Chaney et al., 2004).

Synchrotron μ -XRF, XAFS, and XRD can be used to probe (*in situ*) metal speciation and localization in hyperaccumulator plants with micrometer resolution. Researchers have applied various synchrotron techniques to the investigation of metals in hyperaccumulator plants. Küpper et al. (2004) used XAFS to investigate differences in metal complexation in the Zn hyperaccumulator *Thlaspi caerulescens* exposed to elevated Zn and Cd. Several varieties of *Thlaspi* can simultaneously hyperaccumulate zinc and cadmium. The Cd-challenged plants showed mild symptoms of toxicity during early stages of growth. Zinc was complexed by nitrogen and oxygen ligands in all the tissues analyzed, while a considerable percentage of Cd (~30 %) accumulated by *Thlaspi* was bound to sulfur ligands. Age- and tissue-dependent differences in the metal binding environments were observed for these two metals. These researchers attribute the differences in metal complexation to disparate detoxification strategies, and argue metal detoxification through vacuolar sequestration (by organic acids already functioning as counterions) is energetically favorable for

plants rather than investing excess energy to synthesize large amounts of specialized ligands (e.g. S-rich) required to bind a specific metal.

[Sarrat et al. \(2002\)](#) used bulk and microfocused XAFS to investigate the forms of Zn accumulated in *Arabidopsis halleri*. In aerial parts, Zn was predominantly octahedrally coordinated and complexed to malate. A secondary organic species in which Zn was tetrahedrally coordinated was found in the bases of trichomes by μ -EXAFS but could not be identified. In the roots of hydroponically-grown *A. halleri*, the only Zn species detected was Zn phosphate; the phosphate concentration in nutrient solutions was too high for the Zn accumulation experiment leading to chemical precipitation of ZnPO_4 . Zinc speciation in stem tissue was not determined.

Previous work with Ni hyperaccumulators has demonstrated the importance of organic and amino acids in plant metal homeostasis. For example, nickel absorbed by *Alyssum* roots becomes complexed by free histidine and transported to the xylem ([Krämer et al., 1996](#); [Kerkeb and Krämer, 2003](#)). In the transpiration stream, oxygen-donor ligands (e.g. malate) are involved with Ni detoxification and transport. The majority of nickel translocated to the shoots is compartmentalized in epidermal cell vacuoles, forming a metal–ligand complex unable to exit the tonoplast (vacuolar membrane). Vacuolar sequestration is a key mechanism for metal (hyper)tolerance in hyperaccumulators ([Krämer et al., 2000](#); [Persans et al., 2001](#)), offering a means of metal storage in plants where the least amount of damage to photosynthetic tissues is expected to occur. Accumulated metals

can also be sequestered by association with cell wall material, which have functional groups bearing net-negative charge (bind metals).

It is crucial to know whether accumulated metals are bound by strong (specific) ligands or loosely associated with common organic acids within plant cells and cell vacuoles (i.e. metal speciation) (Küpper et al., 2004). Information on the speciation, localization, and associations of accumulated metals with other elements in hyperaccumulator plants can provide insight into the physiological and biochemical mechanisms of metal tolerance and accumulation. Ultimately, understanding of the mechanisms underlying metal hyperaccumulation and tolerance will permit optimization of metal extraction.

In our previous investigation of Co and Ni accumulation and compartmentalization in Ni/ Co hyperaccumulator *Alyssum murale* (Chapter 2), it was determined that *A. murale* uses a different storage mechanism for Co (exocellular sequestration) than for Ni (vacuolar sequestration), and thus the specialized biochemical processes linked with Ni (hyper)tolerance in *Alyssum* do not confer (hyper)tolerance to Co. Additionally, the formation of Co-rich mineral precipitates on the leaves of Co-treated plants was observed, representing a novel sequestration mechanism involved in Co detoxification (tolerance). The aim of the present study was to determine the chemical form of Co in the Co-rich deposits localized on the surface of *A. murale* leaves as well as determine the speciation of Co in root, stem, and leaf tissues.

3.3 Methods

3.3.1 Experimental Design

Cobalt speciation in the roots, stems, and leaves of Ni/ Co hyperaccumulator *A. murale* “Kotodesh” was investigated *in situ* with bulk and micro-focused X-ray absorption spectroscopy, and results were interpreted in light of elemental and organic acids concentrations. Cobalt localization and elemental associations in plant tissue were observed with μ -SXRF imaging. High-resolution imaging and light-element detection was conducted with scanning electron microscopy coupled with energy dispersive X-ray spectroscopy (SEM-EDX). *A. murale* plants cultivated in Co-enriched nutrient solution were harvested and analyzed for total cobalt content after six weeks metal exposure. Naturally-bleeding xylem fluid was collected from plants grown in Co-enriched and Co-depleted nutrient solutions. Xylem fluid chemistry was investigated with high performance liquid chromatography (HPLC). Randomly selected plants were transported to a synchrotron facility for analysis by μ -SXRF, μ -XAFS and μ -XRD.

3.3.2 Plant Propagation and Cultivation

Alyssum plants were propagated and cultivated by the methods described by [Tappero et al. \(2007\)](#). Briefly, apical cuttings were collected from a mature “mother” plant and treated with Indole-3-butyric acid (rooting hormone). Cuttings were placed into propagation cubes (spun silica glass) and kept in a clone box (constant light and high humidity) until roots protruded from the bottom of the cube.

Alyssum plants were transferred into 4-inch pots filled with acid-washed and rinsed perlite. Plastic mesh covered the drainage holes to retain the perlite, and a layer of inert rock was placed on top of the perlite to minimize light penetration and algal growth. *Alyssum* plants were placed in a greenhouse and pre-cultured for three weeks prior to metal exposure. Photoperiod was set to 16 h with $> 400 \mu\text{mol m}^{-2} \text{s}^{-1}$ photosynthetically active radiation from a combination of high-pressure sodium (HPS) lamps and natural sunlight. The temperature was maintained at 25 and 20° C during the day and night, respectively. Plants were irrigated with a dilute nutrient solution designed to mimic the conditions in a serpentine soil (3.1 mM NO₃; 0.33 mM PO₄; 1.33 mM K; 1.25 mM Mg; 0.5 mM Ca; 0.75 mM SO₄; 10 μM B; 2 μM Mn; 1 μM Zn; 0.1 μM Cu; 0.1 μM Mo; 20 μM Fe-HBED). Iron HBED (Fe-N, N'-di-(2-hydroxybenzoyl)-ethylenediamine-N, N'-diacetic acid) was used to prevent metal chelation interactions (Chaney 1988). Nutrient solution contained basal or elevated Co (25 - 50 μM) and was buffered at pH 6.1 with 2 mM MES (K-salt). Cobalt was added from a stock solution prepared from the nitrate salt. Nutrient solution was replaced weekly. Plants were harvested and analyzed for total Co content after six weeks metal exposure. Xylem fluids were collected from plants and analyzed for organic acid anions.

3.3.3 Plant Tissue Analysis

Immediately following harvest, *Alyssum* shoots were triple-rinsed in deionized water to remove any adhering dust particles. Plant material was oven-dried

at 65° C to a constant weight (approximately 48 h). Dry plant tissue was ground with a plastic herb grinder (420 Grinder Company) and homogenized. Plant tissue samples were acid digested using a modified EPA 3051 method. For each sample, 0.500 gram (+/- 0.05) of plant tissue was microwave digested in 10 mL of concentrated HNO₃. The digest was filtered (0.22 µm) and brought to 30 mL total volume with deionized water. Samples were analyzed for Co, Ni, Zn, Mn, Fe, Mg, Ca, K, S, B, and P by inductively coupled plasma atomic emission spectrometry (ICP–AES). Sample duplicates were within 5 % agreement and the Co and Ni levels measured for the NIST spinach standard were within the range specified by NIST.

3.3.4 Extraction and Analysis of Naturally-Bleeding Xylem Fluid

Plants were cultivated in Co-enriched or depleted nutrient solutions for six weeks, and naturally-bleeding xylem fluid was collected by a method modified from [White et al. \(1981\)](#). Two hours after onset of the photoperiod, plant stems were cut several millimeters above the perlite–rock surface, and naturally bleeding xylem fluid was collected with a needle and syringe. Xylem fluids were placed into light-shielded PCR vials, filtered (0.45 µm centrifugal filter device), and analyzed immediately by HPLC (minimal sample pre-treatment). A separate portion of xylem fluids were stored in PCR vials at –30 ° C; prior to analysis, these xylem fluids were lyophilized to dryness and then reconstituted in potassium phosphate buffer solution (i.e. mobile phase). Organic acid anions (OAAs) in xylem fluid were analyzed with a Dionex high performance liquid chromatography (HPLC) system equipped with a C-18 column

using potassium phosphate solution (25 mM, pH 2.0) as the mobile phase (isocratic). The sample injection volume was 10 μL and the flow rate was set at 1 mL min^{-1} for the separations. Absorbance was monitored at multiple wavelengths and was measured with a UV photodiode array detector at 220 nm wavelength.

3.3.5 Electron Probe Micro-analysis (EPMA)

SEM-EDX was used to collect high-resolution images of leaves from Co-treated *A. murale* plants (i.e. observe Co-rich regions near leaf tips) and to detect correlations between accumulated metals and lighter elements (e.g. Si and S). Scanning electron micrographs were recorded using a Hitachi 4700 FESEM. Leaves were dried over CaCl_2 pellets in a desiccator (48 hrs.) or were flash frozen in liquid nitrogen and then freeze dried under vacuum prior to micro-analysis. Plant tissue samples were mounted on a conductive carbon stub and sputter-coated with carbon to reduce charging effects. Samples were scanned manually at magnifications of 85 to 300 x.

3.3.6 Bulk XAFS Spectroscopy

Cobalt K-edge XAFS spectra of plant tissue samples and Co reference compounds were collected at beamline X-11A at the National Synchrotron Light Source (NSLS), Upton, NY. The electron storage ring operated at 2.5 GeV yielding an electron beam of 300–100 mA. Energy resolution was achieved with a silicon (111) double-crystal monochromator. The ionization chamber (Io) was filled with 10 % N_2 and 90 % Ar, and the beam was detuned by 30 % in Io to reject higher-order

harmonics. The beam energy was calibrated by assigning the first inflection on the K-absorption edge of a metal foil to the elemental edge energy (7709 eV). Data were collected in fluorescence mode using a Stern–Heald (Lytle) detector (filled with Ar) equipped with a Fe (Z–1) filter to minimize elastically scattered radiation (Lytle et al., 1984), or in transmission mode using an ion chamber (I_t) filled with nitrogen gas and trace amounts of argon to achieve optimal absorption in the desired energy range. Powder samples were mounted into Acrylic sample holders, sealed with Kapton tape, and run under ambient conditions (25 °C). Multiple scans were collected until satisfactory signal–to–noise ratios were achieved.

High purity reference compounds were synthesized from reagent grade materials using procedures established in the literature or were purchased as commercial, high-purity chemical reagents; synthetic precipitates are the most reliable reference compounds due to the difficulty of obtaining mineralogically-pure geologic specimens. Reference phases include pure metal hydroxides and carbonates (purchased from Alfa Aesar), a hydrated cobalt carbonate hydroxide (synthesized by the method of Zheng and Xie, 2004), mixed metal-Al hydroxides (synthesized by the method modified from Taylor, 1984 and described in Thompson et al., 1996 and Peltier et al., 2006), metal-bearing hydrous layer silicates (synthesized by the method of Decarreau 1981; Decarreau 1985), metal-ligand coordination polymers such as Co-fumarate_(s) M₃L₂ (synthesized by method of Zheng and Xie, 2004), and aqueous solutions of metal-ligand complexes. Aqueous Co standards (metal–ligand

complexes) were prepared by reacting 300 mM ligand with 30 mM Co(II) at constant pH (6.5). Aliquots of the aqueous standards were sealed into acrylic sample holders with Mylar film, and were refrigerated and stored in the dark until analysis.

3.3.7 Synchrotron-based Spectromicroscopy

Synchrotron-based spectromicroscopic methods for X-ray fluorescence imaging (μ -SXRF) and extended X-ray absorption fine structure spectroscopy (μ -EXAFS) were described in [Tappero et al. \(2007\)](#). Spectra from hydrated plant tissue were collected at beamline 10.3.2 of the Advanced Light Source (ALS), Lawrence Berkeley National Lab, Berkeley, CA. A complete description of the beamline hardware and operation can be found in [Marcus et al. \(2004\)](#). Fresh plant samples were excised from live plants, mounted (with no further preparation) in a thin film of Si grease to a sheet of Mo or Ag foil that was attached to the Peltier (thermoelectric) cooler module on the XY sample stage; tissue samples were rapidly cooled to -30 °C. Multi-element μ -SXRF images of Co-treated *A. murale* leaves were collected to observe elemental localization and spatial associations; the images were used to select regions of interest (ROIs) for μ -XAFS and μ -XRD data collection.

A novel distance (X) vs. energy (E) scan routine was compiled from pre-existing SXRF and XAFS scan routine protocols ([Marcus et al., 2004](#)) and was tested in a line-scan mode. An XE scan records the X-ray fluorescence at each step (e.g. 10 μ m) along a line (X direction) starting with the incident beam energy fixed below the elemental absorption edge and then repeating these absorption measurements with

incrementally higher (e.g. 1 eV) incident beam energies until the desired end energy is reached (e.g. extended region of XAS). In this way, an XAS spectrum is recorded for each pixel area in the XE scan. Likewise, one can collect spatially-resolved spectroscopic information for a defined sample area (e.g. 100 x 100 μm) by performing a series of XE scans (i.e. 'spectromicroscopic imaging'). These large spectral datasets can be analyzed statistically by principle component analyses followed by target transformation and a linear least squares fit procedure. Uniquely identifiable features in the spectral dataset (i.e. contributions from known species) can be isolated with software-based algorithms and used to generate images showing the spatial distribution for each unique chemical species identified within the sample area; a similar protocol is used to generate spectromicroscopic images with Synchrotron Reflectance Fourier Transform Infrared Microscopy (SR-FTIR), Scanning Transmission X-ray Microscopy (STXM), and X-ray microdiffraction, the latter technique yielding "mineral maps" (e.g. map of goethite in soil thin section).

3.3.8 EXAFS Data Analysis

The procedures used for XAFS data analysis were described in [Gräfe et al. \(2008a,b\)](#). XAFS data reduction was performed by standard methods ([Brown et al., 1988](#)). Spectra were energy calibrated, background corrected, and normalized prior to averaging. Normalized spectra were converted from energy units (keV) to photoelectron wave vector units ($\sim\text{\AA}^{-1}$) by assigning the origin (E_0) to the first inflection point of the absorption edge. A spline function was used to extract the chi

oscillations from the XAFS. Fourier transformation (FT) of the raw $k^2\chi^*(k)$ data was performed over a consistent region in k space ($\Delta k = 2.0 - 10.5 \text{ \AA}^{-1}$) and an analog of the radial structure function (RSF) was obtained using the Bessel window function ($\beta = 2$). Single scattering paths for Co–O, Co–N, Co–Si, Co–C, Co–Co, Co–Mg and Co–Mn were generated by FEFF7 (Ankudinov and Rehr, 1997) based on the structures of Co-bearing minerals, or using MO/DFT (molecular orbital/ density functional theory) geometry-optimized molecular clusters of aqueous metal–ligand complexes (Persson and Axe 2005). An estimate of the amplitude reduction factor (S_0^2) was determined by fitting the raw data for a cobalt hydroxide reference material. Multishell fitting (Co–O and Co–Co scattering paths) resulted in a value of approximately 0.85 for S_0^2 when the first-shell Co–O coordination number (CN_{Co-O}) was fixed at 6 (octahedral), and this S_0^2 value was then fixed to fit the experimental data. The errors in the bond distances (R) were estimated to be accurate to $R \pm 0.02 \text{ \AA}$ (first shell) and $R \pm 0.04 \text{ \AA}$ (second shell), and coordination numbers (CN) were accurate to $N \pm 20 \%$ (first shell) and $N \pm 40 \%$ (second shell). Error estimates were determined by a comparison of XRD and EXAFS results for cobalt hydroxide, and were in agreement with estimates previously published (O'Day et al., 1994; Scheidegger et al., 1997). All XAS data analyses were performed with WinXAS version 3.1 (Ressler et al., 1998) or IFEFFIT version 1.2.8 (Newville, 2001; Ravel and Newville, 2005).

Analysis of XAFS spectra collected from multi-component systems often cannot rely on the more rigorous multi-shell fitting procedures. Rather, a spectral dataset obtained from multiple spots throughout the sample can be analyzed statistically using Principal Component Analysis (PCA). Principle components analysis (PCA) describes a large dataset as weighted sums of a smaller number of components, and it has been used by a number of researchers ([Wasserman et al., 1999](#); [Manceau et al., 2000](#); [Grafe et al., 2008b](#)) to analyze spectra from complex, multi-component systems when traditional shell by shell fitting is not appropriate. A statistical fitting approach is requisite to model a dataset from a heterogeneous system because mixed or overlapping atomic shells (within a distance $< 0.1 \text{ \AA}$) may not be separable by shell fitting or may result in erroneous results (e.g. impractically large values for fitting parameters) ([Manceau et al., 2000, 2002](#)). PCA determines the number of abstract factors needed to describe a spectral dataset, and subsequent target transformation (TT) of reference spectra provides the identity of the principle components. Target transformation evaluates reference spectra as components by mathematically removing any part of the signal not describable as a linear combination of the factors, and the amount of signal removed from a reference is measured by a SPOIL value ([Malinowski, 1977](#); [Manceau et al., 2000](#)). Meaningful SPOIL values fall between 0 and 4.5 and have been classified as excellent (0 to 1.5), good (1.5 to 3.0), and fair (3.0 to 4.5) ([Malinowski, 1978](#)). Spectra with the lowest SPOIL values are considered as possible references for the linear least-squares fitting (LLSF) of the

spectral dataset. Linear least-squares fit analysis is used to determine the amounts (weight %) of reference material represented in each sample spectra comprising the experimental dataset (i.e. indicates proportions of mixed-species). Linear least squares fits are often performed with raw chi data; however, the real and imaginary parts of the Fourier transformed data as well as Fourier filtered chi data (i.e. one or more atomic shells isolated by Fourier back-transformation) can be fit by this procedure. Fit residuals defined as the normalized root square difference between the data and the fit are minimized during the fitting procedure. Accuracy of the fit is dependent on the data quality, the data range included in the fit, and how well the standards represent the unknown sample ([Malinowski, 1977, 1978](#)). Components with at least 10 wt % may be detectable by this method ([Manceau et al., 2000](#)).

3.4 Results and Discussion

In our previous investigation of Co and Ni accumulation and compartmentalization in Ni/ Co hyperaccumulator *Alyssum murale* (Chapter 2), it was determined that *A. murale* uses a different storage mechanism for Co (exocellular sequestration) than for Ni (vacuolar sequestration), and thus the specialized biochemical processes linked with Ni (hyper)tolerance in *Alyssum* do not confer (hyper)tolerance to Co. Additionally, the formation of Co-rich mineral precipitates on the leaves of Co-treated plants was observed, representing a novel sequestration mechanism involved in Co detoxification (tolerance). The aim of the present study was to determine the chemical form of Co in the Co-rich deposits localized on the surface of *A. murale* leaves as well as determine the speciation of Co in root, stem, and leaf tissues. Cobalt speciation in *A. murale* was studied by Co K-edge EXAFS on powder samples, and was investigated at the micron scale by X-ray microfluorescence (μ -SXRF) and μ -EXAFS spectroscopy.

3.4.1 Plant Growth and Cobalt Accumulation

All treatments resulted in healthy-looking plants at harvest. Plants in Co-enriched nutrient media had mean \pm S.E. ($n = 4$) shoot Co concentrations of 1420 ± 137 $\mu\text{g/g}$ D.W. (25 μM Co treatment) and 2530 ± 138 $\mu\text{g/g}$ D.W. (50 μM Co treatment); shoot Co reached 4420 ± 122 $\mu\text{g/g}$ D.W. for plants exposed to Co-enriched nutrient solution for 12 weeks. Shoot concentrations of Mn and S were significantly ($P < 0.05$) higher for Co-treated plants than for the control plants. [Tappero et al.](#)

(2007) observed higher shoot S and shoot Mn concentrations for Co-treated *A. murale* plants than for untreated plants, and suggested that elevated uptake of these elements could be related to Co accumulation. Root Co was $871 \pm 40.9 \mu\text{g/g D.W.}$ and stem Co was $411 \pm 49.6 \mu\text{g/g D.W.}$ for the plants from the $50 \mu\text{M Co}$ treatment. The Co translocation factor (i.e. ratio of element concentration in shoot tissue to element concentration in root tissue) was 2.90 and the Co bioconcentration factor (i.e. ratio of metal concentration in shoot tissue to metal concentration in growth media) was 858 for plants treated with $50 \mu\text{M Co}$.

3.4.2 Organic acids in Naturally-bleeding Xylem Fluid

Naturally-bleeding xylem fluid was collected from Co-treated and untreated *A. murale* plants; three independent sets of experimental plants were grown between 03/2006 and 08/2007 to obtain naturally-bleeding xylem fluid for repeat analysis and method optimization. Xylem fluid samples were segregated into a 0 – 1 hr fraction and a 1 – 2 hr fraction. Furthermore, xylem fluids were split into “fresh” (i.e. unaltered) and “lyophilized” samples, the latter were preserved for analysis (i.e. stored at $-30 \text{ }^\circ\text{C}$; freeze-dried under vacuum; reconstituted in 25 mM phosphate buffer, pH=2.0) whereas the “fresh” xylem fluid samples were filtered ($0.45 \mu\text{m}$ centrifugal filtration device) and analyzed immediately for OAAs by HPLC.

Collection time had little influence on the OAA composition of xylem fluids, but it did influence the concentrations of OAA detected in fresh xylem fluids; the 1 – 2 hr fraction was more dilute in OAAs than the 0 – 1 hr fraction. Sample

preservation had minimal influence on the HPLC results for the OAAs detected in *A. murale* xylem fluids; a notable exception was the partial conversion of fumarate to maleate in standard reference materials carried through lyophilization. Therefore, data from the fresh xylem fluids have been reported in this study (Table 3.1).

Table 3.1. Concentrations of major organic acids detected in naturally-bleeding xylem fluid collected from *Alyssum murale* plants.

Treatment	Major organic acids in xylem fluid		
	Fumaric	Citric	Malic
	μM		
Control	74.3 a (4.36)	1090 a (82.7)	1610 a (72.7)
25 μM Co	243 b (11.2)	2030 b (163)	2530 b (120)
50 μM Co	441 c (20.0)	2180 b (167)	2950 b (144)

Values are mean (\pm SE); $n = 3$. Different letters within a column indicate significant difference ($P < 0.05$) with Tukey HSD comparison

The major carboxylic acids ($> 100 \mu M$) detected in *A. murale* xylem exudates are malic and citric acids (control treatment); oxalic acid concentrations are constitutively high as well but efforts to dilute the samples for quantification of this analyte were unsuccessful. Trace amounts of ascorbic and tartaric acids were found in all xylem fluid samples. Succinic and iso-citric acids may also be present in *A. murale* xylem fluids, but these analyte concentrations were near the instrument detection limit and below the practical limit of quantification. Malonic and maleic acids were not

detected in any of the xylem exudates samples. The absence of malonic acid is in apparent contradiction with other studies which have found this organic acid in the extractant solutions prepared from dried and ground whole leaves of other Ni hyperaccumulator species of *Alyssum* (Pelosi et al., 1976; Pancaro et al., 1977; Shaw 1980; Morrison 1980); however, collection and immediate analysis of naturally-bleeding xylem fluid is a direct method that avoids extensive sample pretreatment (e.g. freeze drying, grinding, solvent extraction, volume reduction, treatment with exchange resins, or derivatization).

The concentrations of malic, citric, and fumaric acids increased significantly ($P < 0.05$) upon exposure to Co; however, only fumaric acid concentrations continued to increase with increasing concentrations of Co in nutrient solution. Additionally, fumaric acid showed the greatest magnitude of change upon Co treatment, increasing 3-fold (25 μM Co treatment) and 6-fold (50 μM Co treatment) relative to the control plants. White et al., (1981) measured organic acids in xylem fluids of tomato plants grown with high-Zn and normal-Zn concentrations in nutrient solution, and observed a substantial increase in fumaric acid concentrations for the high-Zn treatment.

Analysis of the xylem fluid chemistry of metal accumulator plants has indicated the involvement of organic acids in metal translocation, transport, and detoxification (Pelosi et al., 1976; Pancaro et al., 1977; Lee et al., 1978; Vergnano and Gabbrielli, 1979; Morrison 1980; Gabbrielli et al., 1991; Homer et al., 1991; Krämer

et al., 1996, 1997; Salt et al., 1999; Sarret et al., 2002). Malic, malonic, and citric acids have consistently appeared as the major ligands associated with Ni in aqueous extracts of leaf material from Mediterranean *Alyssum* species such as *A. bertolonii* (Pelosi et al., 1976; Pancaro et al., 1977; Shaw 1980; Gabbrielli et al., 1991), *A. serpyllifolium* subspecies (Pancaro et al., 1977; Lee et al., 1978; Morrison 1980; Brooks et al., 1981), and *A. troodii* (Homer et al., 1995). Lee et al. (1978) noted malic and malonic acids were the only important acids in purified extracts of the leaves of *A. serpyllifolium* despite Ni stability constants (Ni-malate pK = 3.2; Ni-malonate pK = 3.2) considerably smaller than for citrate (Ni-citrate pK = 5.2), which is the primary ligand responsible for Ni binding in New Caledonian hyperaccumulators. Liddle (1979) argued the malic acid structure allows for a multiplicity of chelate rings to further stabilize the complex formed with nickel. Shaw (1980) evaluated the phytochemistry of several Ni-accumulating *Alyssum* species and confirmed the substantial presence of malic acid in *Alyssum*. Morrison (1980) profiled organic acids in leaf extracts from *A. murale* plus extracts from an accumulator and non-accumulator subspecies of *A. serpyllifolium* and reported noticeably higher citric and isocitric acid levels in the nonaccumulator and observed substantial levels of malic and malonic acids in the two hyperaccumulators.

Krämer et al. (1996) investigated xylem fluid composition in *Alyssum* species exposed to different Ni (and Co) concentrations and observed a linear correlation between the concentration of metal and free histidine in the xylem of *A. murale*, *A.*

bertolonii, and *A. lesbiacum*. At xylem pH, the effective stability constant for the nickel-histidine complex is higher than for any other amino or organic acid; however, at vacuolar pH, amino acids (e.g. histidine) form less stable complexes with Ni and Co. Organic acids (e.g. malate and citrate) produced by the Krebs TCA cycle are known to effectively complex metal ions at pH levels encountered in xylem fluid (pH ≥ 6.5) and plant cell vacuoles (pH ≤ 5.0). Nickel is predominantly complexed with carboxylic acids in shoots, suggesting the primary role of histidine may be to chelate Ni absorbed by root cells and to facilitate xylem loading for long distance transport to the shoot (Baker et al., 2000; Kerkeb and Krämer, 2003).

3.4.3 Cobalt Localization and Elemental Associations using Synchrotron-based Spectromicroscopy and Electron Microprobe Analysis (EMPA)

Micro-SXRF images reveal Co preferentially accumulated at leaf tips and margins of *A. murale* plants (Figure 3.1); an identical localization pattern for Co was first observed for *A. murale* plants cultivated in a mixed-metal (Ni+Co) system (Tappero et al., 2007). Multiple leaves from each plant and leaves from different plants were imaged with SXRF to verify the Co localization pattern is representative.

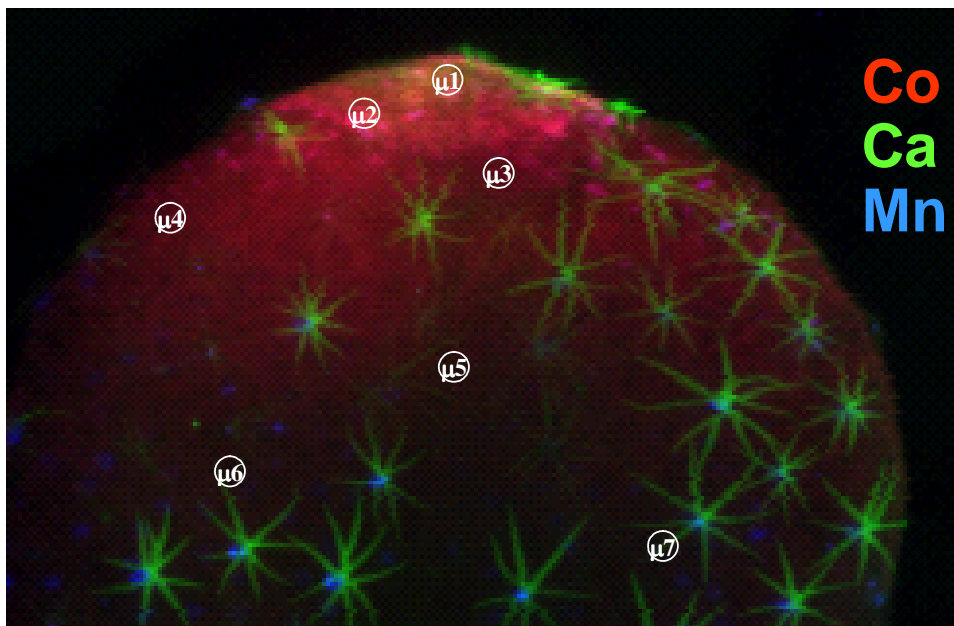


Figure 3.1 μ -SXRF image showing the distribution of Co (red), Mn (blue), and Ca (green) in a hydrated *Alyssum murale* leaf from the 50 μ M treatment plus approximate regions on leaves where μ -EXAFS spectra were collected (indicated with circles).

Synchrotron XRD indicates the stellate trichomes on the leaf surface are composed of calcium carbonate (CaCO_3) rather than calcium oxalate as had been speculated (Figure 3.2). In addition, μ -XRD revealed the presence of silica phytoliths in the Co-rich region near leaf tips; a phytolith (“plant stone”) is a rigid microscopic silica body that forms in many plants. Diffraction data were consistent with a mixture of “amorphous” silica (opal-A) and a poorly-ordered layered framework with a polyhedral local structure resembling that of a sheet silicate (metal octahedra are joined along edges and share corners with ditrigonal SiO_4 rings), presumably a Co-rich phyllosilicate resembling Co-Kerolite (2:1 trioctahedral hydrous silicate of formula $(\text{Co},\text{Mg})_3\text{Si}_4\text{O}_{10}(\text{OH})_2 \cdot n\text{H}_2\text{O}$) (Figure 3.3).

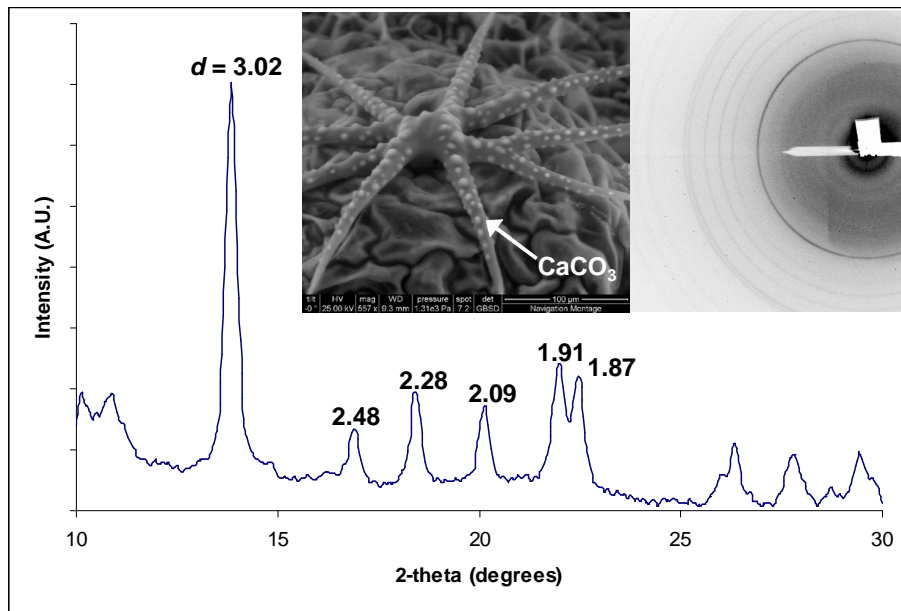


Figure 3.2 One-dimensional XRD pattern for a trichome on an *A. murale* leaf, numbers indicate respective d-spacing for characteristic calcite (CaCO_3) peaks. Inset, SEM image (center) and two-dimensional μ -XRD pattern (right) for the trichome.

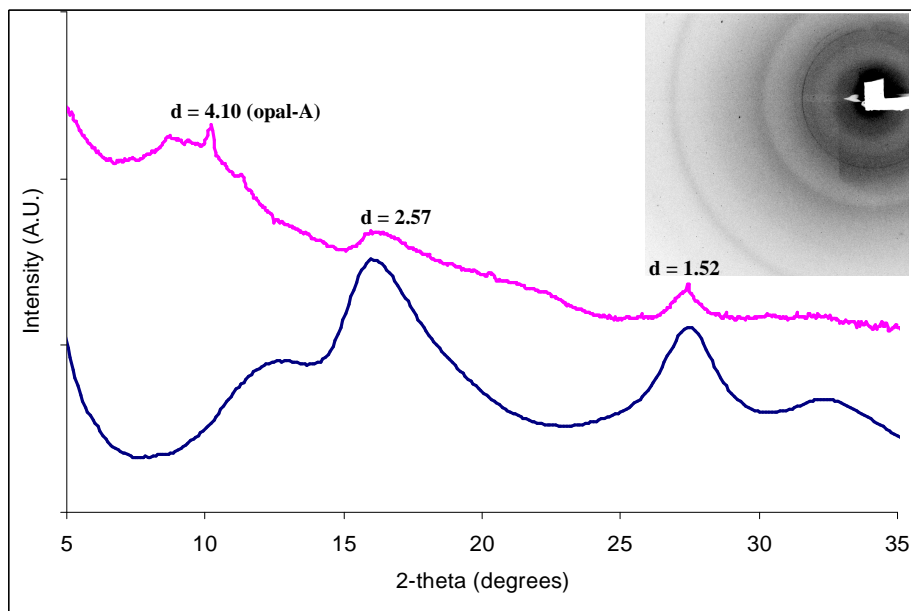


Figure 3.3 Representative one-dimensional XRD pattern for a Co-rich hotspot near the tip of a Co-treated *A. murale* leaf (upper line) and a synthetic, poorly-ordered hydrous Co silicate (lower), numbers indicate respective d-spacing for several characteristic features of the Co-Phyllosilicate (syn. Co-Kerolite; $\text{Co}_3\text{Si}_4\text{O}_{10}(\text{OH})_2$). Inset, two-dimensional μ -XRD pattern (right) for the Co-rich hotspot.

Alyssum murale leaves were investigated with SEM-EDX. Electron microprobe analysis (EMPA) of leaves from Co-treated *A. murale* showed elevated levels of Si, Mg, Ca, and Mn in Co 'hotspots', suggesting these elements were associated with Co on the leaf surface (Figure 3.4). Silicon is the only element associated with the Co-rich deposits that was not detected in the bulk-leaf regions.

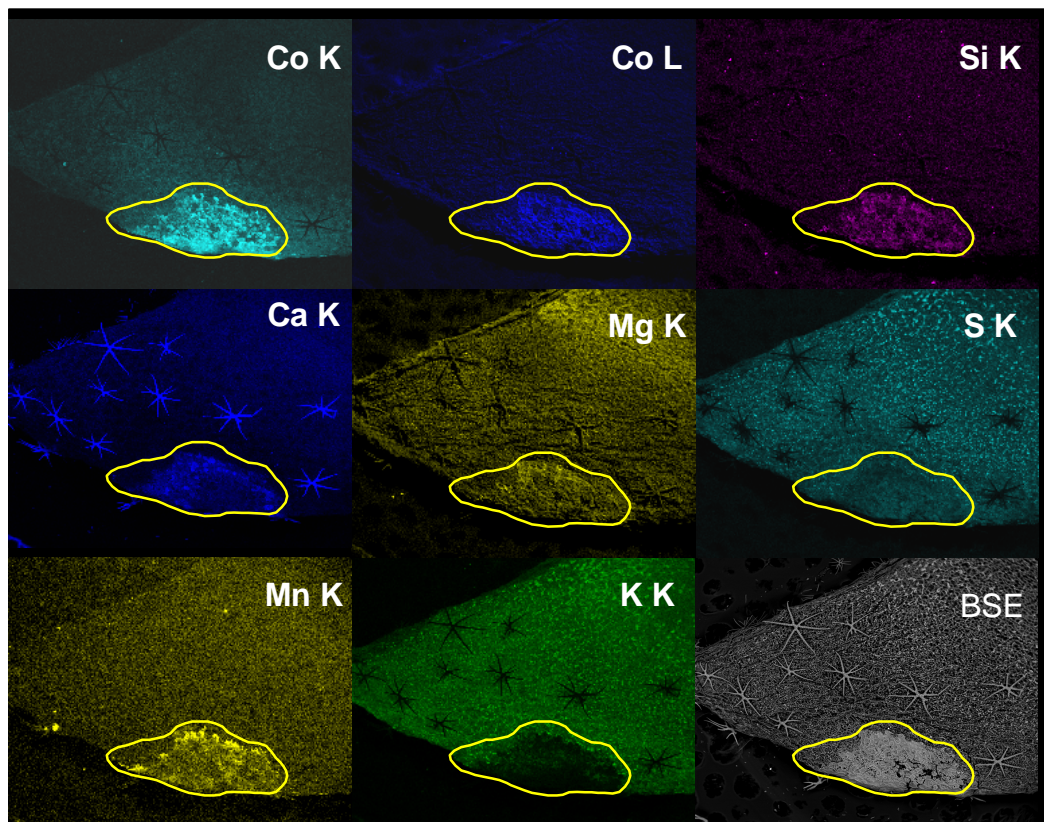


Figure 3.4. EMPA backscattered electron (BSE) image of a leaf from a Co-treated *Alyssum murale* plant and associated X-ray fluorescence maps for Co, Si, Ca, Mg, S, Mn, and K (top panel) plus the corresponding energy-dispersive X-ray spectra (produced by spectral summation) for the Co-enriched and bulk-leaf regions (next page)

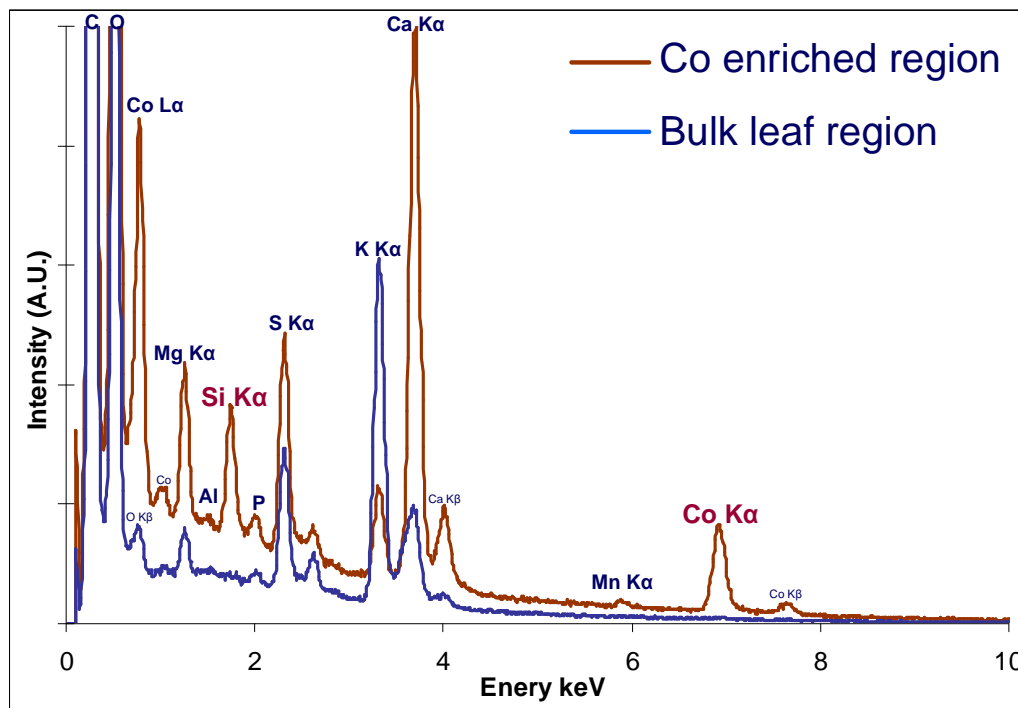
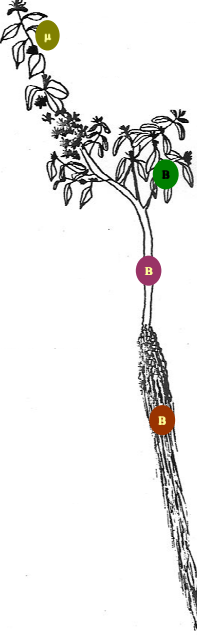


Figure 3.4 (cont) Energy-dispersive X-ray spectra (produced by spectral summation) for the Co-enriched and bulk-leaf regions.

3.4.4 Cobalt Speciation in the Bulk Samples

The principle amino and organic acids involved with Co detoxification and transport in *A. murale* include fumarate, malate, citrate, and histidine. These same ligands are involved with Ni detoxification and transport in *A. murale*. Speciation in leaves of Co+Ni-treated *A. murale* plants ($n = 3$) was investigated with bulk Ni K-edge and Co K-edge EXAFS and the primary Ni species were found to be Ni-histidine (70%) and Ni-malate/Ni-citrate (30%) (Table 3.2 & Figure 3.5). Cobalt speciation in the same leaves from the Co+Ni-treated plants consisted of Co-histidine (62%) and Co-fumarate (36%).

Table 3.2 Summary of Co speciation in hyperaccumulator *Alyssum murale*



Sample ID	Hydrous Co-silicate ^a	Hydrous Co-carbonate hydroxide ^b	Co-fumarate _(s) ^c	Co-histidine _(aq)	Co-fumarate _(aq)	Co-malate _(aq) /citrate _(aq)	Energy shift	NSS ^{d,e}
Bulk XAFS								
Leaves								
B0	6wk (Co+Ni)			62	36		-1.59	3.63E-02
B0 ^f	6wk (Co+Ni)			77 ^f		25 ^f	0.26	2.87E-02
B1	2wk			64	36		-0.88	4.04E-02
B2	4wk			47	55		-1.02	2.01E-02
B3	6wk			37	64		-0.82	1.73E-02
B4	6wk (w/o tips)			34	46	17	-1.01	1.91E-02
Stems								
B5	6wk			52	52		-0.76	1.69E-02
Roots								
B6	6wk			63	37		-3.91	9.57E-02
μ-XAFS (summary)								
μ1	leaf tip	81			16		0.20	4.97E-02
μ2	leaf tip	65	14			21	-0.40	4.95E-03
μ3	leaf tip		86	15			1.62	1.78E-02
μ4	leaf margin		25		18	57	0.85	5.19E-02
μ5	leaf vein			22	31	46	0.83	3.84E-02
μ6	basal			42	20	41	0.65	3.36E-02
μ7	basal				34	67	0.27	3.65E-02

^aCo Kerolite-like [Co₃Si₄O₁₀(OH)₂*xH₂O], ^bCo Widgiemoolthalite-like [Co₅(CO₃)₄(OH)₂*xH₂O], ^cCo-Fumarato Polymer [Co₃(C₄H₂O₄)₂], ^dNormalized Sum of Squares, ^eEstimated error in fitting was ± 10 %, ^fNi K-edge XAS (Ni-Histidine; Ni-Malate/Citrate)

It is noteworthy that fumarate was associated with Co in leaves from both the Co-only (i.e. Co-histidine & Co-fumarate) and Co+Ni treatments (i.e. Ni-Histidine, Ni-Malate, Co-histidine & Co-fumarate). Analysis of the organic acids in naturally-bleeding xylem fluid from *A. murale* control plants revealed that xylem fumarate concentrations are constitutively low (~70 μM); however, xylem fumarate concentrations are elevated (~6 fold) when plants are exposed to nutrient solution with 50 μM Co. In contrast, the xylem fluid concentrations of malate and citrate are constitutively high (> 1000 μM) in both control and Co-treated *A. murale* plants.

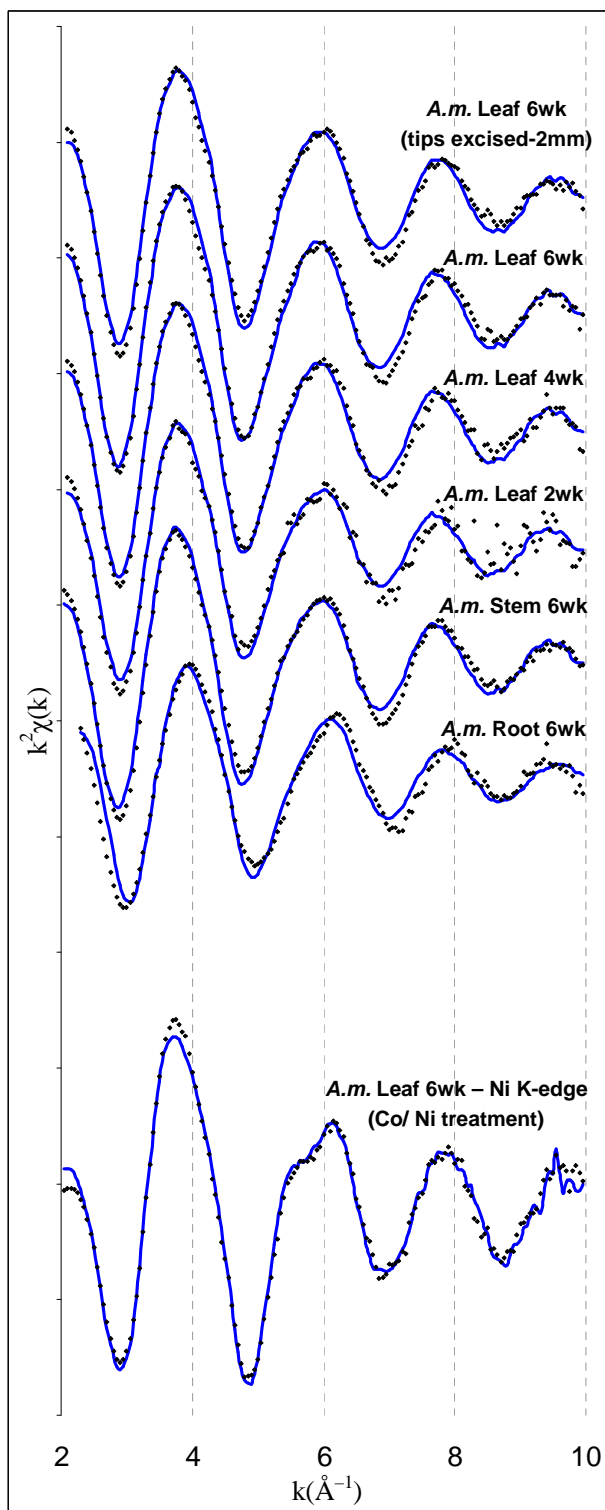


Figure 3.5 Cobalt K-edge EXAFS spectra of bulk plant samples, raw k^2 -weighted $\chi(k)$ spectra (dotted line) and corresponding linear combinations fit (solid line)

Cobalt speciation in the leaves of Co-treated *A. murale* plants was investigated as a function of the time length of metal exposure. Plants were exposed to Co-enriched nutrient media for 2, 4, or 6 weeks and the plant tissues were investigated with bulk Co K-edge EXAFS. Cobalt speciation in the leaves of the 2 week plants consisted of Co-histidine (64%) and Co Fumarate (36%). The proportions of Co species show a trend with the time length of metal exposure. For instance, the fraction of Co bound to histidine in leaves decreases from 64% to 47% to 37% (2wk, 4wk, and 6wk, respectively) while the fraction of Co bound to fumarate increases from 36% to 55% to 64%.

The observed trend in Co speciation could be explained by either the accumulation of Co in leaves as Co-fumarate complexes or the conversion of histidine-bound Co to fumarate-bound Co; other possibilities to consider include a proportional decrease in free histidine (biosynthesis) or an increase in levels of fumarate (biosynthesis). A decrease in histidine biosynthesis could be caused by any number of unrelated reasons including the normal fluctuations in plant metal homeostasis resulting from various stages of plant growth and maturity. With several weeks or more of metal exposure plants can adjust to conditions with elevated metals and compile their biochemical machinery for optimal metal (hyper)tolerance (elevated production of histidine); once stability is reached the machinery is optimized for efficiency (suitable production of histidine). The short-term “histidine response” observed by [Krämer et al \(1996\)](#) may be an early step in a series of biochemical events

leading to the stable phase of sustained metal uptake and elevated resistance to metal toxicity. Therefore, a decrease in Co-histidine species (and an increase in Co-fumarate species) at longer time lengths of metal exposure could reflect changes in the status of plant metal homeostasis.

Another possible explanation for this trend in Co speciation (increase in Co-fumarate species at longer time lengths of metal exposure) is the accumulation of Co-fumarate in leaves and storage as Co-fumarate complexes. Cobalt fumarate solutions are unstable; a Co-fumarate coordination polymer forms rapidly in solution (final pH = 5.5) and crystals develop in a few days at ambient temperature (a few hours at 50°C) (Zheng and Xie, 2004). In the cobalt-fumarate coordination polymer $[\text{Co}_3(\text{H}_2\text{O})_4(\text{OH})_2\text{L}_2 \cdot 2\text{H}_2\text{O}]$ with $\text{H}_2\text{L} = \text{fumarate, HOOCCH}=\text{CHCOOH}$], two CoO_6 octahedra are condensed through hydroxide anions to form edge-shared bi-octahedra, which are bridged by a third CoO_6 to generate a cobalt oxide chain extending indefinitely in the [100] direction (Zheng and Xie, 2004). The bridging CoO_6 octahedral unit is coordinated by four oxygen atoms of different fumarate anions and two hydroxo oxygens. Through the bis-bidentate fumarate anions, the cobalt oxide chains are inter-linked into 3D open framework with rhombic tunnels propagating into the [100] direction (Zheng and Xie, 2004). Therefore, fumarate-bound Co has the potential to accumulate in leaves or at leaf surfaces, condensing into Co-fumarate coordination polymers as the Co- and fumarate- rich vascular fluids (evapo)transpire from leaves (especially near leaf tips and margins).

Histidine- and fumarate-bound Co are the predominant Co species in leaves of Co-treated *A. murale* plants; however, a spectral contribution from Co-malate/citrate becomes more noticeable with increasing plant age (i.e. time length of metal exposure). The spectrum of leaves from the 6 week plants can be correctly reconstructed with reference spectra of Co-malate/citrate (13%), Co-histidine (30%), and Fumarate (56%) (i.e. by allowing a 3rd component), but the NSS value (1.61E-2) does not meet the best established cutoff criteria whereby the fit (judged by the NSS) must improve by more than 10 % and the added component must be weighted more than 10 % of the total contribution (Manceau et al., 2002; Sarret et al., 2002).

Considering the high concentrations of malate and citrate (> 1000 μM) detected in naturally-bleeding xylem fluids collected from *A. murale* plants, it is surprising to find a greater proportion of Co bound to fumarate than to citrate or malate, especially since the latter two should have stronger binding constants (e.g. for Ca and Cu; NIST Critical Database 46 v.8, Smith and Martell, 2004). On the other hand, xylem fluids contain a complex mixture of inorganic ions (e.g. Ca^{2+} , Mg^{2+} , SO_4^{2+}), organic anions (e.g. oxalate) and other solutes and biomolecules that affect metal-ligand equilibria.

Aqueous complexes of Co-citrate and Co-malate are difficult to distinguish by EXAFS spectroscopy. Pure standard reference solutions (pH 6.5) have $\chi(k)$ spectra that match almost perfectly in both phase and amplitude (minus a small deviation in slope that occurs on the left shoulder of an oscillation in the k-range 5.5 – 6.0 \AA), and the Fourier Transforms of the raw $\chi(k)*k^3$ spectra show little differences in

the modulus or the imaginary part (Figure 3.6); pure Ni-malate and Ni-citrate solution standards are equally challenging to distinguish with EXAFS. Since malic and citric acid concentrations are constitutively high in *A. murale* xylem fluid (~1-2 mM) and the Co binding environment is nearly identical for Co-malate and Co-citrate complexes, the spectra for Co-malate and Co-citrate standard reference solutions were merged and the average was included in the fit library as a Co-malate/Co-citrate standard.

Cobalt bound to malate/citrate is detectable in leaves of the 6 week plants when the leaf tips (~2 mm) are excised. SXRF imaging had indicated Co is preferentially localized at leaf tips/ margins, with the greatest enrichment extending ~2000 μm from the average leaf tip. Leaf tips (~2 mm) were meticulously excised from several hundred leaves of Co-treated *A. murale* and the basal segments of leaves were pooled and prepared for analysis by EXAFS. Cobalt speciation in the leaves of the 6 week plants (tips excised) consisted of Co-histidine (34%), Co-fumarate (46%), and Co-malate/citrate (17%), indicating that Co-malate/Co-citrate species are present as minor components in the leaves and become more significant to the total speciation when the leaf tip material is removed ('unmasked'). Additionally, it provides an indication that these species may be present in the leaves from 2, 4, and 6 wk plants; however, including Co-malate/citrate reference spectra (i.e. by allowing a 3rd component) does not change the fit (NSS) for the 2 wk plants, and only improves the fit slightly for 4 week and 6 week plants (4% and 7%, respectively).

Cobalt-fumarate species are more concentrated near the tip of *A. murale* leaves. A comparison of the Co speciation in the leaves of 6 week plants without tips (~2 mm) to the leaves of 6 week plants (whole leaves) reveals that the cut leaves contain overall less Co-fumarate (46% -decreased from 64%) but nearly the same amount of Co-histidine (34% -compared to 37%) as the whole leaves. In other terms, the tips of the leaves tend to contain more Co-fumarate than the basal portions; microprobe findings highlight this trend as well. This finding corroborates the reasoning presented previously to explain the increase in Co-fumarate species observed at longer time lengths of metal exposure (i.e. accumulation and storage of Co-fumarate complexes in leaves).

Cobalt speciation in *A. murale* is influenced slightly by the co-accumulation of Ni (i.e. “simultaneous hyperaccumulation” of Co and Ni). Cobalt speciation in the leaves of 6wk Co+Ni-treated plants consists of Co-histidine (62%) and Co-fumarate (36%), which is most similar to the speciation observed for 2 week plants from the Co-only treatment. However, in comparison to plants from the equivalent 6 wk Co-only treatment, the Co+Ni plants have substantially more Co bound to histidine (63%-increased from 37%) and considerably less Co bound to fumarate (36%-decreased from 64%). The larger fraction of histidine-bound Co observed in the presence of equimolar Ni (Co+Ni treatment) suggests that Ni stimulates histidine production and Co competes for free histidine (Krämer et al., 1996). Thus, Ni may stimulate Co accumulation and elevate Co tolerance in *Alyssum*.

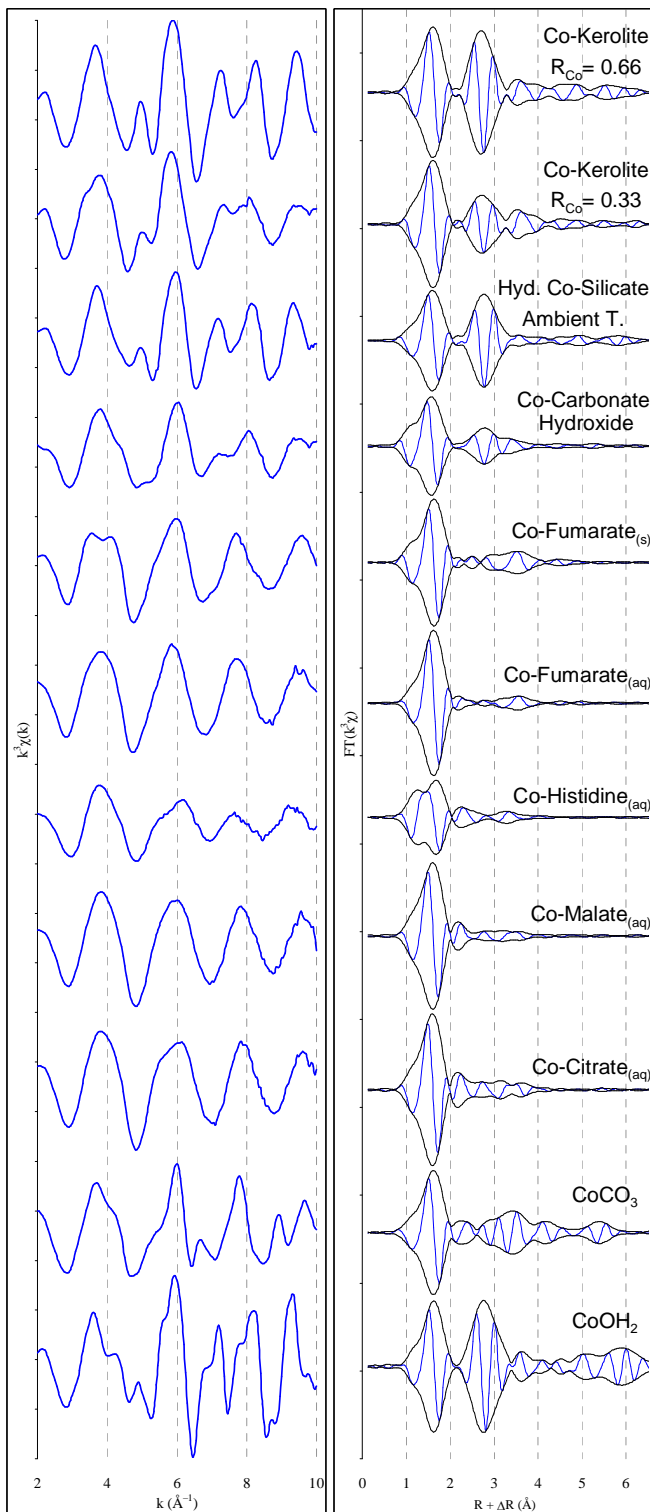


Figure 3.6 Cobalt K-edge EXAFS spectra of Co reference compounds, k^3 -weighted $\chi(k)$ spectra and corresponding Fourier Transforms (modulus and imaginary part).

Similar Co species are detected in *A. murale* tissues but their proportions in root, stem, and leaf tissues reveal an overall trend in bulk Co speciation. Root tissue of the 6 week plants has more histidine-bound Co (63%) than fumarate-bound Co (37%); stem tissue of the 6 week plants contains an equivalent amount of Co-histidine (51%) and Co-fumarate (51%), and leaves of 6 week plants have more fumarate-bound Co (64%) than histidine-bound Co (37%). An overall trend in Co speciation that emerges for the 6 week plants is that the greatest amount of histidine-bound Co occurs in roots (63%) followed by stems (51%) and then leaves (37%).

This unequal distribution of Co-histidine between root, stem, and leaf tissue agrees with the findings of [Krämer et al. \(1996\)](#) and [Kerkeb and Krämer \(2003\)](#), which attribute a role for free histidine in the radial transport and xylem loading of Ni and Co in roots of *Alyssum* hyperaccumulators. In a similar manner the current finding supports the many accounts of hyperaccumulated metals (e.g. Ni, Zn, Co) associated with oxygen-donor ligands (e.g. organic acids) in hyperaccumulator leaves. Furthermore, the observed decrease in histidine-bound Co from root to stem to leaf tissue suggests that a speciation change from histidine-bound Co to fumarate-bound Co (possibly via a ternary-complex intermediate) might occur somewhere along the solute pathway. Metal speciation in hyperaccumulator plants can be expected to vary between plant structures, tissues, cell types, and cellular compartments.

3.4.5 *In situ* Cobalt Speciation in Hydrated *Alyssum* Leaves

Bulk EXAFS spectroscopy shows Co-histidine and Co-fumarate are the predominant Co species in Co-treated *A. murale* plants and that Co-malate/Co-citrate are present as minor species (on a bulk, whole-leaf scale). The increase in Co-fumarate species observed at longer time lengths of metal exposure (2, 4, and 6 weeks) suggests accumulation of Co-fumarate in leaves and possible storage as Co-fumarate coordination complexes. Furthermore, bulk measurements obtained for whole and cut leaves (excised leaf tips, ~2mm) suggests the tips of the leaves tend to contain more Co-fumarate species than the basal segments. Microfocused X-ray absorption spectroscopy (μ -XAS including μ -SXRF, μ -EXAFS, and μ -XRD) can be used to investigate element speciation and distribution in natural, heterogeneous samples at the (sub)micron scale. By utilizing these spectromicroscopic tools in conjunction with electron probe microanalysis (EMPA) and other analytical and wet-chemical techniques it is possible to study the *in situ* speciation of elements in soils and plants, where speciation can vary over tens of microns.

Micro-SXRF and CMT (tomographic) imaging revealed that Co accumulated by *A. murale* is localized in the transpiration stream and is eventually pulled to leaf surfaces, resulting in preferential accumulation of Co at leaf tips/margins and the formation of sparingly-soluble precipitates on leaves. Cobalt enrichment on the surface of leaves is visible with optical microscopy. Electron probe microanalysis (EMPA) of leaves from Co-treated *A. murale* plants shows Co-rich

deposits localized on leaf surfaces; the deposits appear massive in habit (no individual grains or crystals visible) with botryoidal-like morphological features (formed like bubbles or partial bubbles). Electron diffraction did not identify any “crystalline” phases associated with the Co-rich deposits on leaves; the Co-rich deposits may be nanocrystalline or “amorphous”. The electron microprobe beam penetrated only a few microns into the sample, thus the recorded signals were emitted from the leaf surface or cuticle layer. A comparison of the EDS spectra (prepared by spectral summation) for the Co-rich and bulk-leaf regions shows that Si, Mg, Ca, and Mn are spatially associated with the Co-rich deposits; these elements are present at elevated concentrations in Co-rich areas. Silicon is the only element associated with the Co-rich deposits that is not detected in the bulk-leaf regions.

The Co K-edge μ -EXAFS spectra of hydrated leaves from Co-treated *A. murale* are shown in [Figure 3.7](#) and the fit results are shown in [Table 3.3](#). Initial spectromicroscopic measurements revealed differences in speciation between the Co-rich and bulk-leaf regions plus differences in speciation within the Co-rich region. A microfocused X-ray absorption spectroscopy study was initiated to investigate Co speciation in the Co-rich deposits near leaf tips and margins and to determine the ligands involved in Co detoxification and transport in *A. murale* (i.e. *in planta* Co speciation). A suite of spectromicroscopic measurements (including μ -SXRF, μ -EXAFS, and μ -XRD) were performed with fresh, hydrated leaves from healthy, living plants.

Results from Co K-edge μ -EXAFS are in good agreement with those obtained from the bulk EXAFS analysis of dry plant tissues, which identified Co-histidine and Co-fumarate as the predominant forms of Co in leaves. Similarly, μ -EXAFS measurements found that Co-fumarate is the most ubiquitous Co species in hydrated leaf tissue from Co-treated *A. murale*. Co-fumarate was detected at 83 percent of the locations sampled with the micro-focused X-ray beam; it ranged from 15 to 57 % of the total Co species in the sample volume measured by the beam (i.e. spot size x sample thickness). On average, Co-fumarate accounts for about one-third (32%) of the total Co speciation at the locations in the leaf where it is found.

Although bulk XAFS measurements (dry plant material) indicated that Co-malate/Co-citrate species are minor species in Co-treated *A. murale* leaves, they were the second most prevalent *in planta* Co species encountered in hydrated leaves by microspectroscopic analysis. Co-malate/Co-citrate species were detected at 69 percent of the locations sampled with the micro-focused X-ray beam; their proportions ranged from 15 to 57 % of the total Co species in the sample volume measured by the beam. On average, Co-malate/Co-citrate accounts for about one-half (47%) of the total Co speciation at the locations in the leaf where it is found.

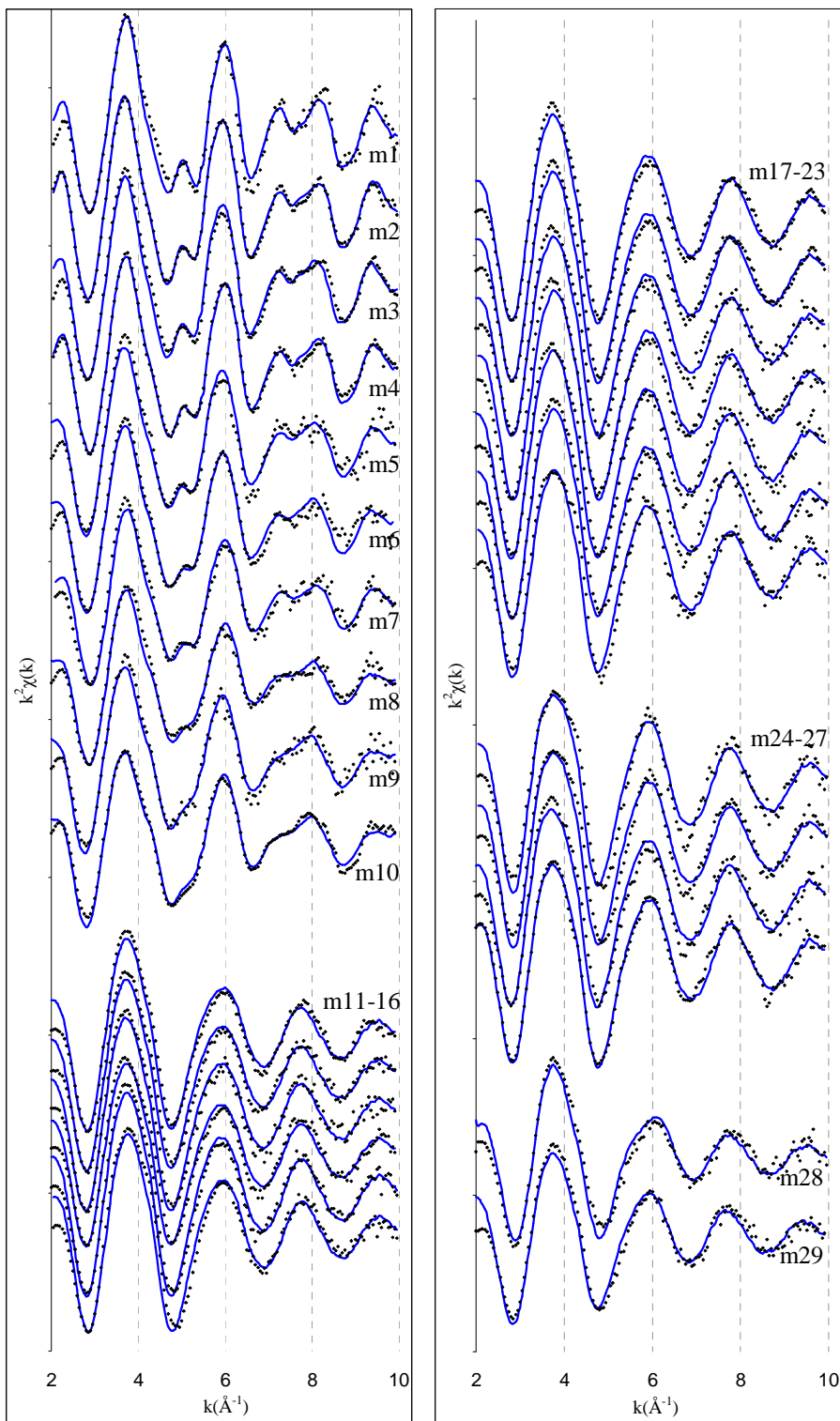


Figure 3.7 Cobalt K-edge μ -EXAFS spectra of hydrated leaves from Co-treated *A. murale* (dotted lines) and corresponding linear combinations fit (solid lines)

Table 3.3 Linear combination fit results for the μ -XAFS spectra of hydrated leaves from Co-treated *A. murale* (shown in **Figure 3.7**)

Sample ID	Hydrous Co-silicate ^a	Hydrous Co-carbonate hydroxide ^b	Co-fumarate _(s) ^c	Co-Histidine _(aq)	Co-Fumarate _(aq)	Co-Malate _(aq) /Citrate _(aq)	delta E ^d	NSS ^{e,f}
m1	81				16		0.20	4.97E-02
m2	65		14			21	-0.40	4.95E-03
m3	67				33		-0.20	3.16E-02
m4	69		18			13	0.27	7.17E-03
m5	45	18			37		1.30	6.72E-02
m6	34	41			25		0.89	3.76E-02
m7	34	40			25		0.71	3.51E-02
m8	25	30		44			0.63	3.87E-02
m9		82			21		2.04	4.32E-02
m10		86	15				1.62	1.78E-02
m11				42	20	41	0.65	3.36E-02
m12				36	25	40	0.87	3.78E-02
m13				26	25	48	1.08	4.01E-02
m14				26	27	49	-0.24	5.07E-02
m15				22	31	46	0.83	3.84E-02
m16				17	33	52	0.50	3.64E-02
m17					33	67	0.42	3.45E-02
m18					34	67	0.27	3.65E-02
m19					39	57	0.11	4.81E-02
m20					41	60	-0.45	3.46E-02
m21					44	57	0.41	5.11E-02
m22					57	43	-0.01	5.39E-02
m23					52	48	-0.22	5.26E-02
m24			25		41	34	-0.20	7.39E-02
m25			21		34	44	-0.37	5.92E-02
m26			25		18	57	0.85	5.19E-02
m27			20		15	65	0.17	1.26E-02
m28				62		33	-0.26	4.93E-02
m29				51	44		0.27	5.08E-02

^aCo Kerolite-like [Co₂Si₄O₁₀(OH)₂*xH₂O], ^bCo Widgiemoolthalite-like [Co₅(CO₃)₄(OH)₂*xH₂O], ^cCo-Fumarate Polymer [Co₃(C₄H₂O₄)₂],

^dEnergy Shift (eV), ^eNormalized Sum of Squares, ^fEstimated error in fitting ($\pm 10\%$)

Cobalt-histidine was detected at 31% of the locations sampled with the X-ray beam, reflecting far fewer occurrences for this Co species than for Co-fumarate (83%) or Co-malate/Co-citrate species (69%). However, Co-histidine species are not spatially associated with the Co-rich regions near tips (~2mm) and are rarely detected in proximity to the leaf tips or margins; instead they are usually found in the basal leaf regions where Co localization is more diffuse (“diffuse leaf region”). A μ -EXAFS scan was collected at midleaf in the center of the main vein of a Co-treated *Alyssum* leaf and the Co speciation consisted of Co-histidine (22%), Co-fumarate (31%), and Co-malate/citrate (46%). This finding is consistent with a report by [McNear \(2006\)](#) of

Ni-histidine species localized in the leaf vein region of a hydrated leaf from Ni-treated *A. murale*. On average, Co-histidine accounts for more than one-third (36%) of the total Co speciation at the locations in the leaf where it is found.

Additionally, the μ -XAS investigation aided in the discovery and identification of sparingly-soluble Co species sequestered on leaf surfaces (near tips/margins). Spectra collected in Co-rich regions near leaf tips showed striking differences from spectra collected in bulk-leaf regions (diffuse Co). The Co K-edge k^3 -weighted $\chi(k)$ spectrum of a Co-rich spot on an *A. murale* leaf had a beat pattern near 5 \AA^{-1} and a split oscillation between 7 and 8.5 \AA^{-1} whereas the $\chi(k)$ spectrum from a bulk-leaf spot did not have these characteristic structural features; spectra with several frequencies are indicative of a long-range ordered binding environment such as that in a mineral structure, while spectra dominated by a single frequency are indicative of a short-range ordered environment. Diffraction data from the Co-rich region are consistent with a mixture of amorphous silica (opal-A) and a poorly-ordered sheet silicate. Micro-EXAFS and EMPA indicate the Co-rich region contains a Co-rich precipitate species with a polyhedral local structure resembling that of sheet silicates (metal octahedral are joined along edges and share corners with ditrigonal SiO_4 rings), presumably a poorly-ordered Co-rich phyllosilicate resembling a Co-Kerolite (2:1 trioctahedral hydrous silicate of formula $(\text{Co,Mg})_3\text{Si}_4\text{O}_{10}(\text{OH})_2 \cdot n\text{H}_2\text{O}$).

Cobalt-rich regions near leaf tips and margins host a mixture of stable and meta-stable phases that form on leaf surfaces via the (evapo)transpiration of biological

fluids rich in Co (i.e. Co-fumarate, Co-malate/citrate, Co-histidine) and other non-essential solute molecules (e.g. $[\text{H}_4\text{SiO}_4]^0$) carried in the transpiration stream. μ -EXAFS and μ -XRD revealed that Co phyllosilicate-like phases (e.g. 2:1 trioctahedral Co-Kerolite-like, $(\text{Co})_3\text{Si}_4\text{O}_{10}(\text{OH})_2 \cdot x\text{H}_2\text{O}$) are the most prevalent species formed in Co-rich leaf regions. These poorly-ordered, biogenic, nano-sized phytoliths consist of two-dimensional hydrous cobalt silicate domains embedded in amorphous opal (opal-A) matrix. Cobalt phyllosilicate-like phases were identified in 28% of the locations sampled with the X-ray beam; proportions of this hydrous Co silicate species at various point locations in the Co-rich region of the leaves ranged from 25 to 81% of the total Co speciation. In addition to Co-Kerolite-like phytoliths on *A. murale* plants (hereso named “**Metallo-Phytoliths**”), spectromicroscopic analysis revealed a significant presence of another Cobaltoan mineral precipitate sequestered on leaf surfaces, a hydrated cobalt carbonate hydroxide.

Widgiemoolthalite ($\text{Ni}_5(\text{CO}_3)_4(\text{OH})_2 \cdot 4\text{H}_2\text{O}$) is the naturally-occurring Ni analogue of hydromagnesite (hydrated magnesium carbonate hydroxide, $\text{Mg}_5(\text{CO}_3)_4(\text{OH})_2 \cdot 4\text{H}_2\text{O}$) that was recently discovered and described (1993). An analogous hydrated Co-carbonate hydroxide mineral can be synthesized by dropwise addition of Na_2CO_3 (1M) to a stirred aqueous solution of Co(II) (0.5M) at ambient temperature (Zheng and Xie, 2003); the violet precipitate is a poorly-ordered, “X-ray amorphous” relative to commercially-available Cobalt Carbonate Basic (a.k.a. hydrated cobalt carbonate hydroxide, $\text{Co}[\text{CO}_3]_{1-a}[(\text{OH})_2]_a \cdot x\text{H}_2\text{O}$). A natural specimen

of the Co-analogue to Widgiemoolthalite ($\text{Co}_5(\text{CO}_3)_4(\text{OH})_2 \cdot x\text{H}_2\text{O}$) has not been discovered or described to date, but the biogenic species observed on leaves of hyperaccumulator *A. murale* is hereso named “**Sqwidgiemoolthalite**”.

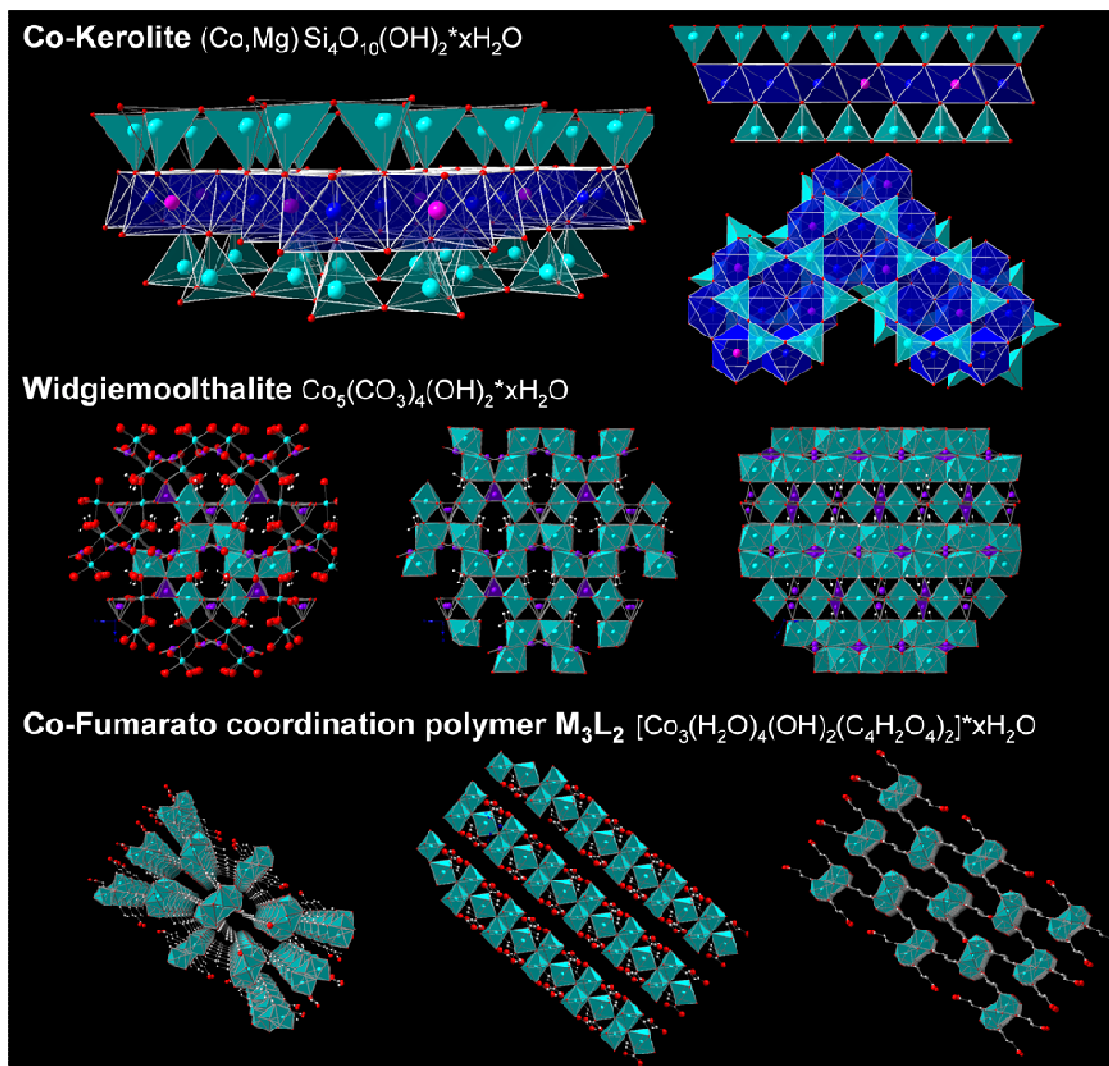


Figure 3.8 Molecular-scale representations of the coordination environment in a Cobalt-rich Kerolite-like 2:1 trioctahedral phyllosilicate, a hydrous Co-carbonate hydroxide mineral precipitate, and a Co-fumarato coordination polymer.

Sqwidiemoolthalite-like mineral precipitates were detected at 21% of the locations sampled with the X-ray beam; proportions of this Co-carbonate hydroxide species at the various point locations in the Co-rich region of the leaf ranged from 18 to 86% of the total Co speciation.

Co-Kerolite-like phytolith and Co-carbonate hydroxide are both observed in the Co-rich region of leaves. Both species are most frequently detected with Co-fumarate. Co-Kerolite-like phytolith and Cobalt carbonate hydroxide are frequently observed as isolated phases surrounded by aqueous Co species, but in other cases they are co-localized with one another and associated with an aqueous Co species (usually Co-fumarate).

Bulk and microfocused EXAFS spectroscopies indicate that Co-fumarate is a primary species in Co-treated *A. murale* plants at both the bulk (whole leaf) and micron (cellular) scale. Bulk EXAFS analysis of cut (leaf tip excised) and whole leaves suggests Co-fumarate may accumulate in leaves and might be stored near leaf tips as Co fumarate coordination complexes. Furthermore, bulk EXAFS revealed that the proportion of Co-fumarate species in leaves increases with longer time lengths of metal exposure. Therefore, Co-treated *A. murale* plants contain localized regions with elevated concentrations of cobalt and fumarate. Cobalt fumarate solutions are unstable; a Co-fumarate coordination polymer forms rapidly in solution and crystals develop at ambient temperature in a few days (a few hours at 50°C) (Zheng and Xie, 2004). For instance, Co fumarate crystals formed serendipitously in a high-purity Co-

fumarate_(aq) solution that had been prepared as a standard reference material for bulk XAFS analysis. Therefore, fumarate-bound Co has the potential to accumulate in leaves or at leaf surfaces, condensing into Co-fumarato coordination polymers as the Co- and fumarate- rich fluids (evapo)transpire from leaves (especially near leaf tips/margins).

A solid-like cobalt fumarate species (Co-fumarate_(s)) was detected on several *A. murale* leaves with μ -EXAFS. Co fumarate_(s) was detected at 24 % of the locations sampled in hydrated leaves and accounted for about 20% of the total Co speciation at locations where it was found. Solid-like Co-fumarate is observed most often near leaf margins. It is commonly localized with Co-malate/Co-citrate and Co-fumarate_(aq) species. Co-fumarate_(s) is a hydrated cobalt hydroxide fumarato coordination polymer of type $M_3L_2 [CO_3(C_4H_2O_4)_2]$. A crystalline form of solid cobalt fumarate was not detected by μ -XRD. Presumably these coordination polymers occur on leaves as a gel-like coating of amorphous solids; their stability on leaf surfaces is anticipated to be rather limited.

In summary, Co-fumarate_(aq) is the predominant species in leaves and accumulates near leaf tips and margins (i.e. regions of maximal transpiration), presumably leading to the formation of cobalt-fumarato coordination polymers (especially near the evaporative interface). These C-rich Co-fumarato polymers are meta-stable on leaf surfaces because of exposure to light, heat, microorganisms and drastically altered chemical conditions (e.g. humidity, air, etc.), all of which facilitate

their degradation. These coordination polymers and their degradation byproducts (bearing resemblance to poorly-ordered Co carbonate hydroxide) may serve as templating agents for the (surface) precipitation of stable Co/Si-rich mineral precipitates (e.g. Co-Kerolite) on *A. murale* leaves. Thus a possible mechanism of deposition involves 1) accumulation of Co-fumarate_(aq) in leaves, 2) condensation of Co-fumarate_(s) near evaporative surfaces (e.g. leaf tips/ margins), 3) partial degradation of C-rich Co-fumarate polymers on leaf surfaces with restructuring to Co carbonate hydroxide-like matrix, and 4) formation of stable Co/Si-rich mineral precipitates (i.e. Co-Fumarate_(aq) → Co-Fumarate_(s) → Co-Widgiemoolthalite → Co-Kerolite).

3.4 References

- Baker, A.J.M., S.P. McGrath, R.D. Reeves, and J.A.C. Smith. 2000. Metal hyperaccumulator plants: a review of the ecology and physiology of biological resources for phytoremediation of metal-polluted soils. *In*: Terry, N., and G. Banuelos (eds.) *Phytoremediation of Contaminated Soil and Water*. Lewis Publishers, Boca Raton. pp. 85-107.
- Brooks, R.R., S. Shaw, and A. Asensi Marfil. 1981. The chemical form and physiological function of nickel in some Iberian *Alyssum* species. *Physiol. Plant.* 51:167-170.
- Brown, G.E. Jr., G. Calas, G.A. Waychunas, and J. Petiau. 1988. X-Ray absorption spectroscopy: Applications in mineralogy and geochemistry. *In* Hawthorne, F.C. (ed.) *Spectroscopic Methods in Mineralogy and Geology*. Mineralogical Society of America, Washington, DC. *Reviews in Mineralogy* 18: 431.
- Chaney, R.L. 1983. Plant uptake of inorganic waste constituents. *In* J.F. Parr, P.B. Marsh, and J.M. Kla (ed.) *Land treatment of hazardous wastes*. pp.50–76. Noyes Data Corp., Park Ridge, NJ.
- Chaney, R.L. 1988. Plants can utilize iron from Fe–N, N’–di–(2–hydroxy–benzoyl)–ethylenediamine–N, N’–diacetic acid, a ferric chelate with 10^6 greater formation constant than Fe–EDDHA. *Journal of Plant Nutrition* 11:1033–1050.
- Chaney R.L., J.S. Angle, and Y.M. Li. 2004. Method for phytomining of nickel, cobalt, and other metals from soil. US patent 5,944,872.
- Decarreau, A. 1981. Cristallogenese a basse temperature de smectites trioctaedriques par vieillissement de coprecipites silicometalloques de formule $(Si_{4-x}Al_x)Mg^{2+}O_{11}nH_2O$, ou x varie de 0 a 1 et $M^{2+} = Mg, Ni, Co, Zn, Fe, Cu, Mn$. *C.R. Acad. Sci. Paris* 292:61-64.
- Decarreau, A. 1985. Partitioning of divalent transition elements between octahedral sheet of trioctahedral smectites and water. *Geochim. Cosmochim. Acta* 49:1537-1544.
- Gabbrielli R, Mattioni C, Vergnano O. 1991. Accumulation mechanisms and heavy metal tolerance of a nickel hyperaccumulator. *J. Plant Nutr.* 14:1067-1080.
- Gräfe, M., R. Tappero, M.A. Marcus, and D.L. Sparks. 2008a. Arsenic speciation in multiple-metal environments: I. Bulk-XAFS spectroscopy of model and mixed compounds. *J. Colloid Interface Sci.* 320:383-399.

Gräfe, M., R. Tappero, M.A. Marcus, and D.L. Sparks. 2008b. Arsenic speciation in multiple-metal environments: II. Microspectroscopic investigations of CCA-contaminated soil. *J. Colloid Interface Sci.* 321:1-20.

Homer, F.A., R.D. Reeves, and R.R. Brooks. 1995. The possible involvement of amino acids in nickel chelation in some nickel-accumulating plants. *Curr. Top. Phytochem.* 14:31-37.

Homer, F.A., R.S. Morrison, R.R. Brooks, J. Clemens, and R.D. Reeves. 1991. Comparative studies of nickel, cobalt, and copper uptake by some nickel hyperaccumulators of the genus *Alyssum*. *Plant Soil* 138:195–205.

Kerkeb, L., and U. Krämer. 2003. The Role of Free Histidine in Xylem Loading of Nickel in *Alyssum lesbiacum* and *Brassica juncea*. *Plant Physiol.* 131:716–724.

Krämer U., Cotterhowells J.D., Charnock J.M., Baker A.J.M., and J.C. Smith. 1996. Free histidine as a metal chelator in plants that accumulate nickel. *Nature* 379:635–638.

Krämer, U., I.J. Pickering, R.C. Prince, I. Raskin, and D.E. Salt. 2000. Subcellular localization and speciation of nickel in hyperaccumulator and non-accumulator *Thlaspi* species. *Plant Physiol.* 122:1343–1354.

Küpper, H., Mijovilovich, A., Meyer-Klaucke, W., and P.M.H. Kroneck. 2004. Tissue- and age-dependent differences in the complexation of cadmium and zinc in the Cadmium/Zinc hyperaccumulator *Thlaspi caerulescens* (Ganges Ecotype) revealed by X-ray absorption spectroscopy. *Plant Physiology* 134:748–757.

Lee, J., R.D. Reeves, R.R. Brooks, and T. Jaffré. 1978. The relation between nickel and citric acid in some nickel-accumulating plants. *Phytochem.* 17:1033-1035.

Lytle, F.W., R.B. Greigor, D.R. Sandstone, E.C. Marques, J. Wong, C.L. Spiro, G.P. Huffman, and F.E. Huggins. 1984. Measurements of soft X-ray absorption spectra with a fluorescent ion chamber. *Nucl. Instrum. Methods Phys. Res. Sect. A.* 226:542–548.

Malinowski, E.R. 1977. Determination of the number of factors and the experimental error in a data matrix. *Anal. Chem.* 49:612–617.

- Malinowski, E.R. 1978. Theory of error for target factor analysis with applications to mass spectrometry and nuclear magnetic resonance spectrometry. *Anal. Chem. Acta* 103:359–364.
- Manceau, A., B. Lanson, M.L. Schlegel, J.C. Harge, M. Musso, L. Eybert–Berard, J.L. Hazeman, D. Chateigner, and G.M. Lamble. 2000. Quantitative Zn speciation in smelter–contaminated soils by EXAFS spectroscopy. *Am. J. Sci.* 300:289–343.
- Manceau, A., M.A. Marcus, and N. Tamura. 2002. Quantitative speciation of heavy metals in soils and sediments by synchrotron X–ray techniques. In Fenter, P. and N.C. Sturchio (Eds.) *Applications of Synchrotron Radiation in Low–Temperature Geochemistry and Environmental Science*, Reviews in Mineralogy and Geochemistry 49:341–428. Mineralogical Society of America, Washington, DC.
- Marcus, M.A., A.A. MacDowell, R. Celestre, A. Manceau, T. Miller, H.A. Padmore, and R.E. Sublett. 2004. Beamline 10.3.2 at ALS: a hard X–ray microprobe for environmental and materials sciences. *J. Synchrotron Rad.* 11: 239–247.
- Morrison, Richard S. 1980. Aspects of the accumulation of cobalt, copper, and nickel by plants. Thesis (PhD in Chemistry). Massey University Library, Palmerton North, New Zealand.
- Newville, M. 2001. IFEFFIT: interactive XAFS analysis and FEFF fitting. *J. Synchrotron Rad* 8:322–324.
- O’Day, P.A., G.E. Brown Jr., and G.A. Parks. 1994. X–ray absorption spectroscopy of Cobalt(II) multinuclear surface complexes and surface precipitates on kaolinite. *J. Colloid Interface Sci.* 165: 269–289.
- Pancarò, L., P. Pelosi, O. Vergnano Gambi, and C. Galoppini. 1977. Further contribution on the relationship between nickel and malic and malonic acids in *Alyssum*. *Soc. Bot. Ital. Congr. Soc., Bardolino (Verona)*.
- Pelosi, P., R. Fiorentini, and C. Galoppini. 1976. On the nature of nickel compound in *Alyssum bertolonii* Desv. II. *Agric. Biol. Chem.* 40:1641–1642.
- Peltier, E., R. Allada, A. Navrotsky, and D.L. Sparks. 2006. Nickel solubility and precipitation in soils: a thermodynamic study. *Clays and Clay Minerals* 54:153–164.
- Persans, M.W., K. Nieman, and D.E. Salt. 2001. Functional activity and role of cation–efflux family members in Ni hyperaccumulation in *Thlaspi goesingense*. *Proceeding of the National Academy of Science* 98:9995–10000.

- Persson, P. and K. Axe. 2005. Adsorption of oxalate and malonate at the water–goethite interface: molecular surface speciation from IR spectroscopy. *Geochim. et. Cosmochim. Acta* 69:541–552.
- Ravel, B. and M. Newville. 2005. Athena, Artemis, Hephaestus: data analysis for X–ray absorption spectroscopy using IFEFFIT. *J. Synchrotron Rad* 12:537–541.
- Ressler, T. 1998. WinXAS: A program for X–ray absorption spectroscopy data analysis under MS–windows. *J. Synchr. Rad.* 5:118–122.
- Salt, D., R. Prince, A.J.M. Baker, I. Raskin, and I. Pickering. 1999. Zinc ligands in the metal hyperaccumulator *Thlaspi caerulescens* as determined by X–ray absorption spectroscopy. *Env. Sci. and Technol.* 33:713–717.
- Sarret, G., P. Saumitou-Laprade, V. Bert, O. Proux, J. Hazemann, A. Traverse, M.A. Marcus, and A. Manceau. 2002. Forms of Zinc Accumulated in the Hyperaccumulator *Arabidopsis halleri*. *Plant Physiology* 130:1815-1826.
- Scheidegger, A.M., G.M. Lamble, and D.L. Sparks. 1997. Spectroscopic evidence for the formation of mixed-cation, hydroxide phases upon metal sorption on clays and aluminum oxides. *J. Colloid Interf. Sci.* 186:118-128.
- Shaw, S. 1980. Some observations on the ecology and phytochemistry of nickel-accumulating *Alyssum* species from the Iberian Peninsula. M.Sc. Thesis, Massey University.
- Smith, R.M. and A.E. Martell 2004. NIST Critically Selected Stability Constants of Metal Complexes Database (version 8.0). NIST Standard Reference Database 46. National Institute of Standards and Technology, Gaithersburg, MD.
- Tappero, R., E. Peltier, M. Gräfe, K. Heidel, M. Ginder-Vogel, K.J.T. Livi, M.L. Rivers, M.A. Marcus, R.L. Chaney, and D.L. Sparks. 2007. Hyperaccumulator *Alyssum murale* relies on a different metal storage mechanism for cobalt than for nickel. *New Phytologist* 175:641-654.
- Taylor, R.M. 1984. The rapid formation of crystalline double hydroxy salts and other compounds by controlled hydrolysis. *Clay Minerals* 19:591-603.
- Thompson, H.A., G.A. Parks, and G.E. Brown. 1996a. Ambient-temperature synthesis, evolution, and characterization of cobalt-aluminum hydrotalcite-like solids. *Clays and Clay Minerals* 47:425-438.

Wasserman, S.R., P.G. Allen, D.K. Shuh, J.J. Bucher, and N.M. Edelstein. 1999. EXAFS and principle component analysis: A new shell game. *J. Synchr. Rad.* 6:284–286.

White, M.C., A.M. Decker, and R.L. Chaney. 1981. Metal complexation in xylem fluid. I. Chemical composition of tomato and soybean stem exudate. *Plant Physiol.* 67:292-300.

Zheng, Y. and H. Xie. 2004. Two fumarato-bridged Co(II) coordination polymers: syntheses, crystal structures and properties of $\text{Co}(\text{H}_2\text{O})_4\text{L}$ and $[\text{Co}_3(\text{H}_2\text{O})_4(\text{OH})_2\text{L}_2] \cdot 2\text{H}_2\text{O}$ with $\text{H}_2\text{L} - \text{HOOCCH}=\text{CHCOOH}$. *Journal of Solid State Chemistry* 177:1352-1358.

Chapter 4

SUMMARY AND RESEARCH NEEDS

4.1 Summary

In this investigation, a combination of novel *in situ* techniques (e.g. synchrotron-based spectroscopies), advanced *ex situ* analytical methods (e.g. electron microprobe analysis), and wet-chemical procedures (e.g. high performance liquid chromatography) were used to investigate the localization and speciation of cobalt in the Ni/Co hyperaccumulator plant (*Alyssum murale*). Synchrotron-based microspectroscopic tools were applied to gain (sub)micrometer-scale information regarding the *in situ* chemical form (i.e. molecular speciation), spatial location, and elemental associations of the plant-accumulated metals (Co and Ni). The first research objective was to investigate aspects of Co accumulation and storage in *A. murale* and to determine the influence of simultaneous hyperaccumulation (i.e. Ni and Co) on metal localization. The second objective was to examine the molecular speciation of Co in various *A. murale* tissues (e.g. roots, stems, shoots, leaf tips) in an effort to improve our understanding of the biochemical mechanisms regulating Co transport and tolerance (i.e. metal homeostasis).

The research findings presented in Chapter 2 revealed a novel metal sequestration mechanism for accumulated Co (exocellular sequestration) that is

potentially involved with Co tolerance in *A. murale*. Furthermore, the sequestration mechanism for Co is completely different from the intracellular mechanism used to sequester Ni in *A. murale* (i.e. vacuolar compartmentation) and other *Alyssum* hyperaccumulators; compartmentalization of metals in the epidermal cell vacuoles of leaves has been established as a key component of the (hyper)tolerance mechanism used by the majority of hyperaccumulator plants.

The specialized biochemical processes linked with Ni (hyper)tolerance in *A. murale* do not confer (hyper)tolerance to cobalt, thus *A. murale* plants alleviate Co toxicity via exocellular sequestration. The two-dimensional μ -SXRF images of Ni in hydrated *A. murale* leaves show the nearly uniform Ni distribution that is indicative of metal enrichment in leaf epidermal tissue. In contrast, images of Co in hydrated leaves show preferential localization of Co at leaf tips and margins, indicating that accumulated Co is not compartmentalized with Ni in the leaf epidermal cells. The three-dimensional tomographic images (CMT) of metals in hydrated *A. murale* leaves show leaf epidermal layers are enriched with Ni but devoid of Co. Additionally, CMT images reveal the majority of Co *in planta* is localized in the apoplasm of leaf ground tissue (i.e. fluid between cells); the majority of Co *ex planta* is sequestered as Co-rich mineral precipitates on leaf surfaces near the leaf tips and margins. The research findings presented in Chapter 2 were published in *New Phytologist* (Tappero et al., 2007).

A mechanistic understanding of the highly selective metal transport system linked to Ni tolerance in shoots of *A. murale* (i.e. vacuolar transporter of leaf epidermal cells) should prove useful for elucidating the biochemical basis for plant metal tolerance or (hyper)tolerance and for unraveling the logistics of metal hyperaccumulation. Ultimately, understanding the physiological and biochemical processes underlying metal acquisition, accumulation, and tolerance will permit optimization of metal phytoextraction and aid developments in the production of nutrient-fortified foods.

The research findings presented in Chapter 3 represent the first report on the occurrence of Co/Si-rich biogenic nanoparticles (e.g. Phytoliths with two-dimensional hydrous cobalt silicate domains) and other Cobaltoan mineral precipitates (e.g. Widgiemoolthalite, Co-analogue) and polymers (e.g. Cobalt hydroxide fumarate coordination polymer, $[\text{Co}_3(\text{H}_2\text{O})_4(\text{OH})_2(\text{C}_4\text{H}_2\text{O}_4)_2]_x\text{H}_2\text{O}$) sequestered on the leaf surface of a metal hyperaccumulator plant.

Analysis of the organic acids in naturally-bleeding xylem fluid from *A. murale* plants revealed constitutively high ($> 1000 \mu\text{M}$) concentrations of malate and citrate. Xylem fumarate concentration was constitutively low ($\sim 70 \mu\text{M}$); however, fumarate concentration was elevated (~ 6 fold) for plants exposed to nutrient solution containing $50 \mu\text{M}$ Co.

The principle amino and organic acids involved with Co detoxification and transport in *A. murale* include fumarate, malate, citrate, and histidine. These same

ligands are involved with Ni detoxification and transport in *Alyssum*. Nickel speciation in leaves of 6 week Co+Ni-treated *A. murale* plants ($n = 3$) consisted of Ni-histidine (70%) and Ni-malate/Ni-citrate (30%); cobalt speciation in the same leaves from the Co+Ni-treated plants consisted of Co-histidine (62%) and Co-fumarate (36%). A Ni-fumarate EXAFS standard should be prepared and tested against Ni-malate in the fitting procedure.

Cobalt speciation in *A. murale* is influenced slightly by the co-accumulation of Ni (i.e. “simultaneous hyperaccumulation” of Co and Ni). Cobalt-treated plants had substantially less Co bound to histidine (37%- decreased from 62%) and considerably more Co bound to fumarate (64%- increased from 36%) than the Co+Ni-treated plants. A larger fraction of histidine-bound Co observed in the presence of equimolar Ni (Co+Ni treatment) suggests that Ni stimulates histidine production (Krämer et al., 1996). Thus, Ni additions have the potential to stimulate Co accumulation and elevate Co tolerance in *Alyssum*.

Cobalt speciation in leaves of Co-treated *A. murale* varied as a function of the time length of metal exposure (2, 4, or 6 weeks). The fraction of Co bound to histidine in leaves decreased from 64% to 47% to 37% (2 wk, 4 wk, 6 wk, respectively) while the fraction of Co bound to fumarate increased from 36% to 55% to 64%. A possible explanation for this trend in Co speciation (increase in Co-fumarate species at longer time lengths of metal exposure) is the accumulation of Co-

fumarate in leaves and storage as Co-fumarate complexes; X-ray microprobe findings highlight this trend.

Cobalt speciation varied between root, stem, and leaf tissues. The greatest amount of histidine-bound Co occurs in roots (63%) followed by stems (51%) and then leaves (37%). This unequal distribution of Co-histidine between root, stem, and leaf tissue agrees with the findings of [Krämer et al. \(1996\)](#) and [Kerkeb and Krämer \(2003\)](#), which attribute a role for free histidine in the radial transport and xylem loading of Ni and Co in roots of *Alyssum* hyperaccumulators. In a similar manner, the current finding supports the many accounts of hyperaccumulated metals (e.g. Ni, Zn, Co) associated with oxygen-donor ligands (e.g. organic acids) in hyperaccumulator leaves. Metal speciation in hyperaccumulator plants can be expected to vary between plant structures, tissues, cell types, and cellular compartments.

A microfocused X-ray absorption spectroscopy study was initiated to investigate Co speciation in the Co-rich deposits near leaf tips and margins and to determine the ligands involved in Co detoxification and transport in *A. murale* (i.e. *in planta* Co speciation). Results from Co K-edge μ -EXAFS are in good agreement with those obtained from the bulk EXAFS analysis of dry plant tissues, which identified Co-histidine and Co-fumarate as the predominant forms of Co in leaves. Similarly, μ -EXAFS identified Co-fumarate as the most ubiquitous Co species in hydrated leaf tissue from Co-treated *A. murale*.

Additionally, the μ -XAS investigation aided in the discovery and identification of the Co species sequestered on leaf surfaces (near tips/ margins) of Co-treated *A. murale*. The Co-rich regions near leaf tips and margins host a mixture of sparingly-soluble phases that form on leaf surfaces via the (evapo)transpiration of biological fluids rich in Co (i.e. Co-fumarate, Co-malate/citrate, Co-histidine) and other non-essential solute molecules (e.g. $[\text{H}_4\text{SiO}_4]^0$) carried in the transpiration stream. μ -EXAFS and μ -XRD revealed that Co phyllosilicate-like phases (e.g. 2:1 trioctahedral Co-rich Kerolite, $(\text{Co},\text{Mg})_3\text{Si}_4\text{O}_{10}(\text{OH})_2 \cdot x\text{H}_2\text{O}$) are the most prevalent species formed in Co-rich leaf regions. These poorly-ordered, biogenic, nano-sized phytoliths consist of two-dimensional hydrous cobalt silicate domains embedded in amorphous opal (opal-A) matrix. In addition to Co-Kerolite-like phytoliths on *A. murale* plants (hereso named “Metallo-Phytoliths”), spectromicroscopic analysis revealed a significant presence of another Cobaltoan mineral precipitate on leaf surfaces, a hydrated cobalt-carbonate hydroxide. Widgiemoolthalite ($\text{Ni}_5(\text{CO}_3)_4(\text{OH})_2 \cdot 4\text{H}_2\text{O}$), a naturally-occurring Ni analogue of hydromagnesite (hydrated magnesium carbonate hydroxide, $\text{Mg}_5(\text{CO}_3)_4(\text{OH})_2 \cdot 4\text{H}_2\text{O}$), has been recently discovered and described (1993). A natural specimen of the Co-analogue to Widgiemoolthalite ($\text{Co}_5(\text{CO}_3)_4(\text{OH})_2 \cdot x\text{H}_2\text{O}$) has not been discovered or described to date, but the biogenic species observed on leaves of Co hyperaccumulator *A. murale* is hereso named “Sqwidgiemoolthalite”. A solid cobalt fumarate species (Co-fumarate_(s)) was detected on several *A. murale* leaves with μ -EXAFS. Solid Co-

fumarate is observed most often near leaf margins. Co-fumarate_(s) is a hydrated cobalt hydroxide fumarate coordination polymer of type M₃L₂ [Co₃(C₄H₂O₄)₂]. A crystalline form of solid cobalt fumarate species was not detected by μ-XRD; these coordination polymers occur as poorly-ordered, amorphous solids, and their stability on the leaf surface is anticipated to be rather limited.

Co-fumarate_(aq) is the predominant species in leaves and accumulates near leaf tips and margins (i.e. regions of maximal transpiration), presumably leading to the formation of cobalt-fumarate coordination polymers (especially near the evaporative interface). These C-rich Co-fumarate polymers are meta-stable on leaf surfaces because of exposure to light, heat, microorganisms and drastically altered chemical conditions (e.g. humidity, air, etc.), all of which facilitate their degradation. These coordination polymers and their degradation byproducts (bearing resemblance to poorly-ordered Co carbonate hydroxide) may serve as templating agents for the (surface) precipitation of stable Co/Si-rich mineral precipitates (e.g. Co-Kerolite) on *A. murale* leaves. Thus a possible mechanism of deposition involves 1) accumulation of Co-fumarate_(aq) in leaves, 2) condensation of Co-fumarate_(s) near evaporative surfaces (e.g. leaf tips/ margins), 3) partial degradation of C-rich Co-fumarate polymers on leaf surfaces with restructuring to Co carbonate hydroxide-like matrix, and 4) formation of stable Co/Si-rich mineral precipitates (i.e. Co-Fumarate_(aq) → Co-Fumarate_(s) → Co-Widgiemoolthalite → Co-Kerolite).

Appendix A

CHAPTER 2 COPYRIGHT PERMISSIONS

Reproduced in part with permission from Tappero, R., E. Peltier, M. Gräfe, K. Heidel, M. Ginder-Vogel, K.J.T. Livi, M.L. Rivers, M.A. Marcus, R.L. Chaney, and D.L. Sparks, Hyperaccumulator *Alyssum murale* relies on a different metal storage mechanism for cobalt than for nickel. *New Phytologist* 175:641-654. DOI: 10.1111/j.1469-8137.2007.02134.x. Copyright © 2007 *New Phytologist*.